Exploitation of Nonlinear Effects in Micro-electromechanical Resonators

Chenchen Deng, St Anne's College

University of Oxford

Trinity Term, 2011

Supervised by Dr Steve Collins

This thesis is submitted to the Department of Engineering Science, University of Oxford, in fulfillment of requirements for the degree of Doctor of Philosophy.

Abstract

Microelectromechanical Systems (MEMS) are well developed in various fields benefiting from the rapid improvement of fabrication technology. Because of the low cost, small mass and high frequency, micromechanical resonators are of great interest to be used in the sensing technology. The mass change of a linear resonator can be identified by monitoring the resonant frequency. Any resonant frequency changes can be detected by the resulting change in amplitude or phase of the resonator's response at a particular frequency. A popular method to increase the sensitivity of the linear resonator is using force feedback to increase the effective Q value of a MEMS resonator by partially cancelling the effects of viscous damping.

Alternative methods to enhance the sensitivity of the resonator have been proposed in this thesis using the non-linear behaviour of the resonator which is known as Duffing non-linearity. A Duffing resonator has sudden transitions in both amplitude and phase at two jump frequencies which could be exploited to enhance the sensitivity of resonator based sensors. Numerical simulations and tests of a 'Duffing' circuit presented a driving scheme to give rise to fast, reliable, sensitive mass sensors. Two types of feedback methods to create a Duffing-like non-linearity are proposed using micromechanical resonators with low native Q values. One is using the force feedback to enhance the Q value and deliberately driving the system into the nonlinear region with a large excitation force. The other one is to generate a displacement cubed feedback term and add it to the primary drive. Both methods show that changes in resonant frequency of a Duffing resonator can create a dramatically larger change in phase than the equivalent linear resonator. In addition to the sensitivity analysis, the transient behaviour of the Duffing resonator following a parameter change has also been investigated in this thesis.

Acknowledgements

The research would not have been possible without the help of many supportive people whom I would like to acknowledge and thank. The long list of acknowledgements must begin with my supervisor Dr. Steve Collins. I really appreciate the chance he gave me by inviting me to Oxford for this research. I take this opportunity to formally thank Steve for his invaluable guidance, thoughtful suggestions and continuing patience throughout my research.

I also would like to express my gratitude to many people who encouraged and advised me throughout this research: Ross Turnbull, Bhaskar Choubey, Mike Ward, Carl Anthony, Xueyong Wei, David Lowe, Rita Gupta, Anthony Cooper, Grahame Faulkner, Jingjing Liu, Danial Chitnis, Dipayan Das and other colleagues and friends. I am very grateful to my fellow colleagues Ross and Bhaskar. Many helpful discussions with them have been a source of inspiration and certainly improved the quality of my research. In many ways I have learnt much from them during my time at Oxford.

Furthermore, I kindly acknowledge China Scholarship Council (CSC) for the generous financial support of my DPhil and the Engineering and Physical Science Research Council for the grant of this research project. I also would like to thank the Department of Engineering Science and St Anne's College for the support of travel funds to attend conferences.

Most importantly, I express my love and gratefulness to my parents and my fiancé Yaokun Dong for their constant support and encouragement throughout my research even though this meant not having me around. To all of them I cannot thank you enough.

Publications

- C. Deng and S. Collins. The transient response of a Duffing resonator following a parameter change. *52nd IEEE International Midwest Symposium on Circuits and Systems*, 2009.

- C. Deng and S. Collins. Sensitivity enhancement using a nonlinear resonator. *2010 IEEE Asia Pacific Conference on Circuits and Systems (APCCAS)*, 2010.

- C. Deng, R. Turnbull, C. Anthony, M. Ward and S. Collins. A non-linear resonator for sensing applications. *Proc. Eurosensors XXIV*, 2010.

- C. Deng, R. Turnbull, C. Anthony, M. Ward and S. Collins. Effect of phase-shifts in force feedback loops on Q-enhanced MEMS resonators. *IET Science, Measurement & Technology*, 2011. (submitted)

Contents

List of Figures

List of Tables

Chapter 1

MEMS/NEMS resonator for sensing

1.1 Introduction

Micro/nanoelectromechanical systems (MEMS/NEMS) are of great interest because of the low cost, compact size, low power consumption and feasibility of integration with IC technology [1]. These features have driven a variety of MEMS/NEMS applications into the commercial market such as ink jet printer head, mirror devices and sensors [2]. With the rapid development of miniaturization technology, it is possible to manufacture MEMS/NEMS devices with smaller masses and higher frequencies. In particular the small mass of the micro/nanomechanical resonator means that it can be sensitive to the absorption of an even smaller additional mass onto its surface if it is coated with a specific receptive layer [3]. In this chapter, a brief review of MEMS/NEMS resonant sensors, mass sensor in particular, will be discussed. The system responses of linear resonator and Duffing resonator will be introduced in the following sections.

1.2 Brief overview of MEMS/NEMS resonant sensors

For a micro/nanomechanical resonator, a change in mass of the resonator causes a change in the resonant frequency. Change to the resonant frequency of a resonator, with a functionalised surface, has been used as a method of detecting exposure to chemical or biological substances [3–6]. By monitoring the resonant frequency change, various studies have demonstrated mass sensors based on MEMS [3, 7–10] or NEMS [11–17].

Most MEMS/NEMS mass sensors have been driven with a conservative driving force to ensure that the resonator is operated in the linear region. The sensitivity of the linear resonator for mass sensing is closely related to the Q value (quality factor) of the resonator and many ultra-sensitive mass sensors have been implemented with a extremely high natural Q by placing the resonator in a deep vacuum environment [13, 16, 17]. However, this is not convenient, especially for environmental sensing. When operated at atmospheric pressure for sensing applications, micromechanical systems are likely to have low Q values because of the high damping effects due to the surrounding environment, particularly the interaction with air. Consequently, it is desirable to enhance the Q value, and therefore increase the sensitivity, of the sensor. Force feedback that is proportional to the velocity of resonator have been employed to cancel part of the damping term [5, 18–23]. Merz, Tamayo, and with their respective collaborators, have used displacement detection to generate the required velocity signal which is then added to the primary drive. For this technique, extra electronics are required to convert the displacement signal to a signal proportional to velocity [5, 18–20]. With the same aim of generating a feedback voltage that is proportional to the velocity, Nguyen and Turnbull have both measured the velocity of the resonator directly with a comb structure, which is a simple and convenient method of obtaining the required feedback signal [21–23]. The resulting effective high Q value leads to a rise in the sensitivity of the linear resonator [5, 20, 23].

There has also been growing interest in investigating the non-linear behaviour of MEMS/NEMS resonators [24–27], including research on mass sensing using non-linear behaviours. The investigations of the non-linear behaviours for mass sensing can be divided into two categories that use different driving methods: parametric excitation and direct excitation. For systems with parametric excitation one of the parameters of the system is time-varying. One important characteristic of these systems is that they either remain stationary or oscillate with a high amplitude depending upon the parameters in the equation of the motion. There is a rapid transition between these two behaviours as either the frequency or the amplitude of the parameter variation is changed [28]. Tracking this boundary of stability in the parameter space has been used in applications including non-contact atomic force microscopy [29], microgyroscopes [30] and mass sensing [31, 32]. For mass sensing applications, the position of the sharp boundary between two states is monitored to detect any change in mass, because the position of the transition boundary depends upon the parameters of the equation, including the mass of the oscillator [33]. Mass sensing based on parametric resonance has been shown to be two orders of magnitude more sensitive than the equivalent linear micro-resonator [34].

A similar concept has been explored by Younis, who utilised the escape-from-a-potential-well and jump phenomena in electrostatically-actuated resonator for mass sensing. When parallel plate electrostatic force is beyond a certain value, there is a band of frequencies in which the microbeam cannot have a steady state response [35] and within this band of frequencies the microbeam is pulled in after it escapes from the potential well of the electrostatic force. Since the position of this pull-in band is related to the value of the mass, if the driving frequency is well chosen a dramatic amplitude change from a stable state towards escape phenomenon can be used for mass detection. This method is applicable when it is not necessary to quantify the change in mass. In addition, Younis claims that the jump in amplitude response near a bifurcation point can be used to quantify the mass change but the sensitivity requires further investigation [35].

The other type of excitation method used to investigate the non-linear behaviour of resonators is direct drive. Within this category the most common nonlinearity is a restoring force that is proportional to the cube of displacement which converts a simple harmonic resonator to a Duffing resonator. Duffing behaviour in micro/nano mechanical resonators has been exploited for sensing [36–41], electromechanical signal processing [42,43], signal amplification and noise squeezing [44,45]. For mass sensing, Dai studied the possible application of carbon nanotubes (CNT) resonators to mass detection using a continuum elastic model. These numerical studies show that the Duffing-like nonlinear behaviour of the CNT may improve the detection sensitivity. However, unlike the linear resonators this method has not been confirmed experimentally [36].

In another widely cited theoretical paper, Buks predicted that a nanomechanical resonator in its non-linear region acts as a phase-sensitive mechanical amplifier. The performance of the nanomechanical resonator when it is driven into a non-linear regime has been studied and an increase in mass sensitivity compared with the behaviour in the linear regime has been predicted. More importantly, Buks also claims that the sensitivity increase, achieved by driving the resonator at a critical frequency which forms one edge of a bistability region, is accompanied by a dramatic reduction in the speed of response of the resonator to any change in mass [37]. However, the important conclusion that increased sensitivity is associated with a delayed response of the non-linear resonator has not been confirmed experimentally.

From the above review of previous work, it is clear that there have been several reports of the use of non-linear behaviours to increase the mass sensitivity of MEMS/NEMS resonators. However, the only paper to deal with the potentially equally important speed of response of the resonator is a theoretical study that predicts very slow responses. The motivation of this thesis is to investigate the sensitivity of Duffing-like non-linear resonators and their temporal responses. Before the transient response is discussed, the steady state responses of the linear and the Duffing resonators before and after the parameter change will be introduced in following sections.

1.3 Linear resonator

A linear micromechanical resonator can be modelled as a simple spring-mass-damper system. Assuming a linear damping term proportional to velocity, the displacement x responding to the driving force F at an angular frequency ω is represented by

$$m\ddot{x} + c\dot{x} + kx = Fe^{j\omega t} \tag{1.1}$$

where m is the effective mass of the resonator, c is the damping constant and k is the spring constant. Dividing both sides of Equation 1.1 by the effective mass gives the motion for the micromechanical resonator:

$$\ddot{x} + \frac{\omega_0}{Q}\dot{x} + \omega_0^2 x = F_d e^{j\omega t} \tag{1.2}$$

with resonant frequency $\omega_0 = \sqrt{\frac{k}{m}}$, quality factor $Q = \frac{m\omega_0}{c}$ and normalized driving force $F_d = \frac{F}{m}$. The resonant frequency would change because of the mass change or the change in the spring constant of the resonator. Assuming the displacement takes the form $x = Xe^{j\omega t}$, the transfer function of linear system is given by

$$G(j\omega) = \frac{X}{F_d} = \frac{1}{\omega_0^2 - \omega^2 + \frac{j\omega\omega_0}{Q}} \tag{1.3}$$

which has magnitude and phase :

$$|G| = \frac{1}{\sqrt{(\omega_0^2 - \omega^2)^2 + (\frac{\omega\omega_0}{Q})^2}} \tag{1.4}$$

$$\angle G = -arctan(\frac{\alpha}{Q(1-\alpha^2)}) \tag{1.5}$$

where $\alpha = \frac{\omega}{\omega_0}$ is defined as the frequency ratio. A change in mass Δm changes the equation of the motion to:

$$\ddot{x} + (\frac{c}{m+\Delta m})\dot{x} + (\frac{k}{m+\Delta m})x = (\frac{F}{m+\Delta m})e^{j\omega t} = F_n e^{j\omega t} \tag{1.6}$$

Assuming that the mass change Δm is small relative to the mass m, hence

$$\frac{\Delta\omega_0}{\omega_0} = -\frac{\Delta m}{2m} \tag{1.7}$$

Equation 1.7 shows that to a first approximation the percentage change in resonant frequency is half of that in mass change. Amplitude and phase responses before and after the increase in mass are compared in Figure 1.1. As expected, a 1% increase in mass leads to a decrease in the resonant frequency. In addition, the peak amplitude response after the mass change also rises slightly. Similarly, a decrease in spring constant k can also reduce the resonant frequency. If the spring constant k is decreased by Δk which is small compared with k, the relationship between the resonant frequency and spring constant can be approximated by:

$$\frac{\Delta\omega_0}{\omega_0} = \frac{\Delta k}{2k} \tag{1.8}$$

Although the mass change also modifies other parameters in the equation of the motion, the simulated results in Figure 1.1 show that the 1% increase in mass and 1% decrease in spring constant have the same amplitude and phase response with the same amount of decrease in the resonant frequency. Consequently, the investigation of a mass sensor can be performed by changing the spring constant because both of them requires an effective method to detect the resonant frequency with good sensitivity. For the micromechanical resonator fabricated for this research project, the spring constant of the resonator can be effectively changed by a DC voltage. This meant that it is easier to change the effective spring constant reproducibly than changing the mass of the resonator and this technique will be further discussed in Section 4.4.3.

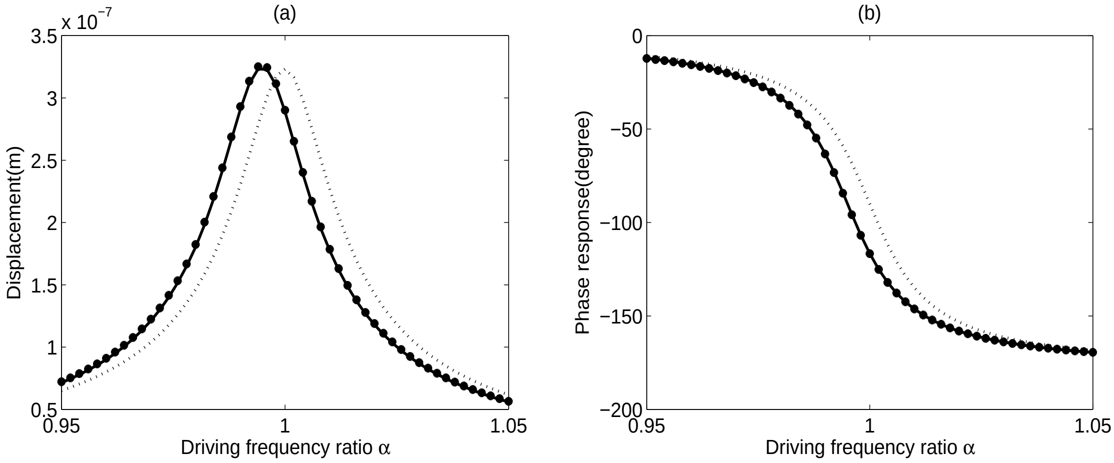

Figure 1.1: Amplitude(a)and phase(b) response of linear resonator before any changes (dotted line) and the responses with mass increases for 1% (solid line) or spring constant decrease for 1% (stars).

Changes in resonant frequency can be detected by monitoring the resulting change in either the amplitude or phase response at a particular frequency and the sensitivity of the sensor will be proportional to the rate of change of amplitude or phase with resonant frequency. This rate of change is closely related to the Q value (quality factor). Q value equals to the ratio of the centre frequency to the bandwidth and describes the sharpness of the systems response as shown in Figure 1.2(a). The comparison of amplitude responses with various Q values shows that the response is quite flat and broad for a low Q system while a narrow response and clear peak can be seen for a high Q value. In addition, Figure 1.2(a) shows that the high-Q system resonates with a greater amplitude than system with a lower Q at the resonant frequency.

The maximum amplitude A_m from Equation 1.4 is seen at a frequency ω_m near the resonant

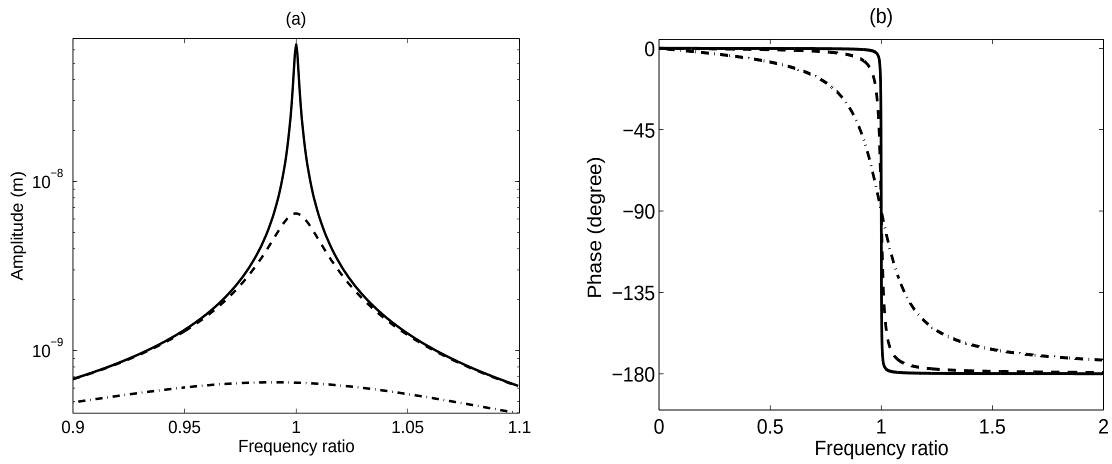

Figure 1.2: Amplitude (a) and phase (b) responses against the normalized frequency ratio α at different Q values (dash-dot:Q=5;dashed:Q=50;solid:Q=500).

frequency defined by [46]:

$$\omega_m = \omega_0\sqrt{1-\frac{1}{2Q^2}} \tag{1.9}$$

$$A_m = (\frac{F}{k})\frac{Q}{\sqrt{1-\frac{1}{4Q^2}}} \tag{1.10}$$

This indicates that monitoring the frequency of peak amplitude to identify a mass change is not desirable, because changes in Q value also shift the frequency of maximum amplitude (Equation 1.9) which might give a wrong impression of mass change. More importantly, tracking maximum amplitude means that the peak value in the magnitude corresponds to the minimum change rate. This is not desirable in term of detection resolution.

There is even a combination of circumstances that mean that some changes cannot be detected because the mass increase will cause the peaks shift to lower frequency (Equation 1.9) as well as an increase in amplitude (Equation 1.10). This means that in some circumstances the amplitude of the response at the original resonant frequency does not change even though the mass increases. Figure 1.3 demonstrates this phenomenon for a system with a 10% change in mass while the amplitude at the driving force does not change as shown at the black rectangle in the figure.

An alternative method of determining the resonant frequency is to monitor the phase difference between the force and the response. Equation 1.5 shows that, at resonance, the phase

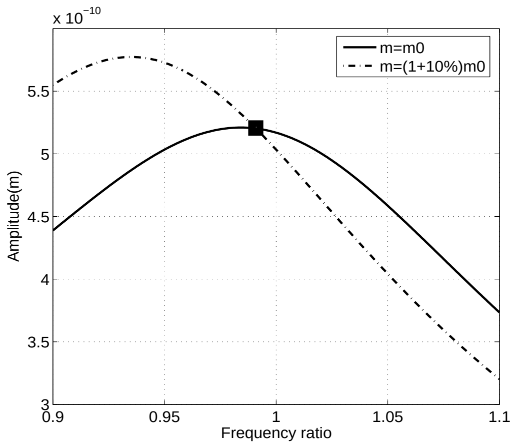

Figure 1.3: Amplitude responses against normalized frequency ratio showing that no change in amplitude corresponding to a 10% mass change.

difference between the excitation signal and the output signal is always -90 degrees and independent of the Q value, while the amplitude response varies with different Q values. Figure 1.2(b) shows that phase responses at different Q values are the same at resonance while the behaviours of phase responses near resonance are determined by the quality factor. Low values of quality factor result in a wide linear region of phase change($\frac{\mathrm{d}\phi}{\mathrm{d}\omega_0}$) around the resonant frequency, whereas at high Q values the phase changes very quickly and rapidly saturates at zero or -180 degrees. From Equation 1.5 the phase response at resonance with respect to the resonant frequency change or driving frequency change are approximated by

$$\frac{\mathrm{d}\phi}{\mathrm{d}\omega}|_{\omega=\omega_0} = -\frac{2Q}{\omega_0} \tag{1.11}$$

$$\frac{\mathrm{d}\phi}{\mathrm{d}\omega_0}|_{\omega=\omega_0} = \frac{2Q}{\omega_0} \tag{1.12}$$

The comparison of Equation 1.11 and Equation 1.12 shows that when the resonator is driven at resonance, the amount of phase change caused by changes in resonant frequency or driving frequency is the same but with opposite sign which means resonant frequency change can be quantified using Equation 1.11. As shown in the Figure 1.2(b), when the Q value increases, $\frac{\mathrm{d}\phi}{\mathrm{d}\omega_0}$ is approaching infinity. Consequently in order to maximize the detection resolution high quality factor is desired. Combining Equation 1.7 and Equation 1.12, the phase change is related to the mass change by

$$\frac{\Delta m}{m} = \frac{\Delta \phi}{Q} \tag{1.13}$$

There are a number of benefits offering by monitoring the phase between displacement and driving force as opposed to amplitude. Firstly, at resonance the phase response changes at a maximum rate while the amplitude response is at the minimum change rate around peak value. Secondly, note that the value of phase response at resonance is constant (-$\pi/2$) and is independent of quality factor. Furthermore, since the only effect of a change in resonant frequency is a shift along the frequency axis, the phase always changes as shown in Figure 1.1(b).

Equation 1.13 shows that one of the key factors that will determine the performance of any of these MEMS resonator based sensors is the Q value of the resonator and high Q will be desirable. Unfortunately, it is very difficult to achieve a high Q in air, when viscous drag is the dominant damping mechanism. As a result there is an interest to enhance the Q value to improve the sensitivity of the sensor. Since viscous damping is dependent upon the velocity of the resonator, this damping can be partially cancelled using a feedback force, $F_{FB}(j\omega)$, that is proportional to the velocity of the resonator [23, 47]. Then the governing equation of the linear resonator becomes:

$$\ddot{x} + \frac{\omega_0}{Q}\dot{x} + \omega_0^2 x = F_d e^{j\omega t} + \lambda\frac{\omega_0}{Q}\dot{x} = F_D(j\omega) + F_{FB}(j\omega) \tag{1.14}$$

where λ is defined as the feedback fraction which determines the amount of damping force to be cancelled. The transfer function is then modified:

$$\hat{G}(j\omega t) = \frac{X}{F_D + F_{FB}} = \frac{1}{\omega_0^2 - \omega^2 + \frac{j\omega\omega_0(1-\lambda)}{Q}} = \frac{1}{\omega_0^2 - \omega^2 + \frac{j\omega\omega_0}{Q_{eff}}} \tag{1.15}$$

where the effective quality factor is defined as:

$$Q_{eff} = \frac{Q}{1-\lambda} \tag{1.16}$$

In order to achieve a high effective Q value, the feedback fraction λ is required to approach unity. However, in practice it is quite difficult to control the λ to ensure that it will not cause positive feedback when the feedback fraction approaches unity. To prevent the resonator from self-oscillation, the effective Q value is limited by the resolution of the feedback gain control. Therefore, the sensitivity of the Q-enhanced resonator in the linear region is restricted as well.

1.4 Duffing resonator

To increase the accuracy with which the resonant frequency can be detected, large rate of phase change with respect to frequency is required. The Duffing resonator has two sharp phase changes at two frequencies which means that the rate of change of phase can in theory approach infinity without increasing the Q value. This makes Duffing resonators attractive as a resonant frequency sensor. The motion of the Duffing resonator can be described by Equation 1.17 which has a cubic non-linear restoring force.

$$\ddot{x} + \frac{\omega_0}{Q}\dot{x} + \omega_0^2 x + \gamma x^3 = F_d \cos \omega t \tag{1.17}$$

If the non-linear parameter γ is positive then the spring constant is stiffer and the amplitude curve bends towards the larger frequency which is called hardening Duffing resonator. It can also be negative which makes resonator softer and reduce the frequency where maximum amplitude occurs which is called softening Duffing resonator. In this chapter, all the analysis will be based on the hardening resonator as an example and the softening resonator has similar behaviour.

The only difference between a linear resonator (Equation 1.2) and a Duffing resonator (Equation 1.17) is the non-linear part γx^3. When the driving force is sufficiently small, the amplitude of x is also small, so that the non-linear restoring force is much smaller than the linear restoring force $\omega_0^2 x$. The amplitude response of the Duffing resonator is the same as the linear resonator represented by a symmetrical curve (Figure 1.4 (a) stars and solid line). As the driving force increases, the curve changes its shape to become asymmetrical. At this stage, only one value of amplitude corresponds to every frequency (Figure 1.4(a) dashed line). When the driving force reaches a critical value, however, the nature of the curve changes. There is a

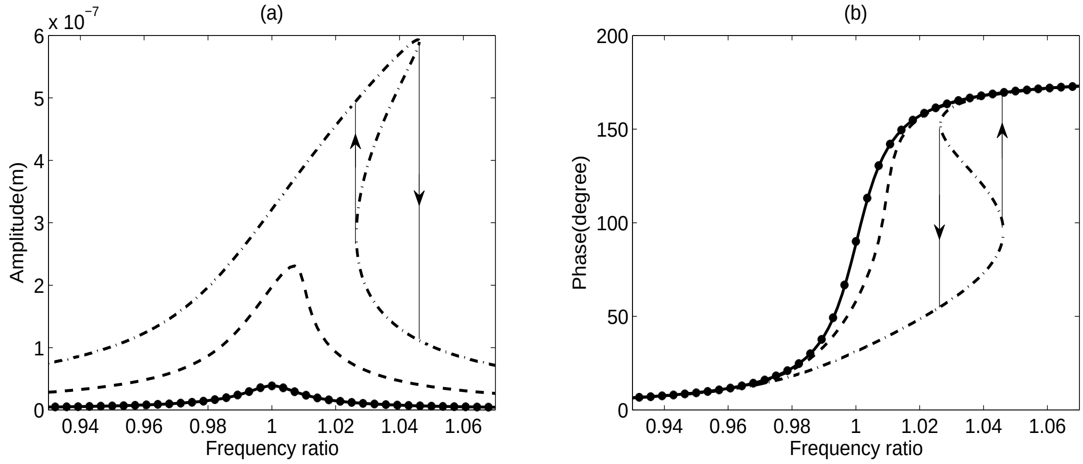

Figure 1.4: Amplitude(a) and phase(b) response of different driving force in Duffing resonator (solid:$F_d = 5N/kg$; dashed:$F_d = 30N/kg$; dash-dot:$F_d = 80N/kg$) compared with a linear resonator(dots:$F_d = 5N/kg$).

range of frequencies which have more than one amplitude response value (Figure 1.4(a) dash-dot line). The two ends of this line are two jump frequencies which determine the frequency range over which multiple amplitudes exist. If the non-linearity is weak then the solution will be very similar to that of the linear system. The solution for a damped Duffing system can be assumed to be the same as the linear resonator as a first approximation [48]:

$$x = A\cos(\omega t + \psi) \tag{1.18}$$

where there is a phase difference ψ between the applied force and response. Usually, the applied force is prescribed first and then the phase of the solution is determined. However, in this case, it is more convenient to fix the phase of the solution in form of $x = A\cos\omega t$ and keep the applied force as a quantity to be determined. As a result, the Duffing Equation 1.17 is converted to:

$$\ddot{x} + \frac{\omega_0}{Q}\dot{x} + \omega_0^2 x + \gamma x^3 = F_d\cos(\omega t + \phi) = A_1\cos\omega t - A_2\sin\omega t \tag{1.19}$$

where the amplitude $F_d = (A_1^2 + A_2^2)^{\frac{1}{2}}$ of the applied force is considered fixed, but the amplitude ratio $\tan\phi = \frac{A_2}{A_1}$ is to be determined.

By substituting $x = A\cos\omega t$ into Equation 1.19 and making use of the following equation:

$$\cos^3\omega t = \frac{3}{4}\cos\omega t + \frac{1}{4}\cos 3\omega t \tag{1.20}$$

Equation 1.19 leads to:

$$(-A\omega^2 + A\omega_0^2 + \frac{3}{4}\gamma A^3)\cos\omega t - \frac{\omega_0}{Q}A\omega\sin\omega t + \frac{1}{4}A^3\frac{\omega_0}{Q}\cos 3\omega t = A_1\cos\omega t - A_2\sin\omega t \tag{1.21}$$

Since the third harmonic is much smaller than the first harmonic, the term involving $\cos 3\omega t$ can be disregarded as an approximation. Equating the coefficients of $\cos\omega t$ and $\sin\omega t$ on both sides of Equation 1.21 yields:

$$-A\omega^2 + A\omega_0^2 + \frac{3}{4}\gamma A^3 = A_1 \tag{1.22}$$

$$\frac{\omega_0\omega}{Q}A = A_2 \tag{1.23}$$

The relationship between the amplitude of the applied force and the quantities A and ω can be obtained by squaring and adding the Equation 1.22 and Equation 1.23

$$(-A\omega^2 + A\omega_0^2 + \frac{3}{4}\gamma A^3)^2 + (\frac{\omega_0}{Q}A\omega)^2 = A_1^2 + A_2^2 = F_d^2 \tag{1.24}$$

and the amplitude ratio gives the expression of phase response

$$\tan\phi = \frac{A_2}{A_1} = \frac{\frac{\omega_0\omega}{Q}}{\omega_0^2 - \omega^2 + \frac{3}{4}\gamma A^2} \tag{1.25}$$

The Equation 1.24 could be converted to a cubic function of A^2 [49]

$$(\frac{3}{4}\gamma)^2(A^2)^3 + \frac{3\gamma}{2}(\omega_0^2 - \omega^2)(A^2)^2 + [(\omega_0^2 - \omega^2)^2 + (\frac{\omega_0}{Q})^2\omega^2]A^2 = F_d^2 \tag{1.26}$$

The cubic equation $x^3 + ax^2 + bx + c = 0$ can be reduced to $y^3 + py + q = 0$, in which $p = -\frac{a^2}{3} + b$; $q = 2(\frac{a}{3})^3 - \frac{ab}{3} + c$ by the substitution $x = y - \frac{a}{3}$. The discriminant of the cubic equation is $D = \frac{q^2}{4} + \frac{p^3}{27}$, which is a function of the driving frequency and driving force, and if one of them is fixed the other one determines the number of the solutions as well as the type of them.

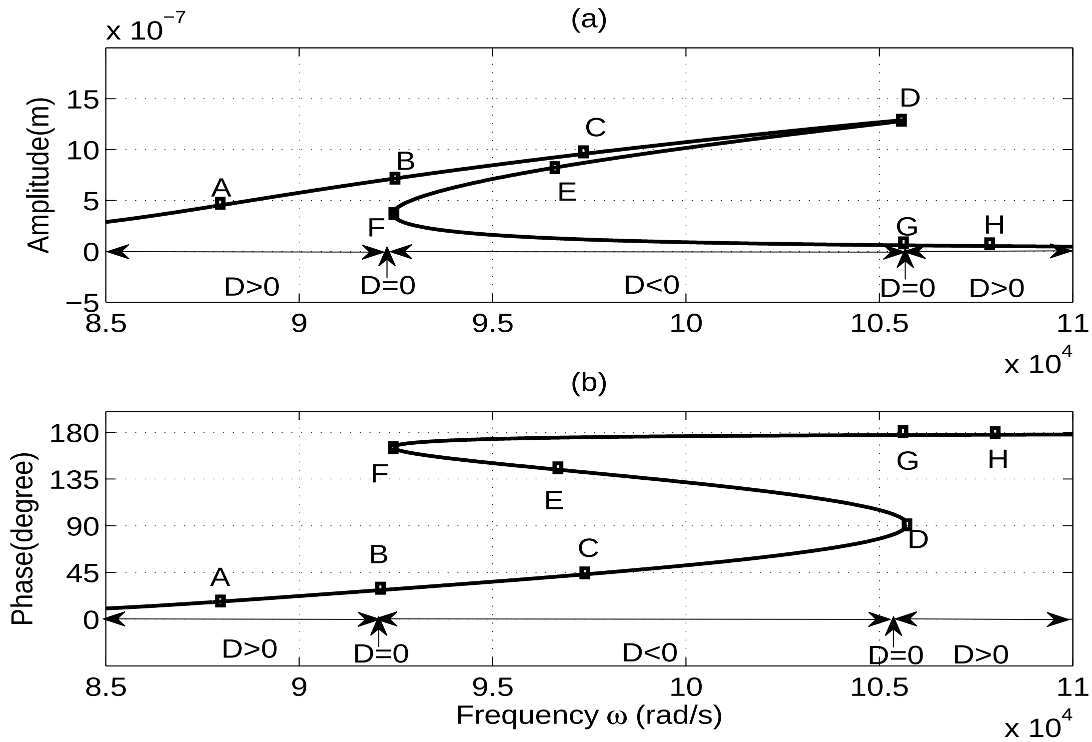

Figure 1.5: Amplitude (a) and phase (b) response of a Duffing resonator with fixed driving force $F_d = 200N/kg(f_0 = 14kHz, Q = 60, \gamma = 2.7 \times 10^{21}N/(kg \cdot m^3))$.

If $D > 0$, one root is real and two are complex conjugates; If $D = 0$, all roots are real and two are equal; If $D < 0$, all roots are real and different. The roots for the cubic equation are the square of amplitude and the amplitude response must be real, so the roots of the cubic equation should be real and positive. So when $D > 0$ there is one root but when $D < 0$ there are three roots for the same frequency. The jump points for the Duffing resonator are where $D = 0$. Figure 1.5 shows the simulated results by solving the cubic equation 1.26 and Equation 1.25. The value of resonant frequency used in the simulation is the designed value for micro-mechanical resonator.

In Figure 1.5(a), the region $D < 0$ has three real roots at the same frequency among which two solutions are stable and the other one is unstable [50]. The portions ABCD and FGH of the response curve correspond to amplitudes of stable resonance while the segment DEF corresponds to the unstable ones. As the driving frequency ω is increased from a very low value, the amplitude response increases along the curve ABCD, and a further increase in ω

causes a jump in amplitude to point G and a decrease of amplitude along the curve GH. If the starting point is point H corresponding to a large value of ω, as ω decreases, the amplitude response increases until point F is reached. The amplitude then jumps to the point B, where if ω is further decreased, the amplitude decrease along BA. This system therefore exhibits hysteresis due to the existence of multi-amplitude [51].

Figure 1.5 (b) shows the behaviour of the phase ϕ as a function of ω . The points marked by letters correspond to the same points in the Figure 1.5 (a). Notice that the rate of change of phase at point D is almost infinite as there is a discontinuity in phase response. The Duffing resonator therefore has the same $\frac{\Delta\phi}{\Delta\omega}$ as a linear system with an infinite Q value at resonance. If the displacement of the resonator is not too large the cubic equation can be utilized to determine two jump frequencies.

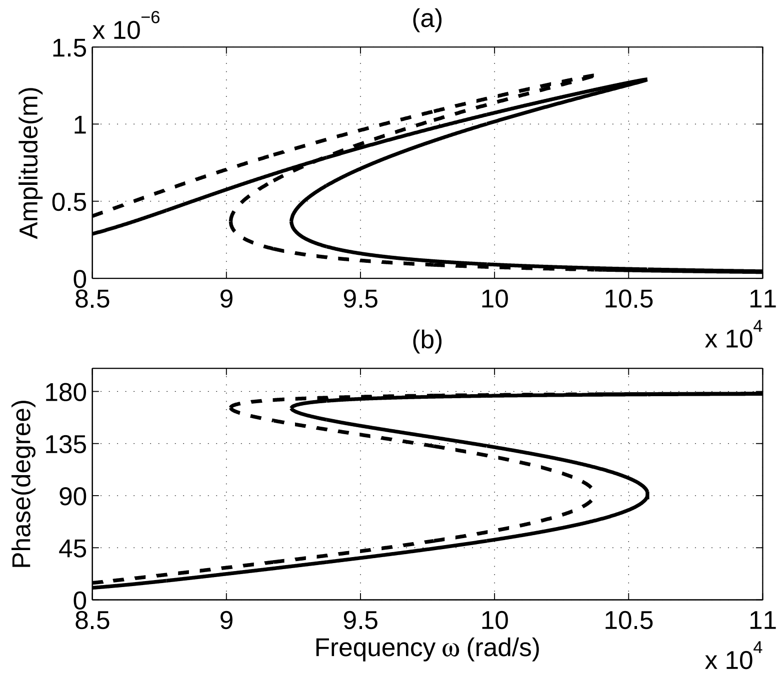

Figure 1.6: Amplitude(a) and phase(b) response of a Duffing resonator when the mass changes for 5%(dotted line).

When the driving force is small enough, the Duffing resonator can be considered as a linear system (Figure 1.4). When the mass increases, the amplitude and phase response of the linear resonator will shift towards smaller frequency (Equation 1.7) and similar behaviour of the Duffing resonator is expected. Figure 1.6 shows the expected shifts for both amplitude and phase response. Consequently, an increase in mass of the resonator can be detected by driving it at the higher jump frequency. In this case, when the mass changes, the amplitude is expected to drop dramatically at the same driving frequency. Unlike the linear system, the amplitude response following a mass change for the Duffing resonator can therefore be used to detect a change in mass. Similarly, the phase response in Figure 1.6(b) shows that at this same frequency $\frac{\mathrm{d}\phi}{\mathrm{d}\omega}$ is infinite. This suggests that both amplitude and phase response at the jump frequency can be used for detecting the mass change for the Duffing resonator.

1.5 Summary

The small size of MEMS/NEMS resonators make them attractive as mass sensors and any mass change is usually detected using a change to the resonant frequency. In this Chapter, the analysis of linear harmonic resonator shows that it is desirable to monitor the phase response instead of amplitude response to detect a change in resonant frequency. To increase the sensitivity at resonance, velocity feedback has been shown to cancel part of linear damping and therefore increase the effective Q value.

However, the control of the feedback gain to achieve the high effective Q value that is required whilst ensuring that the resonator does not become an oscillator is very difficult. Studies of the steady state response of a Duffing resonator suggest that its phase response will be more sensitive to changes in resonant frequency when the resonator is in its non-linear mode than it is when it is operated in its linear mode with the same Q value. If the Duffing resonator is excited by a sufficiently large driving force, there are two frequencies where both the amplitude and phase responses are discontinuous. This means that the rate of change of amplitude and phase with respect to the driving frequency can be considered to approach infinity. This makes the Duffing resonator a promising sensor with high sensitivity.

1.6 Thesis overview

This thesis will investigate the exploitation of Duffing-like nonlinearities to enhance the sensitivity of micromechanical resonators. In addition, the transient behaviour of these resonators following a parameter change will also be investigated experimentally.

In Chapter 2 simulation results for a model of a MEMS Duffing resonator are presented that show an unexpected delay in the response of a resonator to a change in its mass. The possible reason of this undesirable behaviour is discussed and a solution to avoid this problem is also proposed. This solution is based upon driving the resonator at a particular frequency and force that have to be calculated from the resonator's parameters. Hence a parameter extraction procedure is presented with simulation results. To confirm the unexpected long transient response, a circuit whose response is described by the Duffing equation is investigated in Chapter 3. The Duffing circuit will be characterised before measuring the response following a parameter change which is equivalent to a change in mass of the micromechanical resonator. Responses following the ”mass” changes under different driving conditions will be compared.

Chapter 4 describes a micromechanical resonator with a low native Q in air and the actuation and measurement electronics for this resonator. A velocity feedback system has been used to partially cancel damping and therefore increase the effective Q value of the resonator. The sensitivity of the linear resonator with Q-enhancement will be discussed when the displacement response is small and the corresponding model of this velocity feedback system will be characterised. This is followed in Chapter 5 by the analysis of an unexpected Duffing-like nonlinearity that occurred when the resonator was driven to increase its maximum displacement. A model describing the motion of the Q-enhanced resonator showing non-linear behaviour will be developed and experimental results will compare the sensitivity and dynamic range of the different driving voltage levels.

An alternative method of creating the Duffing non-linearity without increasing the amplitude of the resonator is presented in Chapter 6. This will be implemented by generating a displacement cubed term to add to the primary drive. The model of this feedback method will be characterised and the response of different feedback gains will be discussed. Finally, Chapter 7 contains the conclusion remarks and some possible areas of future work.

Chapter 2

Transient response of the Duffing resonator following a mass change

2.1 Introduction

The analysis in Section 1.4 shows that Duffing resonator has the potential to detect small mass change with large amplitude and phase jumps. This suggests that the Duffing resonator can be implemented as a mass sensor with great sensitivity. As a mass sensor, another crucial characteristic is the transient response time which means that the sensor should be able to respond to the mass change in a reasonable time reliably. Buks has suggested the response time for detection will approach infinity when the resonator is operated near the jump frequency, but this does not seem to have been investigated experimentally before [37]. In this chapter, the transient response of the Duffing resonator following the mass change will be simulated and investigated.

2.2 Transient response of the Duffing resonator

For the Duffing resonator whose response is shown in Figure 1.5 and Figure 1.6, the higher jump frequency is estimated to be $\omega = 105716\ rad/s$ by solving the cubic Equation 1.26. To simulate the transient response at this frequency, Equation 1.17 was solved using the MATLAB $ode45$ solver. The initial condition for the simulation is essential because if the resonator is driven from rest the response will be the stable response with lower amplitude as shown in Figure 1.5. Consequently, the initial condition of the simulation for the high jump point is chosen to be similar to the displacement and velocity of its higher branch of the steady states. The displacement x and velocity v of the movement at a driving frequency ω can be described by:

$$x = A\cos(\omega t - \phi) \tag{2.1}$$

$$v = \dot{x} = -A\omega\sin(\omega t - \phi) \tag{2.2}$$

where the amplitude A and the phase ϕ of the displacement at the high jump point are obtained from the jump point D in Figure 1.5 of $A = 1.291 \times 10^{-6}m$ and $\phi = 90°$ with a normalised driving force $F_d = 200N/kg$. From Equation 2.1 and Equation 2.2, the initial conditions can therefore be obtained and in particular if $x_0 = 0$ then $v_0 = 0.136m/s$. The simulation with these initial conditions at the frequency $\omega = 105716\ rad/s$ shows a high stable amplitude response. When the mass is increased by 1% a large decrease in the amplitude response is expected. However, a slight increase in amplitude is observed in the simulated results.

From the analysis in Section 1.4, the cubic equation has been obtained by disregarding the higher order harmonics and is only valid when the non-linear restoring force is much smaller than the linear one. The ratio between these two forces in Figure 1.5 at the peak amplitude is approximately 0.8 which is too large. Consequently, the algebraic solution of the higher jump point obtained from the cubic equation is an approximation. The reason for the slight increase in amplitude following the mass change is probably that the calculated higher jump frequency is actually slightly lower than the actual higher jump frequency and that the mass change is not sufficient to lead to amplitude collapse. If this hypothesis is true, then an amplitude jump is expected when a larger mass change occurs. This has been observed in Figure 2.1 which shows the amplitude response before and after mass increases by 3% at $t = 0.1s$ with all other conditions unchanged.

Figure 2.1 confirms the reason for the unexpected response to a mass change of 1% is the errors in predicting the higher jump frequency using the cubic equation, and therefore a better estimate of the higher jump frequency needs to be obtained. The process of obtaining

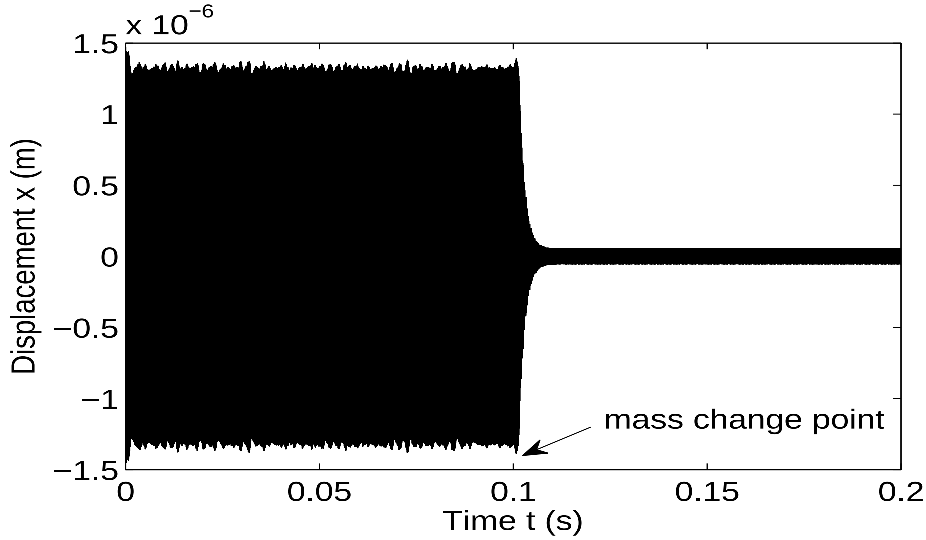

Figure 2.1: Transient behaviour when mass changes by 3% at $t = 0.1s$ with $F_d = 200N/kg$.

this better estimate starts with simulating the amplitude response with respect to time at the estimated jump frequency $\omega = 105716rad/s$ with the initial conditions that can lead to a high stable state using MATLAB $ode45$ solver. Then the last displacement and velocity within the simulated window will be used as the initial condition for the next simulation with a small increase in driving frequency. In this way, the driving frequency of the simulation will be gradually increased by a pre-determined step each time and for each driving frequency, the initial conditions are the solutions of displacement and velocity of the previous stage. This simulates the process of sweeping the driving frequency continuously along the high amplitude stable state. As the rise of the driving frequency, it becomes increasingly difficult to remain in the high stable state which requires a smaller frequency increment each time.

After gradually increasing the driving frequency, the higher jump point for the same Duffing system was found to be $\omega = 107500rad/s$, rather than the original estimate of $\omega = 105716rad/s$ which was calculated from the cubic equation. Repeating the simulation with a mass change for 1%, the transient response is shown in Figure 2.2. Now a 1% mass change can cause a collapse in amplitude.

Although the driving frequency is a better approximation to the jump frequency than in the previous calculation, the response time of the resonator still depends upon the time during an oscillation at which the mass change occurs. To compare the transient behaviours when mass change occurs at different times of an oscillation cycle, Table 2.2 shows the response time

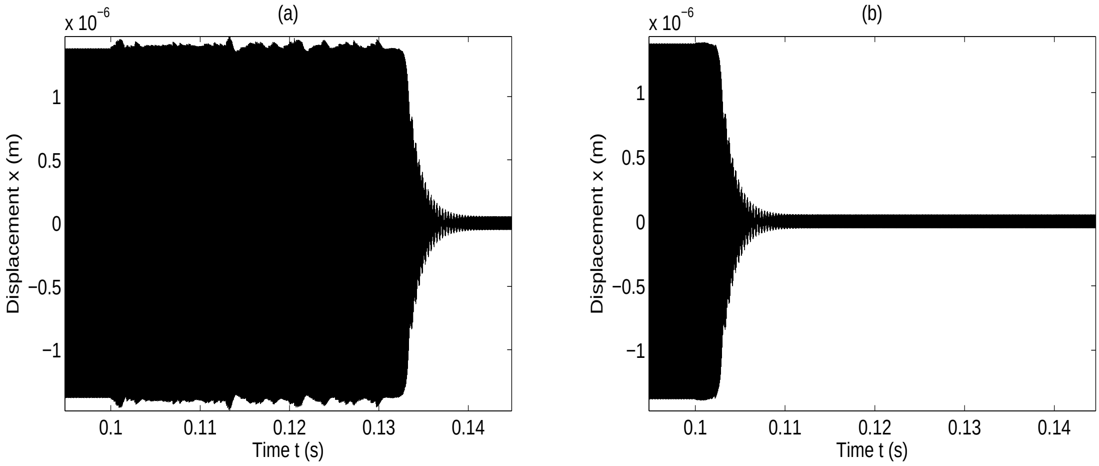

Figure 2.2: Transient behaviours with more accurate driving frequency when mass changes 1% at different time in the cycle.

under different conditions. The notations of mass change position correspond to the position in Figure 2.3. The mass change time for the case in Figure 2.2 (a) is point H in the Figure 2.3 while the result in Figure 2.2 (b), which corresponds to point G, shows a much shorter delay.

Table 2.1: Response time for the mass change 1% with different initial positions for the mass change.

Mass change points	A	B	C	D	E	F	G	H
$F_D = 200$	164T	167T	253T	173T	346T	234T	162T	1297T

where $T = \frac{2\pi}{\omega}$ and ω is the jump frequency obtained by creeping up to the high amplitude with the method described previously.

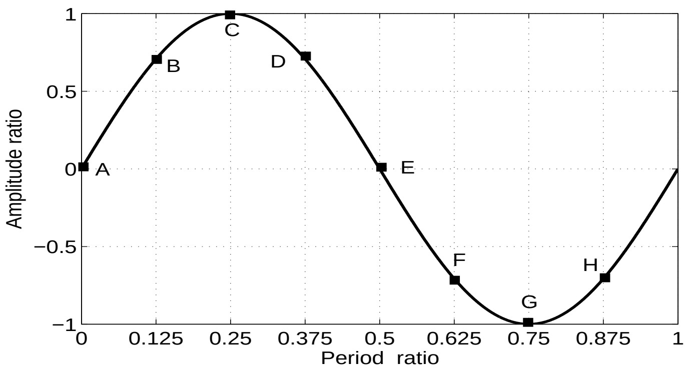

Figure 2.3: Notations for the initial position when the mass change occurs.

The response time of a mass sensor is as important as the sensitivity, so it is essential to make sure the response time is independent of the time when the mass changes. The timing for the mass change determines the initial condition for the new system which has a different mass. In the case of a linear system with positive damping, the steady-state forced response is independent of the initial conditions. However, in non-linear systems the initial condition can play a crucial role. In particular, when there is more than one stable solution the initial condition determines which steady state is physically realized by the system and each of the stable responses has a domain of attraction in the space formed by the initial conditions [52]. When an initial condition falls on the boundary between two domains of attraction small changes in the initial condition can produce a large difference in the system's response.

In the Duffing system, there are a range of driving frequencies with two stable solutions and one unstable solution. This unstable solution is the boundary between the domains of attraction of two stable solutions [53]. All initial conditions in one domain will lead to the corresponding steady state solution following different trajectories. If some of these trajectories remain close to the unstable state before finally ending in the low amplitude stable state then some initial conditions could result in a long transient response. The observed variable transient response of the system may therefore be caused by the existence of an unstable state near to the high amplitude stable state.

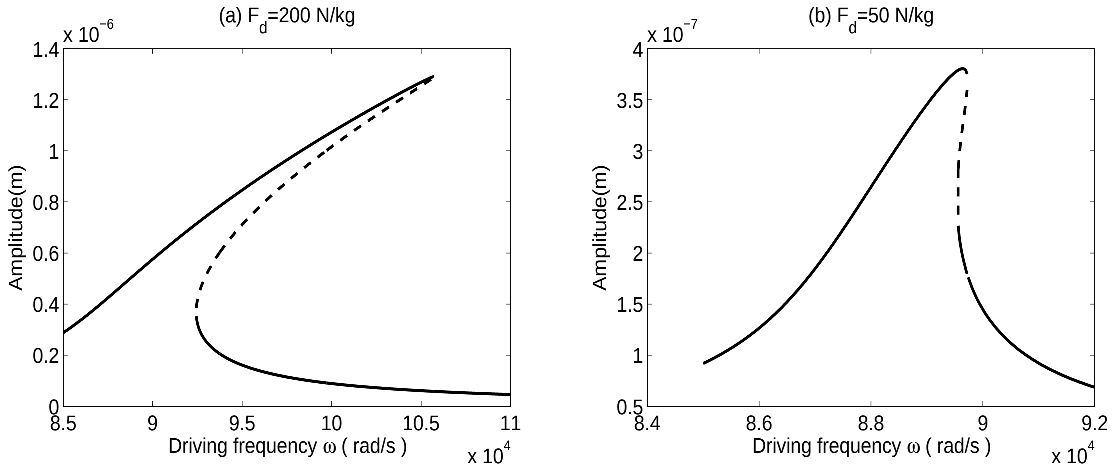

Figure 2.4: Amplitude response of different driving forces (Solid line for the stable solutions; dashed line for the unstable solutions).

To confirm the above hypothesis, the amplitude responses of two different driving forces are compared in Figure 2.4. Figure 2.4 (a) shows that when the resonator is driven with $F_d = 200N/kg$ to create a large hysteresis loop the high amplitude stable solution (solid line) and the unstable solution (dashed line) are very close to each other around the frequency at which the resonator must be driven if its amplitude is to collapse when the resonant frequency changes. This proximity means that just after a small change in mass has occurred the resonator may find itself in the part of phase space that is very close to the unstable solution. The very slow escape of the resonator for this part of the phase space to the region close to the low amplitude stable state may cause the long delays observed in Figure 2.2(a). If this hypothesis is true, then this undesired long transient behaviour can be avoided by driving the system with smaller driving force because the unstable solution is nearly vertical and the stable solution separates quickly from the unstable solution near the jump frequency as shown in Figure 2.4(b). To investigate this possibility the same Duffing system has been simulated but with a smaller driving force $F_d = 50N/kg$. The results obtained showed that a reliable collapse of amplitude occurs when the mass changes at several different times during a cycle. In particular for the times shown in Figure 2.3 the response time is constant at approximately 100 periods and all these cases showed a transient behaviour very similar to that shown in Figure 2.5. Although the initial condition is described by its amplitude and velocity, the analysis of the amplitude response in Figure 2.4 and Figure 2.5 is able to explain the phenomenon of long transient response and propose a practical solution. In addition, another benefit of driving the Duffing resonator weakly is that the analytic approximation used is more accurate and so the solution of the cubic equation is a better approximation to the true jump frequency.

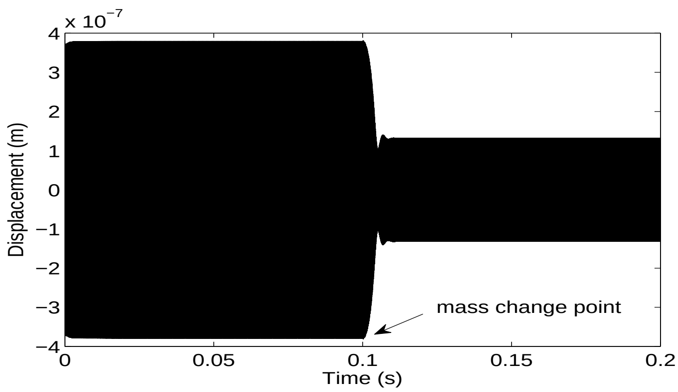

Figure 2.5: Transient behaviours when mass changes for 1% at $t = 0.1s$ with $F_d = 50N/kg$.

A comparison between two cases has clearly demonstrated that it is much more effective and reliable to drive the Duffing system with a weak driving force. It is essential to determine a proper driving force to achieve a weak non-linearity with a very high rate of change of phase at a certain frequency. Figure 1.4 shows there is a critical value of driving force which just creates a non-linear jump. If the driving force is smaller than this critical value, there is only one value of amplitude response at each driving frequency (Figure 1.4 solid and dashed line). If a greater force is applied, there is a region with more than one amplitude response value at each frequency and this is a typical non-linear system (Figure 1.4 dash-dot line).

A method to determine the critical driving force value is required. The relationship between the driving frequency and amplitude response is determined by the cubic Equation 1.26. The range for three roots at one frequency is limited by $\frac{\mathrm{d}A}{\mathrm{d}\omega} = \infty$, and the two ends are the jump points (Points D and F in Figure 1.5 (a)). Differentiating the Equation 1.26 with respect to ω, the equivalent equation to $\frac{\mathrm{d}A}{\mathrm{d}\omega} = \infty$ is as follows:

$$\frac{27}{16}\gamma^2(A^2)^2 + 3\gamma(\omega_0^2 - \omega^2)(A^2) + [(\omega_0^2 - \omega^2)^2 + (\frac{\omega_0}{Q})^2\omega^2] = 0 \tag{2.3}$$

As a result, the jump points are determined by the solutions of Equation 2.3. For a Duffing resonator driven by sufficiently large force, there is a range with three roots coexisting and two jumps frequencies. This means that the quadratic Equation 2.3 with respect to A^2 has two different roots. If there is no range of frequencies in which cubic equation 1.26 has three roots, then there is no real solution to the quadratic equation 2.3. Consequently, when the quadratic equation has only one real root, the only solution is the threshold point which give the critical frequency where the only jump occurs. The critical driving frequency ω_c can be calculated by equating to zero the discriminant for the Equation 2.3.

$$36\gamma^2(\omega_0^2 - \omega^2)^2 - 27\gamma((\frac{\omega_0}{Q})^2\omega^2 + (\omega_0^2 - \omega^2)^2) = 0 \tag{2.4}$$

Thus,

$$\omega_c = \frac{\sqrt{3}\omega_0}{2Q} + \sqrt{\frac{3\omega_0^2}{4Q^2} + \omega_0^2} \tag{2.5}$$

which is determined by the natural frequency and quality factor but this critical frequency is independent of the non-linearity parameter. Applying the binomial theorem and disregarding the small parts gives:

$$\omega_c = \frac{\sqrt{3}\omega_0}{2Q} + \omega_0(1 + \frac{3}{8Q^2}) = \omega_0(1 + \frac{\sqrt{3}}{2Q}) \tag{2.6}$$

The corresponding amplitude is the only root of Equation 2.3 :

$$A_c^2 = x = -\frac{b}{3a} = \frac{8(\omega^2 - \omega_0^2)}{9\gamma} \tag{2.7}$$

Substituting the amplitude A_c and driving frequency ω_c into the cubic Equation 1.26, the critical driving force F_{d_c} is given by:

$$F_{d\_c} = \sqrt{\frac{32\sqrt{3}\omega_c^3\omega_0^3}{27Q^3}}/\sqrt{\gamma} \tag{2.8}$$

where F_{d_c} is inversely proportional to the square root of the non-linearity parameter γ.

2.3 Parameter extraction for the Duffing resonator

To determine the critical driving force and frequency of a Duffing resonator (Equation 1.17), the parameter values are required. It is essential to implement parameter extraction before the sensing application because the properties of the resonators with the same design vary after the manufacture process [54]. There are three key parameters: the resonant frequency ω_0, the quality factor Q and the non-linear parameter γ that determine the response of the Duffing resonator (Equation 1.17).

When the Duffing resonator is driven with a sufficiently small force, the amplitude and phase response can be modelled by a linear resonator as the non-linear restoring force is much smaller than the linear one (Figure 1.4). The resonator parameters used to simulate the parameter extraction process are the same as those in Chapter 1: $f_0 = 14kHz$, $Q = 60$ and $\gamma = 2.7 \times 10^{21} N/(kg \cdot m^3$ (Figure 1.5 and Figure 1.6.

The amplitude and phase response of its linear mode with $F_d = 5N/kg$ have been simulated by solving the Equation 1.17 with MATLAB $ode45$ solver as shown in Figure 2.6. The maximum amplitude in Figure 2.6(a) and -90 degrees phase shift in Figure 2.6(b) both give the resonant frequency to $f_0 = 14.0kHz$ which is exactly the same as the model.

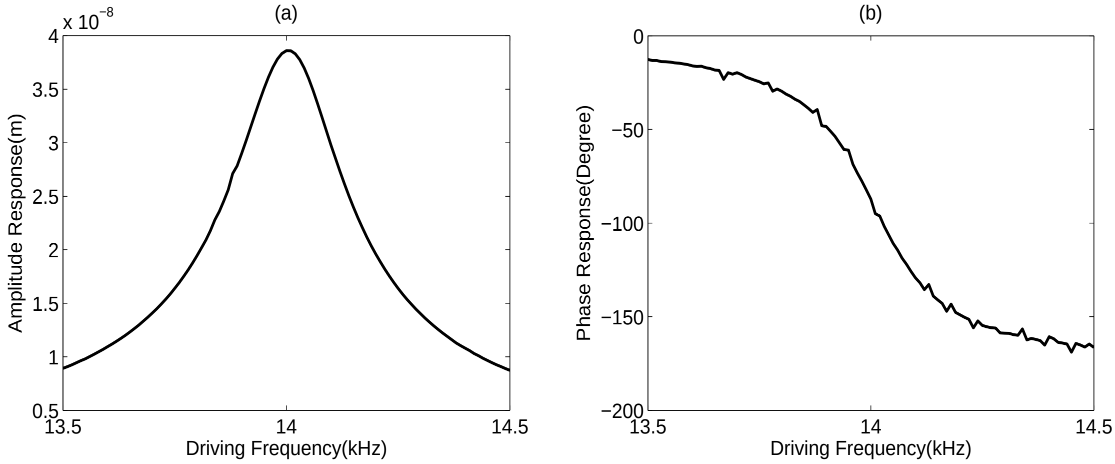

Figure 2.6: The simulated amplitude (a) and phase response (b) of the Duffing resonator with $F_d = 5N/kg$.

The Q value is defined as the ratio of resonant frequency and the $-3dB$ bandwidth which can be obtained from amplitude response in Figure 2.6(a) [46]. The extracted Q is 59.63 and the error is about 0.6% compared with the expected Q of 60. The difference is probably caused by the numerical error from the simulation but the method for extracting the Q value is feasible.

The phase response of the Duffing resonator Equation 1.25 describes the relationship between the phase response and non-linear parameter at each driving frequency. Consequently, to extracted the non-linear parameter γ, Equation 1.25 can be rearranged to give

$$\gamma = \frac{\omega^2 - \omega_0^2 + \frac{\omega\omega_0}{Q\tan\phi}}{\frac{3}{4}A^2} \tag{2.9}$$

Equation 2.9 suggests that for each driving frequency, the non-linear parameter γ can be calculated with the corresponding phase as well as amplitude response. The extracted value, in theory, is expected to be constant throughout the whole frequency range. Figure 2.7 shows the simulated response of the resonator to four different driving forces.

For each driving frequency ω the non-linear parameter γ can be calculated using the amplitude A and phase response ϕ with the extracted resonant frequency ω_0 and Q using Equa-

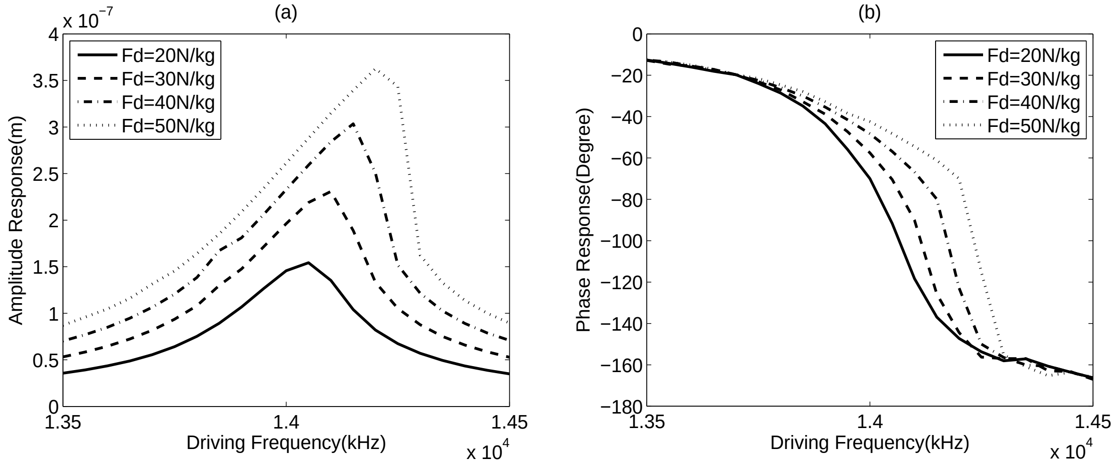

Figure 2.7: The simulated amplitude (a) and phase (b) response of the Duffing resonator with different driving forces.

tion 2.9.

The calculated non-linear parameter has been plotted in Figure 2.8, and there is more variation in the extracted values around the frequencies which are far off resonance. This could be explained in two aspects: the first element is that the absolute value of amplitude off peak is small so that the relative error will be significant; the second element is that the $\tan\phi$ approaches 0 when the phase response is near 0 or -180 degrees so that any minor error in the value will affect the extracted parameter dramatically. To eliminate these two problems, only those responses with amplitude greater than $1/\sqrt{2}$ of the peak response which corresponds to the amplitude at $-3dB$ point and with absolute value of $\tan\phi$ greater than 10 are used for extracting the non-linear parameter. Under this condition, the average and standard deviation value are summarised in Table 2.2.

Table 2.2: Standard deviation and average value for extracted γ with MATLAB simulation

	Standard Deviation ($\times 10^{20}$)	Average $\gamma(\times 10^{21})$
$F_d = 20N/kg$	9.76	2.68
$F_d = 30N/kg$	3.49	2.66
$F_d = 40N/kg$	2.24	2.69
$F_d = 50N/kg$	2.15	2.71

The standard deviation is decreasing as the driving force increases, and the error compared with expected $\gamma = 2.7 \times 10^{21}$ of these driving forces are between 0.4% and 1.5% which is probably caused by the numerical errors of the simulation. As a result, the non-linear

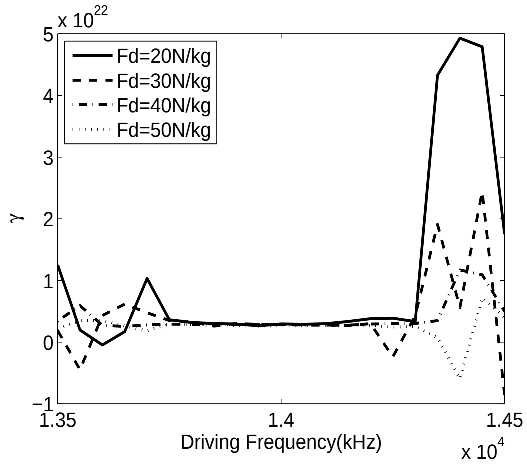

Figure 2.8: Extracted non-linear parameter from the simulated amplitude and phase responses.

parameter can be extracted if the data is taken under conditions that: the amplitude response and the absolute value of $\tan\phi$ are both above certain values which have been chosen to be the $-3dB$ amplitude and $\tan\phi = 10$ in the discussion above. The other condition is that the non-linear restoring force is not too large because the amplitude and phase response can not be described by the cubic equation accurately when the non-linear restoring force is comparable with the linear one as the driving force increases. This parameter extraction method will be confirmed by experimental results in the following chapters.

2.4 Summary

The sensitivity and the response time are both essential to a sensor but the response time has not been previously investigated experimentally. The transient behaviours of a Duffing resonator following the mass changes have been simulated. Unexpected varied long transient responses have been observed when the resonator is driven hard to create a large hysteresis loop. Since the response of the Duffing resonator critically depends on the initial conditions, it is believed that this problem is due to the high stable state's proximity to the unstable state near the jump frequency.

To improve the speed and the consistency of the response time, the driving force has been reduced to just create a small hysteresis loop. In this way, the stable solution and the unstable solution near the jump frequency separate from each other quickly and therefore the increase in mass can lead to quick repeatable jump in amplitude. The simulations with smaller driving force, which can give instant amplitude collapse no matter when the mass change occurs, have confirmed this solution.

Harmonic balance has been used for solving the Duffing equation and the amplitude response is described by a cubic equation. With this cubic equation, the method of determining the critical force which is the threshold value for the jumps to occur has therefore been identified. This critical force will be used as a reference to choose the desired driving force for the mass change sensing.

Due to manufacturing variations, parameter values for each resonator are different. To determine the critical force for the resonators, parameter extraction is needed. A procedure to extract parameters has therefore been suggested.

Chapter 3

Duffing Circuit resonator

3.1 Introduction

In previous chapters, a series analysis of the Duffing resonator has been simulated with MATLAB which includes the transient behaviour following the mass change, the parameter extraction method and the prediction for the critical driving force. Experiments are needed to check the numerical results, particularly the unexpected transient results. Since the numerical results suggest that the transient response can be critically dependent upon the initial condition, these experiments need to be reproducible. Before the investigation of the behaviour of micromechanical resonator, an electronic system called Duffing circuit, with similar resonant frequency and Q value as the micromechanical resonator, has been designed, built, and tested. In this Chapter, the methods for the parameter extraction, the sensor implementation techniques and observations of transient behaviour will be confirmed with the Duffing circuit.

3.2 Duffing circuit resonator design

An electrical circuit whose response is the solution of the hardening Duffing Equation 1.17 is shown in Figure 3.1 [55]. The components in the dotted rectangle compose a linear resonator. Op-amp $OPA404(a)$ functions as an integrator and the $OPA404(b)$ is an inverting amplifier with a gain of $\frac{R_{2b}}{R_{1b}}$. $OPA404(c)$ integrates all the signals coming into the inverting input including the driving voltage from the signal generator. If the output from $OPA404(a)$ is x,

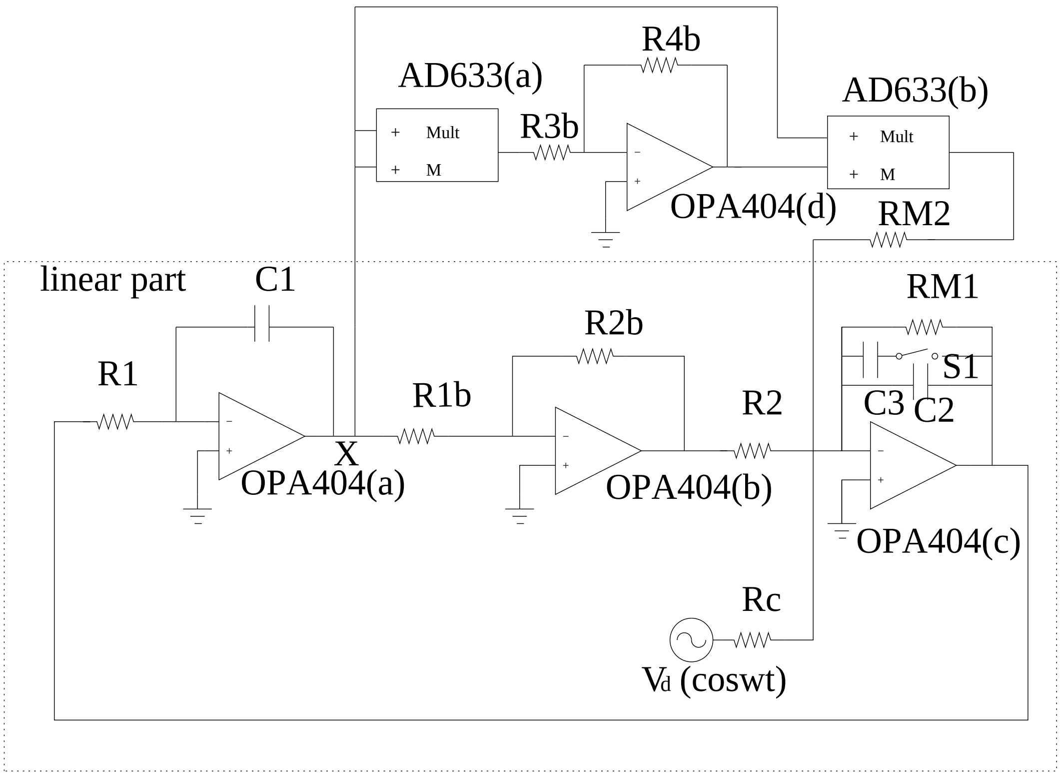

Figure 3.1: Schematic diagram of the Duffing resonator circuit.

then the linear resonator in the rectangle can be described by:

$$\ddot{x} + \frac{1}{R_{M1}C_2}\dot{x} + \frac{R_{2b}}{R_{1b}R_2C_2R_1C_1}x = \frac{1}{R_1C_1R_cC_2}V_d\cos\omega t \tag{3.1}$$

The components outside the rectangle create the non-linear term γx^3, the multipliers $(AD633)$ generate the squared term and then the cubic term and $OPA404(d)$ works as an amplifier to compensate the reduced gain from the multiplier. If the output from the amplifier is fed into the linear resonator then the equation for the response of the hardening Duffing resonator circuit is

$$\ddot{x} + \frac{1}{R_{M1}C_2}\dot{x} + \frac{R_{2b}}{R_{1b}R_2C_2R_1C_1}x + \frac{M^2R_{4b}}{R_{3b}R_{M2}C_2R_1C_1}x^3 = \frac{1}{R_1C_1R_cC_2}V_d\cos\omega t \tag{3.2}$$

Compared with the typical motion for a Duffing resonator Equation 1.17 discussed in

Section 1.4, the parameters of the circuit could be determined as follows:

$$\mu = \frac{\omega_0}{Q} = \frac{1}{R_{M1}C_2} \tag{3.3}$$
$$\omega_0^2 = \frac{R_{2b}}{R_{1b}R_2C_2R_1C_1} \tag{3.4}$$
$$\gamma = \frac{M^2R_{4b}}{R_{3b}R_{M2}C_2R_1C_1} \tag{3.5}$$
$$F_d = \frac{1}{R_1C_1R_cC_2}V_d = d_0V_d \tag{3.6}$$

The resonant frequency of the micromechanical sample which is going to be tested in the following chapters is around 17kHz, so the circuit design aims for a similar frequency range. The resonant frequency of the circuit has been chosen to be 10^5 rad/s. The designed quality factor Q for the mechanical system in air is approximately 10, as a result the same Q has been chosen for the Duffing circuit which means $\mu = 10^4$. Given that the displacement is around "$1V$", the non-linear parameter γ is chosen to be 10^9. This ensures that the ratio between the cubic and the linear restoring force is around 10% which is small but significant to create a hysteresis jump within the driving voltage limit. Equation 3.2 shows that C_2 is the only common factor in the terms of μ,ω_0^2,γ and F_d, the "mass" of the circuit is represented by C_2. The minimum available value of the polystyrene capacitor is $10pF$, to ensure the "mass" can be changed by a small amount of ratio (0.01%), C_2 is chosen to be $100nF$. Then R_{M1} can be calculated from Equation 3.3:

$$R_{M1} = \frac{1}{C_2\mu} = 10^3\Omega \tag{3.7}$$

OPA404(b) is designed as an inverting buffer between two integrators with a gain of -1 which is determined by $-R_{2b}/R_{1b}$. Since the resistor value should not be less than $1k\Omega$ otherwise current flow will be too large which is not desirable, choose $R_{1b} = R_{2b} = 1k\Omega$. Recall from Equation 3.4 and suppose $R_1 = R_2 = 1k\Omega$ and so

$$C_1 = \frac{R_{2b}}{w_0^2R_{1b}R_1R_2C_2} = 1nF \tag{3.8}$$

The transfer function of the multiplier AD633 defined in the manual is:

$$W = \frac{(X_1 - X_2)(Y_1 - Y_2)}{10V} + Z \tag{3.9}$$

In this circuit, $X_2 = Y_2 = Z = 0$. Since the output of the AD633(a) is divided by 10, the Opa404(d) functions an inverting amplifier with the Gain of 10. Therefore, $R_{4b} = 10k\Omega$; $R_{3b} = 1k\Omega$. From Equation 3.5 the value of R_{M2} is given by

$$R_{M2} = \frac{M^2 R_{4b}}{R_{3b} C_2 R_1 C_1 \gamma} = 10^3\Omega \tag{3.10}$$

Recall from Equation 1.10, that describes the maximum magnitude for a linear resonator, the peak amplitude of the Duffing circuit can be approximated by

$$|G|_{max} = \frac{X}{F_d} = \frac{X}{\frac{1}{R_1 C_1 R_c C_2} V_d} = \frac{Q}{\omega_0^2} = \frac{1}{\mu\omega_0} = R_{M1} C_2 \sqrt{\frac{R_{1b} C_1 R_1 C_2 R_2}{R_{2b}}} \tag{3.11}$$

Letting $\frac{X}{V_d} = 1$, then

$$\frac{X}{V_d} = \sqrt{\frac{R_2 C_2}{R_1 C_1}} \frac{R_{M1}}{R_C} = 1 \tag{3.12}$$

Thus, R_C is obtained from Equation 3.12 of $10k\Omega$. There is an additional parameter d_0 resulting from the circuit design. The value obtained from the Equation 3.6 is 10^9.

The resistors and capacitors used for this Duffing circuit have $\pm 1\%$ and $\pm 10\%$ manufacturing tolerance respectively so that the key characteristic values ω_0, Q, γ and d_0 may deviate from the designed value by more than 20%. Therefore it is necessary to extract the parameter value before performing the experiments.

3.3 Duffing circuit characterisation

3.3.1 Actuation and measurement

Two types of commercially available bench top signal generators were used for testing the Duffing resonator circuit. The first signal generator (WW5064) has a digital input to give the user accurate control of its output frequency and the frequency resolution is $1\mu Hz$. However, experience showed that this system only ever found the low amplitude response. This problem was traced to the fact that this signal generator stops generating an output when the frequency is changed. With the other (older) signal generator (TG550) that was used the user controls the output frequency using a dial. The higher amplitude response could be observed by slowly turning the dial to increase the frequency used to drive the resonator. However this method has two disadvantages. First, manually increasing the frequency results in uneven frequency increases which will affect the results of experiments. Second, it is impossible to reach the jump frequency repeatedly to the required accuracy. An automatic method of creating and controlling the frequency used to drive the circuits is therefore required. To characterise the hysteresis loop of the Duffing resonator, a system has been designed to exploit the accuracy and stability of direct digital frequency synthesis as shown in Figure 3.2.

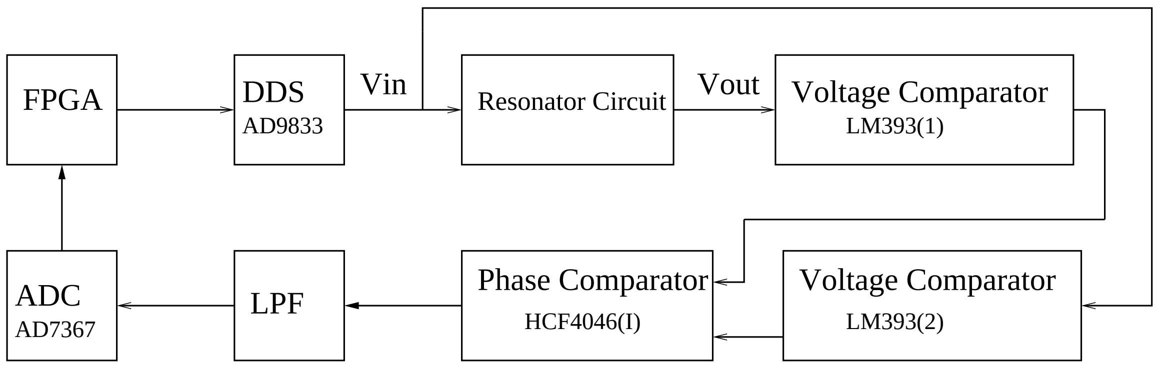

Figure 3.2: Driving and control electronic systems for the Duffing resonator circuit test.

The desired accuracy and stability of the driving signal is provided by a programmable waveform generator IC (AD9833) which is controlled by an FPGA. The sine output signal from the AD9833 both drives the resonator and provides an input to a comparator which creates a square wave that is in phase with the sine wave. The phase shift between the driving voltage and the output voltage is then detected by an XOR gate phase comparator. The output from this comparator is low pass filtered to create a DC voltage that represents the phase shift between the input voltage and the circuit's response. An ADC then converts this phase information into digital words which can be processed by the FPGA. In addition, during experiments the DC voltage from the Low Pass Filter(LPF) also provides a real-time channel to monitor the resonators phase shift.

For those experiments which do not require continuous sweep, the bench top digital signal generator (WW5064) was used to replace the FPGA and the DDS as it has more stable output in terms of frequency and the amplitude than the DDS system.

3.3.2 Parameter extraction

The Duffing circuit is composed of several resistors and capacitors and the actual values of these components are different from the labelled values due to the manufacturing tolerance. To check if the combined effects of the differences between ideal and actual component values has a significant effect, the Duffing circuit is driven at a sensitive condition. This condition is choosing the driving voltage to be the estimated critical driving force calculated with the ideal component values. As discussed in Section 2.2, the critical driving voltage is the threshold value to lead to a range of frequencies with multi-amplitude solutions. Therefore, if the driving voltage is less than the critical driving voltage, no jump will be observed and there will be a hysteresis loop if the driving voltage is larger than the critical value. The response of the resonator driven with the critical force is expected to bend to the right but with no jumps. The critical driving voltage is calculated using Equation 2.8 with the designed components value to be $V_{d\_c1} = 1.63V$. The amplitude and phase response driven with this critical voltage are shown in Figure 3.3 which has obvious but unexpected jumps both in amplitude and phase response. Therefore the parameter extraction is needed to predict the parameter ranges especially as they are important when determining a driving force and frequency.

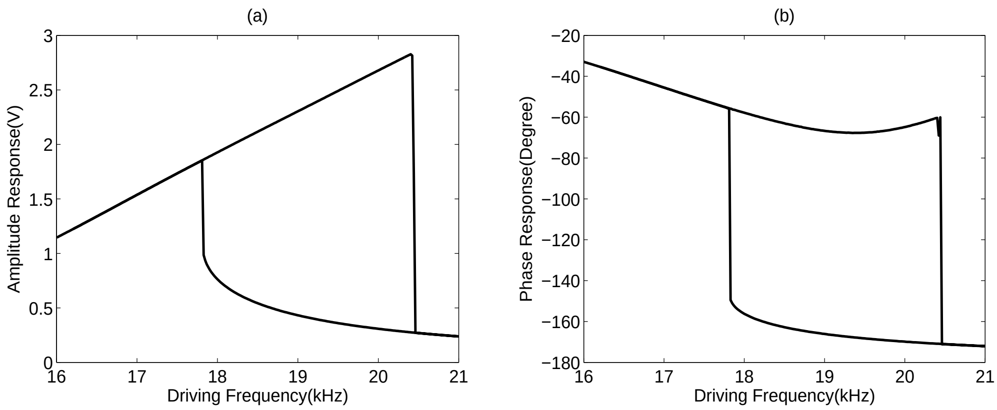

Figure 3.3: Amplitude(a) and phase(b) response driven with the designed critical driving voltage $V_{d\_c1} = 1.63V$.

When the Duffing resonator is driven with a force which is far less than the critical value (e.g. one tenth), the amplitude response can be considered as a linear system. The Duffing circuit is driven with $V_d = 0.18V$ and the amplitude and phase response is shown in Figure 3.4 (solid line).

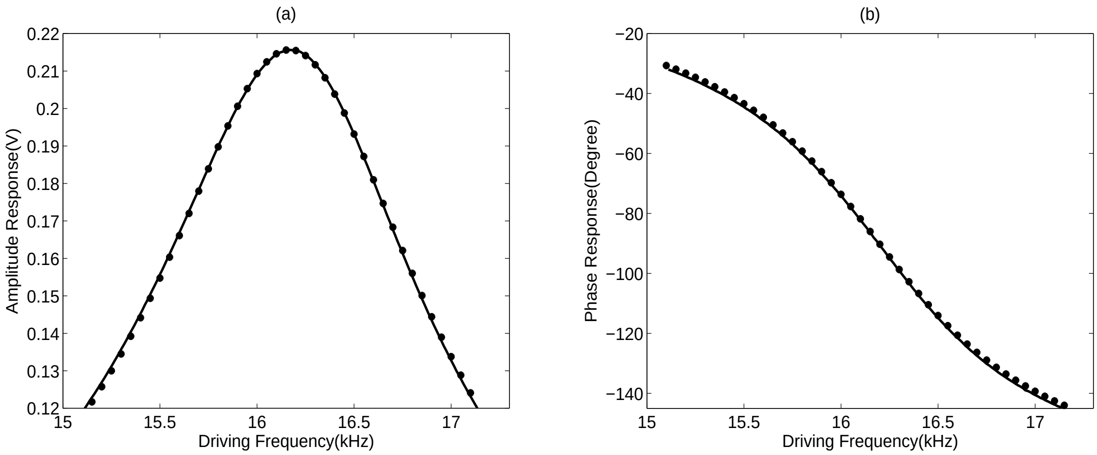

Figure 3.4: Amplitude (a)and phase (b) comparison of simulation (dots) and experimental (solid line) results driven with a small force $V_d = 0.18V$ showing linear behaviour.

With the transfer function of the linear resonator (Equation 1.4), linear parameters ω_0, Q and d_0 are extracted using the MATLAB curve fitting tool. The extracted and the expected parameter values are compared in Table 3.1 and these extracted parameters are all within the expected range of $\pm 20\%$. The dots in Figure 3.4 plot the simulated transfer function of a linear resonator with those extracted parameters in Table 3.1 which proves that the chosen force was small enough to model a linear resonator.

Table 3.1: Comparison of expected and extracted linear parameter values for the Duffing resonator circuit

Parameter	Expected value	Extracted value	Relative difference
ω_0	15915.5Hz	16190.6Hz	2%
Q	10	12.02	20%
d_0	1.049×10^9	1.0×10^9	5%

The method of extracting the non-linear parameter γ has been discussed in Section 2.3, and the non-linear parameter can be extracted with Equation 2.9. Since Equation 2.9 is valid on condition that the non-linear cubic restoring force $m\gamma x^3$ is relatively small compared with the linear restoring force $m\omega_0^2 x$. Therefore the driving force chosen to extract the non-linear parameter should be smaller than the driving voltage in Figure 3.3. It shows that the ratio reaches 0.55 at the peak amplitude which is too large. Four different smaller driving voltages are applied to the Duffing circuit, and the response comparison is shown in Figure 3.5.

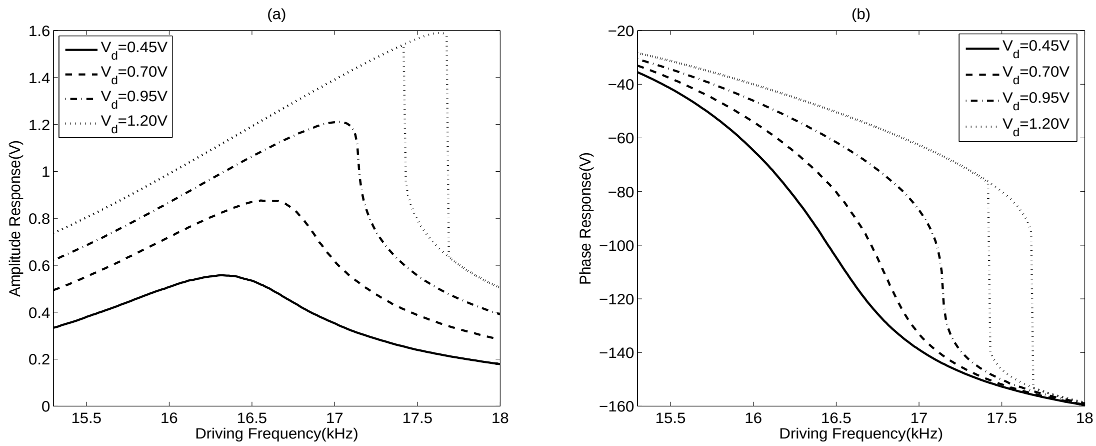

Figure 3.5: Amplitude(a) and phase (b) response driven with the voltages to extract the non-linear parameter.

The extracted γ using the Equation 2.9 with the data in Figure 3.5 is illustrated in Figure 3.6. The extracted non-linear parameter varies widely corresponding to different driving forces and frequencies. For the same noise level, the small amplitude responses have lower signal to noise ratio. Therefore, the responses with amplitude less than the amplitude at $-3dB$ point have been discarded.

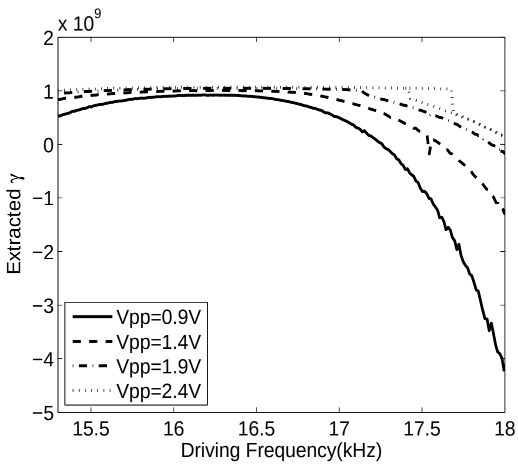

Figure 3.6: Extracted non-linear parameter with four different driving voltages.

In addition, it is $\tan\phi$ instead of phase response ϕ that determines the non-linear parameter in Equation 2.9 and the values of $|\tan\phi|$ have been plotted in Figure 3.7 which have a wide range of values from 0.5 up to 200. Those small values are more likely to be influenced by the noise so that only the experimental data with the absolute value of $\tan\phi$ larger than a certain value (for example 10) are considered as a good estimation. Under these two conditions for amplitude and phase response, only some of the experimental results are used to extract the non-linear parameter. The standard deviation and average value for each driving voltage are compared in Table 3.2.

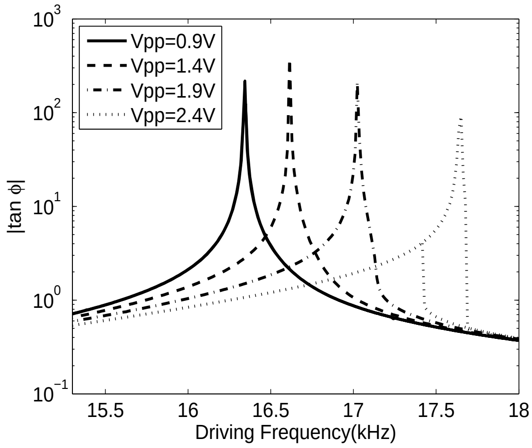

Figure 3.7: Comparison of $\tan\phi$ with four different driving voltages.

Table 3.2: Standard deviation and average value for extracted γ for the Duffing resonator circuit.

	Standard Deviation ($\times 10^6$)	Average $\gamma(\times 10^9)$
$V_d = 0.45V$	5.64	0.91
$V_d = 0.70V$	4.75	0.99
$V_d = 0.95V$	4.12	1.02
$V_d = 1.20V$	3.85	1.04

From the Table 3.2, $V_d = 1.2V$ gives the least standard deviation and the average value of extracted $\gamma = 1.04 \times 10^9$ is within the tolerance range compared with the expected value $\gamma = 1 \times 10^9$. So far, the four key parameters have been extracted. Then, the critical driving voltage using the Equation 2.8 with the extracted parameters can be recalculated to $V_{d\_c2} = 1.2V$. This result is still not consistent with the expected results as in Figure 3.5 the driving voltage $V_d = 1.2V$ shows a clear hysteresis loop.

To check the extracted parameters, the experimental data with the driving voltage $V_d = 0.18V$ are compared with the simulation results by solving the Duffing resonator (Equation 1.17) using the MATLAB $ode45$ solver at each frequency instead of the linear transfer model in Figure 3.4. The simulation results in Figure 3.8(a) show that the estimated resonant frequency is a bit low compared the experimental results. The reason is probably that the small driving force does not produce an absolute linear response, so the parameters extracted have some tiny error resulting from the curve fitting method. After careful adjustment, the resonant frequency is changed from $16960.6Hz$ to $16171.6Hz$ and this gives a better fit as shown in Figure 3.8(b).

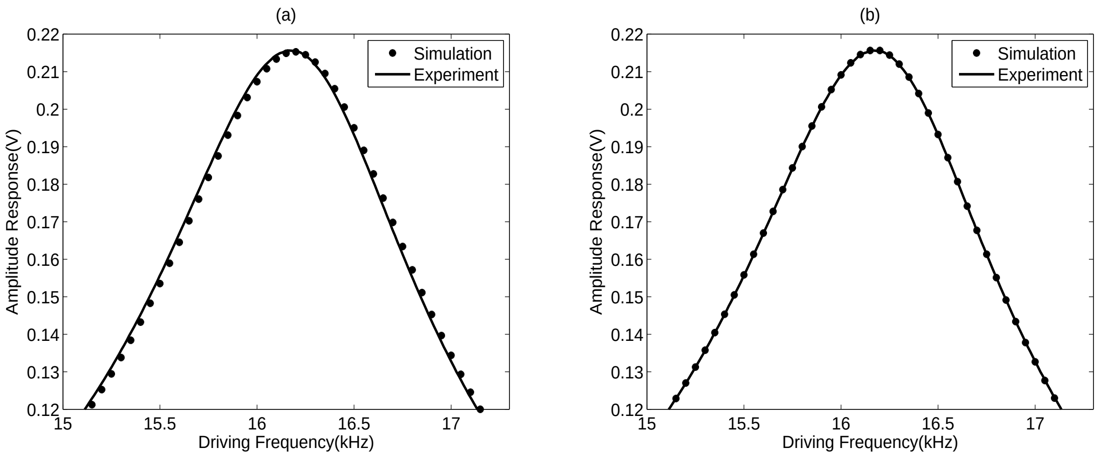

Figure 3.8: Amplitude comparison of simulation and experimental results with $V_d = 0.18V$.

If driving voltage is changed to $V_d = 1.2V$ with the updated parameters in the Figure 3.8(b), the simulation results are compared in the Figure 3.9(a). The simulated results represent the lower branch for the amplitude response as the initial condition for the $ode45$ solver is zero, however, the simulation behaves quite differently from the experimental results in terms of the peak amplitude as well as the jump frequency where the amplitude discontinuity occurs. If the non-linear parameter is increased by 10% to 1.14×10^9 as shown in the Figure 3.9(b), the jump frequency is the same as expected, but the peak amplitude is much smaller than the experimental results.

As the resonant frequency is easy to identify from the linear system and it has been confirmed with the simulation of the linear response in Figure 3.8, simulations with different parameter combinations are implemented to find a best fit with the experimental data with $V_d = 1.2V$. A three dimension (γ, d_0, and Q) search strategy is developed to find the best estimation for the non-linear response. For each entry of the three dimension parameter matrix, three frequencies (16.5kHz,17kHz and 17.5kHz) that can describe the shape of the peak and jump in general are simulated and return the maximum difference compared with the

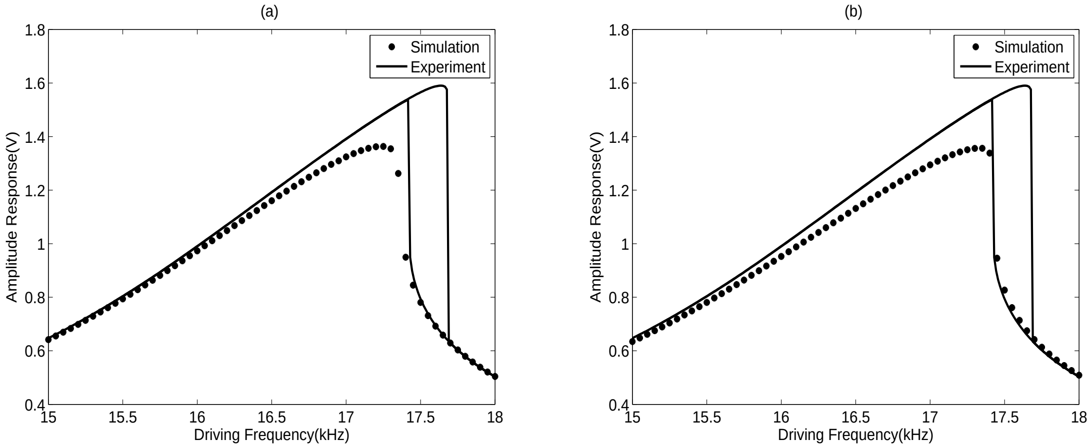

Figure 3.9: Amplitude comparison of simulation and experimental results with $V_d = 1.2V$ with (a) $\gamma = 1.04 \times 10^9$ and (b) $\gamma = 1.14 \times 10^9$.

experimental results. By comparing these returned values the minimum value gives the best estimation of the system parameters. The search starts with a general cover of the range around the previous extracted values then based on the minimum value obtained a finer search is implemented. The parameters for the two searches and the results obtained are listed in the Table 3.3.

Table 3.3: Entries for optimising the parameter extraction and the parameters for best fit

	First Search(general)	Second Search (detail)
$\gamma(\times 10^9)$	0.85:0.1:1.15	1:0.025:1.1
$d_0(\times 10^9)$	0.9:0.05:1.1	1::0.025:1.1
Q	12:1:15	13:0.2:15
Minimum difference(V)	0.0168	0.0049
Best entry	$\gamma = 1.05 \times 10^9$ $d_0 = 1.05 \times 10^9$ $Q = 13$	$\gamma = 1 \times 10^9$ $d_0 = 1.05 \times 10^9$ $Q = 14.4$

The parameters from the second search in Table 3.3 are used in the simulation with more driving frequencies. Figure 3.10(a) shows a good fit between the simulated and the actual test results when it is driven by $V_d = 1.2V$. However, the simulation with same parameters but driven with $V_d = 0.18V$ do not agree with the experimental results at all in Figure 3.10(b). This implies that the response of the designed Duffing circuit does not obey the standard Duffing equation (Equation 3.2).

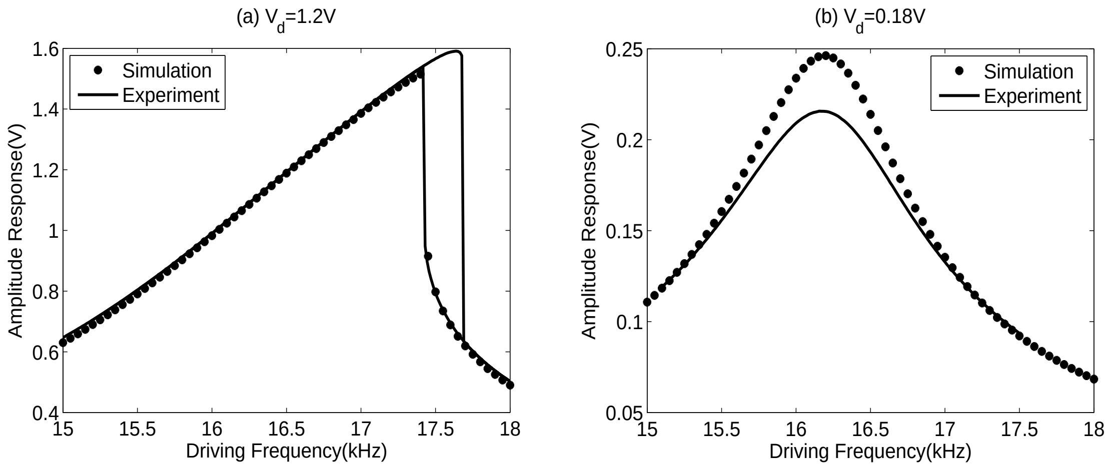

Figure 3.10: Amplitude response comparison of simulation and experimental results with parameters extracted for the best fit of $V_d = 1.2V$.

3.3.3 Improved Model

To identify the real model of the circuit, the extracted parameter values for two different driving voltages are compared in Table 3.4 and it shows that the most significant difference is the Q value. Comparing Figure 3.10 (a) and (b), it shows that the damping term decreases a lot when the amplitude response increases so there seems to be an amplitude dependent Q. This implies that the non-linear feedback circuit might not produce a pure displacement cubed term and there probably is some amplitude dependent damping term missing from the previous model.

Table 3.4: Extracted parameter values with two driving voltages

	$V_d = 0.18V$	$V_d = 1.2V$	Relative difference
$\gamma(\times 10^9)$	1.04×10^9	1×10^9	4%
$d_0(\times 10^9)$	1.049×10^9	1.05×10^9	0.1%
Q	12.02	14.4	17%

If the hypothesis is correct, then the softening Duffing circuit with an inverted non-linear feedback should behave in the opposite way. The damping term will increase when the amplitude response becomes larger. To confirm this, the same parameter extraction experiment is performed on a softening Duffing circuit with a negative non-linear parameter γ. This circuit was created by adding a unity gain inverting amplifier before the non-linear term is added to the linear part. Similar to the hardening system, the response with different driving force can not be fitted with same parameters but there is one difference from the hardening system.

Compared with the data fitting in Figure 3.10, the parameters extracted from the response to the same driving force are simulated and compared in Figure 3.11. The linear simulation with the parameters that fit the non-linear response in Figure 3.11 (b) shows that the damping term is smaller for the small amplitude response which is in the opposite way to the hardening system. This proves that the output from the non-linear feedback term has some effect on the Q value of the system.

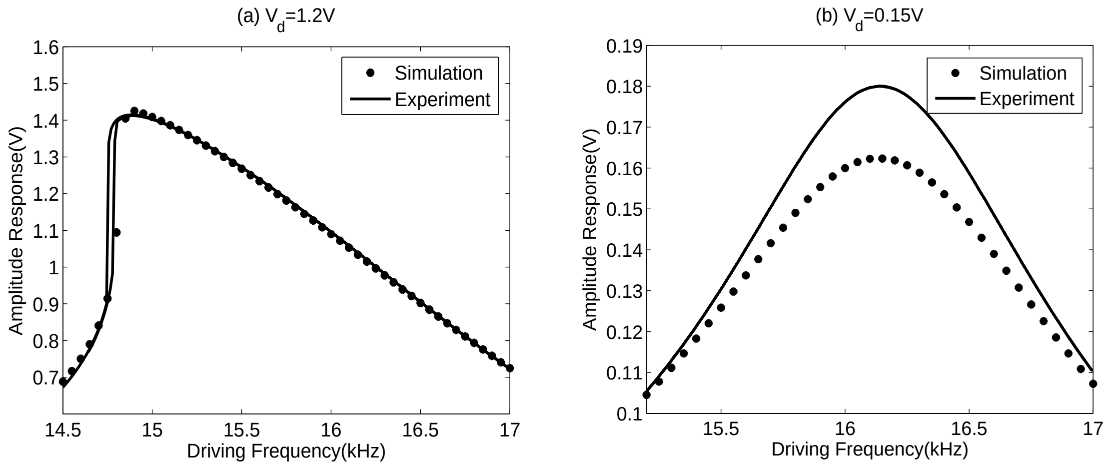

Figure 3.11: Amplitude comparison of simulation and experimental results with parameters extracted for the best fit of $V_d = 1.2V$ (Softening Duffing circuit).

If the multipliers are perfect, the non-linear feedback is not expected to have a damping term. However, the multipliers might have some delays which is probably the cause of the amplitude dependent Q. The data sheet for the multiplier AD633 indicates that the settling time to 1% at $\Delta V_0 = 20V$ is about $2\mu s$. The input of the test is a square waveform with $1V$ amplitude and $1V$ DC offset at 10kHz. An oscilloscope snapshot (Figure 3.12) has demonstrates the delay caused by the multiplier and it is about $1.5\mu s$ which is equivalent to about -5 degrees with a period of $0.1ms$.

Although the phase shift caused by the multiplier is only about -5 degrees the output from the multipliers will affect the behaviour of the Duffing circuit significantly because the effective coefficient for the non-linear term will be multiplied by non-linear parameter $\gamma = 10^9$. To simplify the analysis, suppose the input of the first multiplier is the displacement of the resonator $x = Acos\omega t$. If the effective phase shift caused by the multiplier is θ, then the

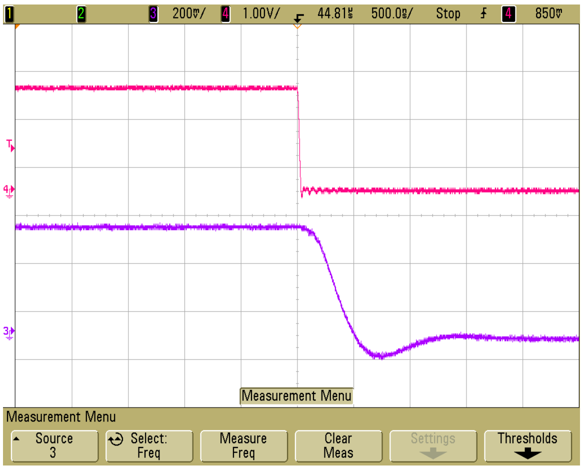

Figure 3.12: Settling time for the multiplier AD633(Pink:input;Purple:output).

non-linear term fed into the linear resonator is

$$\begin{aligned}
Y &= A^2\cos^2(\omega t+\theta)A\cos\omega t \\
&= A^2(\cos\omega t\cos\theta-\sin\omega t\sin\theta)^2 A\cos\omega t \\
&= A^3(\cos^3\omega t\cos^2\theta+\sin^2\omega t\cos\omega t\sin^2\theta-\sin\omega t\cos^2\omega t\sin 2\theta) \\
&= x^3\cos^2\theta+\dot{x}^2x\frac{\sin^2\theta}{\omega^2}+x^2\dot{x}\frac{\sin 2\theta}{\omega} \qquad (3.13)
\end{aligned}$$

where $\dot{x} = -A\omega\sin\omega t$ and the first term is the slightly attenuated amplitude cubed term. The size of the second term is negligible compared with the other two terms because $\sin^2\theta$ is much smaller than $\cos^2\theta$ and $\sin 2\theta$ when θ is around -5 degrees. The third term is the non-linear damping term. As the displacement increases, this term cancels more damping in the hardening system, but causes more damping for the softening system which explains the behaviour in Figure 3.10 and Figure 3.11.

To quantify the phase shift, the output spectrum from the second multipliers in Figure 3.1 is measured in Figure 3.13. If the circuit is perfectly ideal as designed, the output spectrum is expected to contain the first and the third harmonics only and the magnitude of the first harmonic should be three times that of the third harmonic according the Equation 1.20. From Figure 3.13, it shows only the first and third harmonics without any DC component or the even harmonics. The magnitude of the first harmonic is $78.0mV$ while the third one is $26.2mV$, and the ratio between these two is 2.974 which is slightly less than 3. To analyse the output

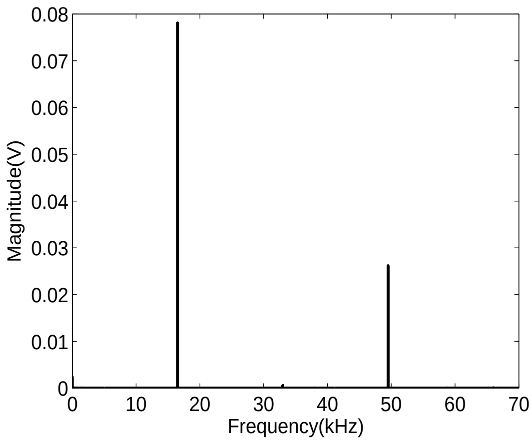

Figure 3.13: Spectrum response of the multipliers with $V_d = 1V$ at 16.5kHz.

spectrum, Equation 3.13 can be rewritten to:

$$\begin{aligned}
Y &= x^3 \cos^2 \omega t + x^2 \dot{x} \frac{\sin 2\theta}{\omega} \\
&= A^3 (\cos^3 \omega t \cos^2 \theta - \sin \omega t \cos^2 \omega t \sin 2\theta) \\
&= A^3 [(\frac{3}{4} \cos \omega t + \frac{1}{4} \cos 3\omega t) \cos^2 \theta - (\frac{1}{4} \sin \omega t + \frac{1}{4} \sin 3\omega t) \sin 2\theta] \\
&= \frac{1}{4} A^3 [\sqrt{9 \cos^4 \theta + \sin^2 2\theta} \cos(\omega t - \varphi) + \sqrt{\cos^4 \theta + \sin^2 2\theta} \cos(3\omega t - \delta)] \\
&= \frac{1}{4} A^3 [\sqrt{9 + 4 \tan^2 \theta} \cos(\omega t - \varphi) + \sqrt{1 + 4 \tan^2 \theta} \cos(3\omega t - \delta)] \qquad (3.14)
\end{aligned}$$

in which $\tan \varphi = -\frac{2}{3} \tan \theta$, $\tan \delta = -2 \tan \theta$ and the ratio between the two harmonics is

$$Ratio = \frac{A_\omega}{A_{3\omega}} = \sqrt{\frac{9 + 4 \tan^2 \theta}{1 + 4 \tan^2 \theta}} \qquad (3.15)$$

Substituting the magnitude at the first and third harmonics in Figure 3.13 into the above equation, it gives $\theta = -4^\circ$ which is in an acceptable range. Then, the Duffing circuit model will be converted to:

$$\ddot{x} + \frac{\omega_0}{Q} \dot{x} + \omega_0^2 x + \gamma (x^3 + \frac{2 \tan \theta}{\omega} x^2 \dot{x}) = V_d \cos(\omega t) \qquad (3.16)$$

where $\gamma = \gamma_0 \cos^2 \theta$ and γ_0 is real non-linear parameter for the Duffing circuit and γ is the extracted value. Then, the cubic Equation 1.26 to solve the amplitude is modified as well:

$$[(\frac{3}{4}\gamma)^2 + (\frac{1}{4}\beta)^2](A^2)^3 + [\frac{3\gamma}{2}(\omega_0^2 - \omega^2) + \frac{1}{2}\beta\frac{\omega\omega_0}{Q}](A^2)^2 + [(\omega_0^2 - \omega^2)^2 + (\frac{\omega_0}{Q})^2\omega^2]A^2 = V_d^2 \tag{3.17}$$

where $\beta = 2\tan\theta\gamma$ and the phase response becomes:

$$\tan\phi = \frac{\frac{\omega_0\omega}{Q} + \frac{1}{4}\beta A^2}{\omega_0^2 - \omega^2 + \frac{3}{4}\gamma A^2} \tag{3.18}$$

The best fit has been achieved by solving the cubic Equation 3.17 and Equation 3.18 using the extracted data in Table 3.5.

Table 3.5: Parameters values used to simulate amplitude and phase response with the improved model.

Parameter	f_0	Q	γ	d_0	θ
Value	16171.6Hz	12.02	1.04×10^9	1.049×10^9	$-6.86°$

In Table 3.5, all parameter values except θ were obtained by parameter extraction in Section 3.3.2 (Table 3.1 and Table 3.2) but the resonant frequency f_0 has been slightly adjusted by solving the Duffing resonator with MATLAB $ode45$ when $V_d = 0.18V$ instead of using the linear transfer function. The phase shift θ has been extracted by searching the best fit between the simulated and experimental results for both $V_d = 1.2V$ and $V_d = 0.18V$ as shown in Figure 3.14.

In Figure 3.14, the new model with amplitude dependent damping arising from a phase shift gives a much better fit with the real circuit tests. The critical driving voltage for a hardening system with the new model based on the Equation 2.8 is $V_{d\_c} = 0.963V$. The amplitude and phase response recorded in Figure 3.15 shows that shows that no hysteresis loop is observed but there is a driving frequency with a very high $\frac{d\phi}{d\omega}$ which indicates that a jump will occur if the driving force is increased further. Although it requires further investigation about the critical force it is able to confirm the phase shift model.

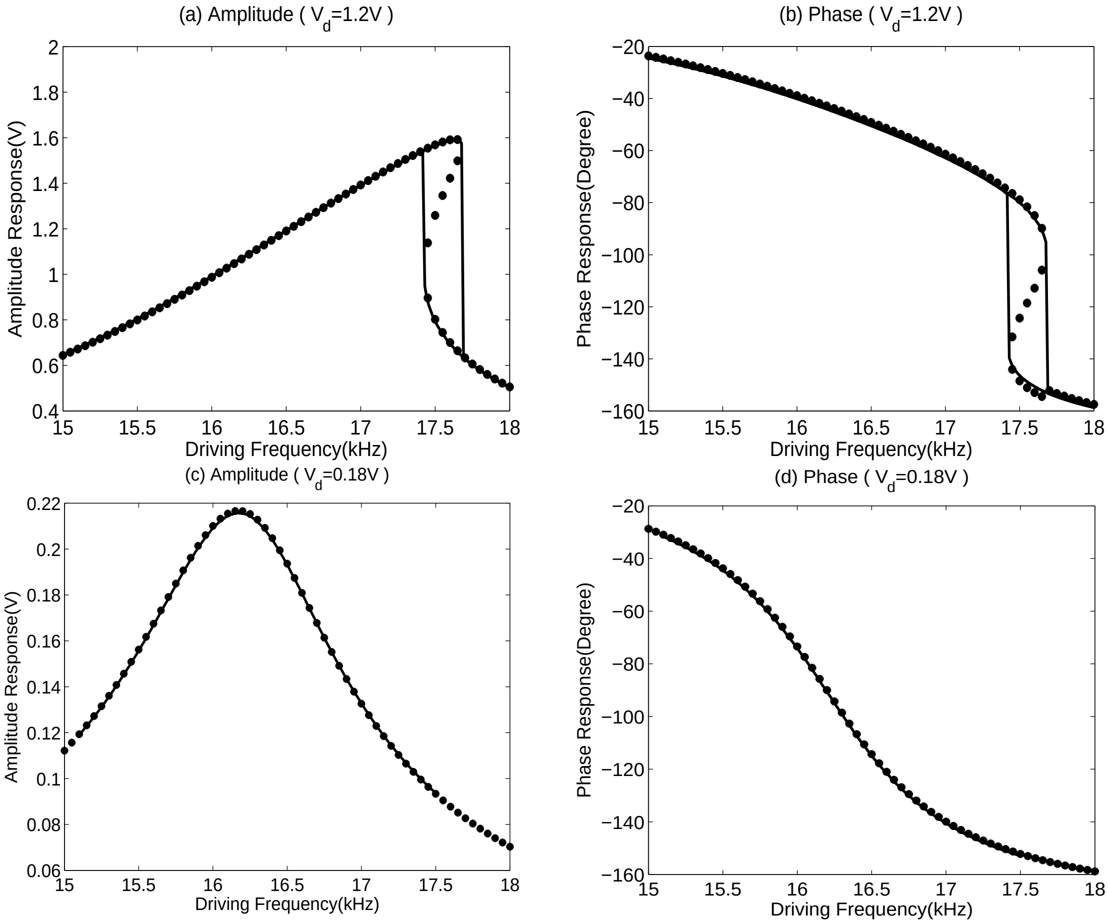

Figure 3.14: Comparison of simulated (dots) and experimental (solid line) results with the improved Duffing model driven by $V_d = 1.2V$ or $V_d = 0.18V$.

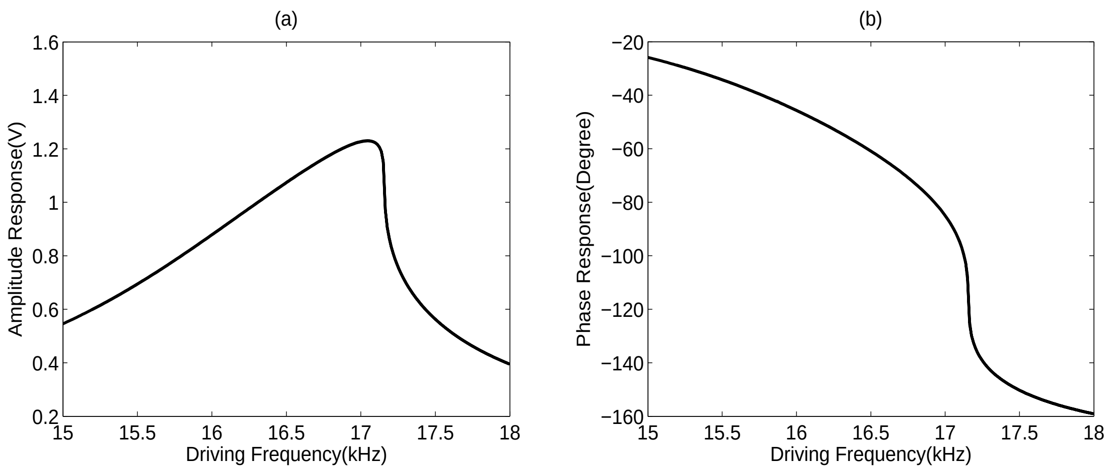

Figure 3.15: Amplitude and phase response driven with calculated critical voltage $V_d = 0.963V$.

3.4 Duffing circuit response following the ”mass” change

3.4.1 Control electronics

The aim of the this project is to detect the mass change of the micromechanical resonator but undesired long transient response following the mass change has been observed in the simulated results. To investigate this behaviour, it is required to be able to change the effective ”mass” of the Duffing circuit repeatedly. A comparison of the Equation 1.17 and Equation 3.2 show that capacitor C_2 is equivalent to the mass of a micromechanical resonator as C_2 is the only common factor in the terms of μ, ω_0^2, γ and d_0. By turning on the switch S1 in Figure 3.1, the equivalent value for C_2 increases to $C_2 + C_3$. In order to control the switch of the voltage signal which can be well monitored and recorded, the S1 is composed of an analogue switch and a voltage comparator as shown in Figure 3.16.

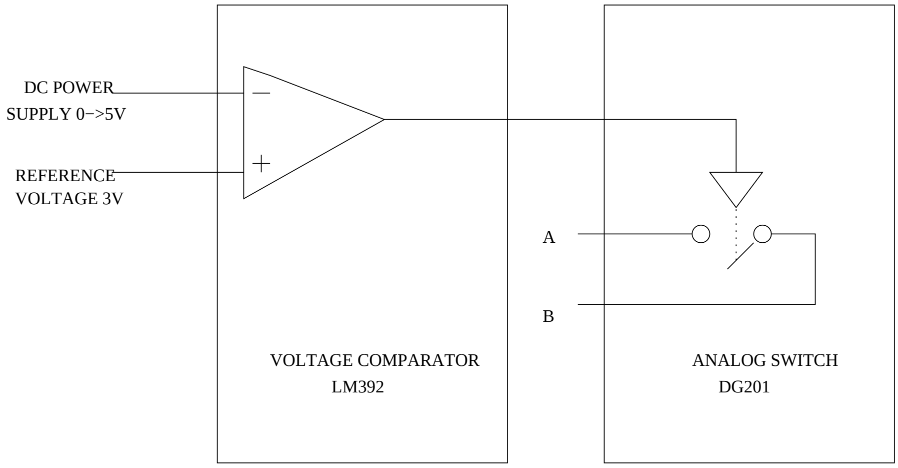

Figure 3.16: The circuit diagram for the parameter change control switch.

The analogue switch is controlled by a DC voltage and it will be turned ON when the input control changes from logic 1 to logic 0. Then, C_3 is connected to the circuit, and the ”mass” of the Duffing resonator is increased. The output of a power supply unit (Agilent E3631A) can be connected to the control input of the analogue switch directly, but it takes approximately $4.6ms$ to change its output from $0V$ to $5V$. Compared with the resonant frequency of the resonator, the rising time is 75 times of the period of the movement which is not desirable for determine the exact time when the parameter change occurs. Therefore, a voltage comparator LM392 is used to speed up the voltage rising/falling rate. With a $3V$ reference voltage at the non-inverting input and the power supply at the inverting input, the output is connected to the control signal of the analogue switch DG201. The measured rising time for the same voltage change is approximately $10\mu s$ which is close to one fifth of the period. Therefore, by connecting this control voltage to the data acquisition device, the behaviour of the switch with respect to time is recorded in terms of voltage signals.

The actuation and measurement system for investigating the transient behaviour following the parameter change is the same as the system for characterising the Duffing circuit as shown in Figure 3.2. The driving frequency for detecting the parameter change can be achieved by programming the FPGA which can control the AD9833 to start increasing the driving frequency until the resonator phase shift or the driving frequency reaches a predetermined value. This value, the frequency accuracy and the rate at which the frequency is increased can be set by the user using the FPGA so that the driving frequency for detecting the resonant frequency change can be located repeatedly.

3.4.2 Linear resonator circuit

Before investigating the transient behaviour of the non-linear resonator, the linear circuit in the dotted rectangle in Figure 3.1 has been tested. It has been characterised with the switch in its two positions with C_3 chosen to be $0.1\% C_2$ which means that the ”mass” of the Duffing circuit will be increased by 0.1% when the switch is turned on. The 0.1% increase in ”mass” will result in a 0.05% decrease in resonant frequency (Equation 1.7). Although ”mass” change also will affect value of other parameters such as Q and the scaled force, those changes are negligible compared with the influence of the change in resonant frequency for such a small percentage change in mass. In the following discussion, the effect of ”mass” C_2 increase will be considered to be equivalent to the effect that the resonant frequency is decreased by twice the percentage change in ”mass”(Equation 1.7).

The relative values of C_2 and C_3 means that the resonant frequency is shifted by 0.05%, which with a resonant frequency of $16kHz$ is approximately $8Hz$. A comparison of the amplitude and phase responses observed in these two experiments, Figure 3.17, shows that as expected the phase response is -90 degrees at resonance and there is a slight difference between the two observed responses. If the resonant frequency of a linear circuit changes from ω_0 to $\omega_0 + \Delta\omega_0$ then the phase change at resonance $\Delta\phi$ is

$$\frac{\Delta\omega_0}{\omega_0} = -\frac{\Delta\phi}{2Q} \tag{3.19}$$

where Q is the quality factor of the resonator. The Q of this linear system is approximately 10 and the percentage change in the resonant frequency is 0.05%. The expected phase change is therefore $0.01rad(0.57°)$. An important effect that will limit the ability of the system to detect such a small change is the noise on the DC voltage that represents the phase difference. Results show that when the linear circuit is driven at its resonant frequency the noise on this voltage signal is equivalent to a phase of approximately 0.5 degree.

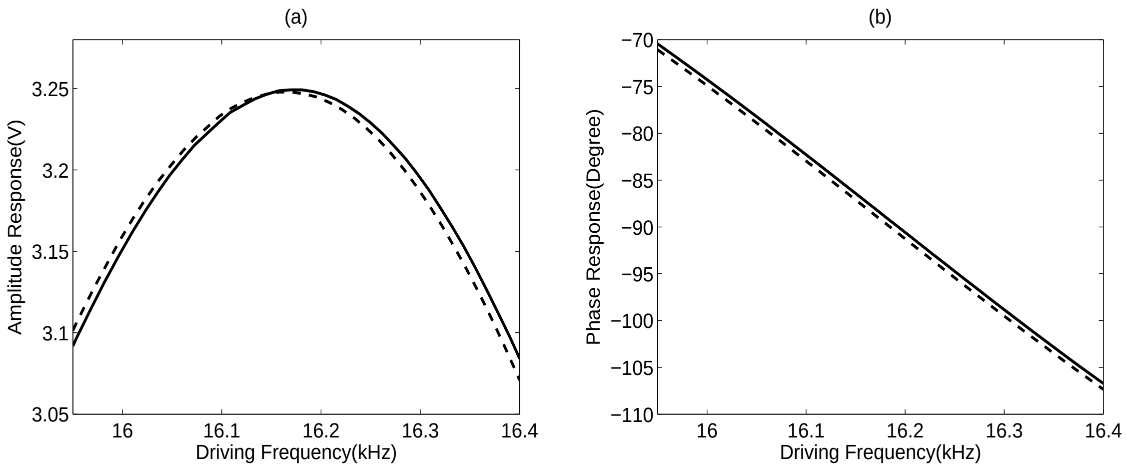

Figure 3.17: Comparison of amplitude (a) and phase (b) response of the equivalent linear resonator circuit before (solid line) and after (dashed line) an 0.05% change in resonant frequency with $V_d = 2.8V$.

Since the resonant frequency of the linear resonator can be achieved without continuous sweep of the driving frequency, the linear circuit is directly driven by the bench-top signal generator with the resonant frequency obtained in Figure 3.17. To test the ability of the system to detect a change in resonant frequency of 0.05%, the switch was closed to decrease the resonant frequency. The time at which this occurred is shown as the vertical line in Figure 3.18. The amplitude response in Figure 3.18 (a) does not change much following the resonant frequency change while Figure 3.18 (b) illustrates that before this event the resonators phase shift was the expected -90 degrees. The figure also shows the expected change in phase shift after the resonant frequency has changed. Overall the results in Figure 3.18(b) suggest that by averaging these results a system could be created that detects a change in resonant frequency of 0.05%, but that this is close to the limit of sensitivity of the system.

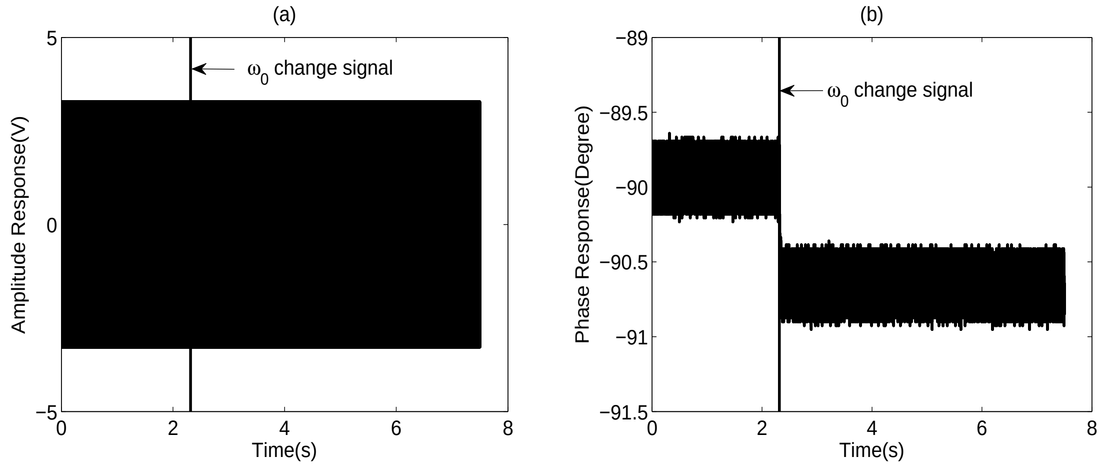

Figure 3.18: The measured transient amplitude (a) and phase (b)behaviour of the linear resonator circuit at resonance and the resonant frequency changes by 0.05% with $V_d = 2.8V$.

3.4.3 Long transient behaviour

To compare with the linear resonator, the initial investigation of the response of the hardening Duffing circuit starts with a large driving force which can lead to large amplitude and phase changes at a jump frequency following a resonant frequency change.

The experiment with the two slightly different values of capacitance was performed by sweeping the driving frequency from very low frequency until the phase response of the resonator changes suddenly, see Figure 3.19. As expected the increase in capacitance has caused a reduction in frequency at which the amplitude and phase response of the system changes suddenly. The black rectangles in Figure 3.19 suggest that if the Duffing resonator is being driven at this jump frequency then the resonant frequency change will result in a change in phase of more than 100 degrees which is increased dramatically compared with the linear resonator with the same change in resonant frequency.

Based on the phase response from Figure 3.18(b), the higher jump frequency can be obtained. This can then be programmed into the FPGA so that it stops increasing the DDS output frequency when this frequency is reached. The phase response can not be used as the sweep

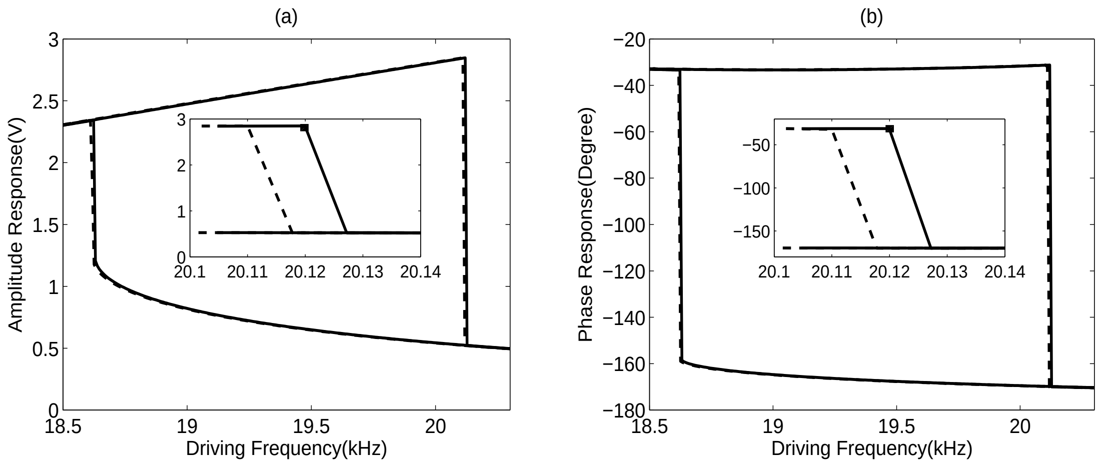

Figure 3.19: Comparison of amplitude (a)and phase (b)response of the hardening Duffing circuit before (solid line)and after (dashed line) an 0.05% change in resonant frequency with $V_d = 2.8V$. The inset shows the detailed amplitude and phase responses near the higher jump frequency.

reference in this case as the phase response is quite flat before reaching the jump point. The DC voltage representing the phase has been recorded whilst the FPGA first finds the jump frequency and then a change in resonant frequency is induced. Figure 3.21 shows four sets of the transient behaviour following the resonant frequency change. Under the same conditions, the experiments have been performed repeatedly and the expected large amplitude and phase changes have been observed. However, the transient behaviour varies dramatically in terms of the response time. This confirms the simulation results in Chapter 2 that large driving forces are likely to cause varied transient responses after the small parameter change.

3.4.4 Over-critical driving voltage

Previous simulated analysis in Section 2.2 has shown that the undesirable temporal response can be avoided by driving the system slightly greater than the critical driving force which will be called over-critical driving voltage. In this section, the Duffing circuit will be driven with an over-critical driving voltage to implement a reliable sensor. Figure 3.21 shows that the system is driven by a smaller voltage than the one in Figure 3.19 so that the hysteresis loop is small and the high amplitude stable state separates quickly from the unstable state. For the same change in resonant frequency, the system will not start in the region of phase space close

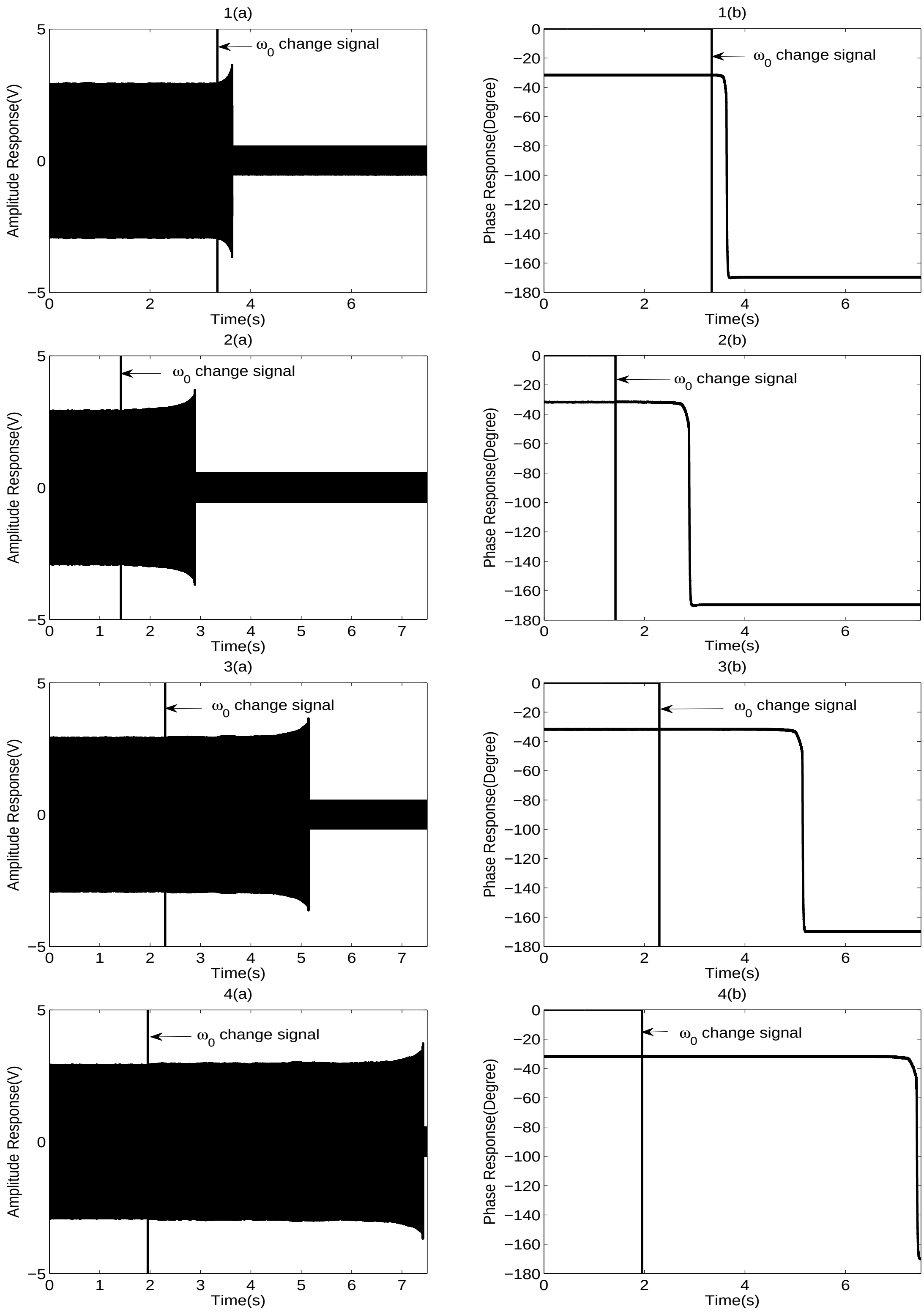

Figure 3.20: Four sets of measured transient amplitude (a) and phase (b)behaviour of the hardening Duffing resonator at higher jump frequency and the resonant frequency changes by 0.05% with $V_d = 2.8V$.

to the unstable state and an immediate collapse in amplitude is therefore expected.

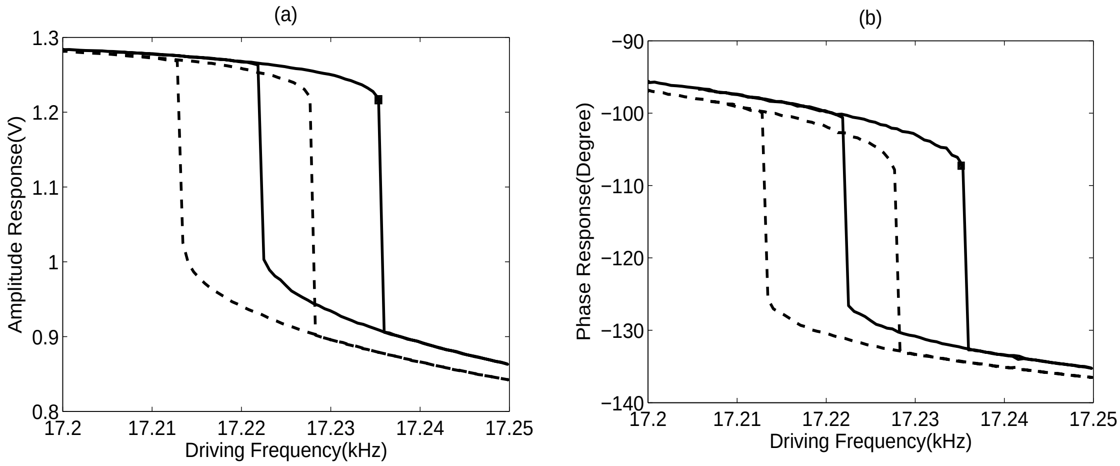

Figure 3.21: Comparison of amplitude (a)and phase (b)response of the hardening Duffing circuit before (solid line)and after (dashed line)an 0.05% change in resonant frequency with $V_d = 1V$.

Figure 3.22 shows the phase response obtained from a typical experiment implementation. Since the whole process takes around ten minutes, it would be very difficult for the data acquisition device to capture all the real time samples continuously. Instead, 1MHz sampling rate for the phase measurement has been used and therefore the x-axis in Figure 3.22 is the sample number rather than time. This figure clearly shows that initially, step I, the detected phase response is changing as the system changes the output frequency from the DDS chip. This phase change ends when the system observed the desired phase response of $-107°$ and during step II the resonator is then driven at a constant frequency. Finally the resonant frequency of the system is changed by 0.05% at sample 58 and there is a large change in detected phase. Compared with phase response to the same resonant frequency change of the linear resonator in Figure 3.18, the results in Figure 3.23 show that using a Duffing resonator it is much easier to detect a change in resonant frequency.

Similar tests are performed with the softening Duffing circuit by adding a unit gain inverting amplifier in the non-linear feedback loop. Figure 3.24 shows that a reduce in the resonant frequency will cause the amplitude and phase response shift towards the smaller frequencies as well for the softening circuit. If the resonator is driven at the higher jump frequency indicated by the rectangles in Figure 3.24, jumps in amplitude and phase are expected to be observed.

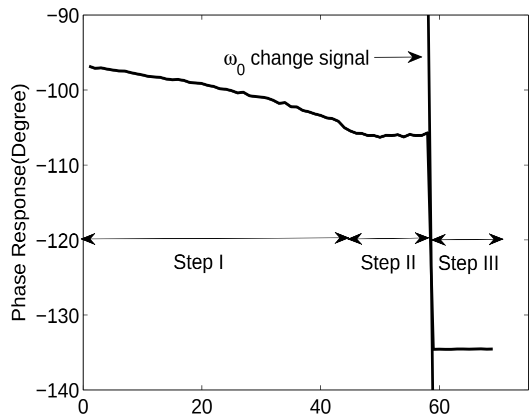

Figure 3.22: Measured transient responses of a Duffing resonator to (I) Sweep up frequency to the higher jump frequency;(II) Keep frequency unchanged and waiting for the resonant frequency change signal; (III) After the resonant frequency changes by 0.05% the phase response suddenly jumps.

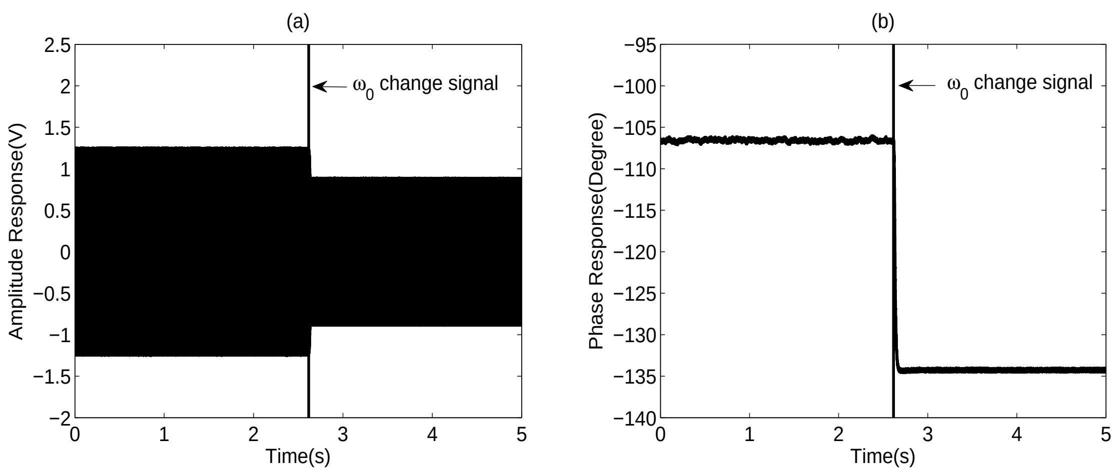

Figure 3.23: The measured transient amplitude (a) and phase (b)behaviour of the hardening Duffing resonator at higher jump frequency and the resonant frequency changes by 0.05% with $V_d = 1V$.

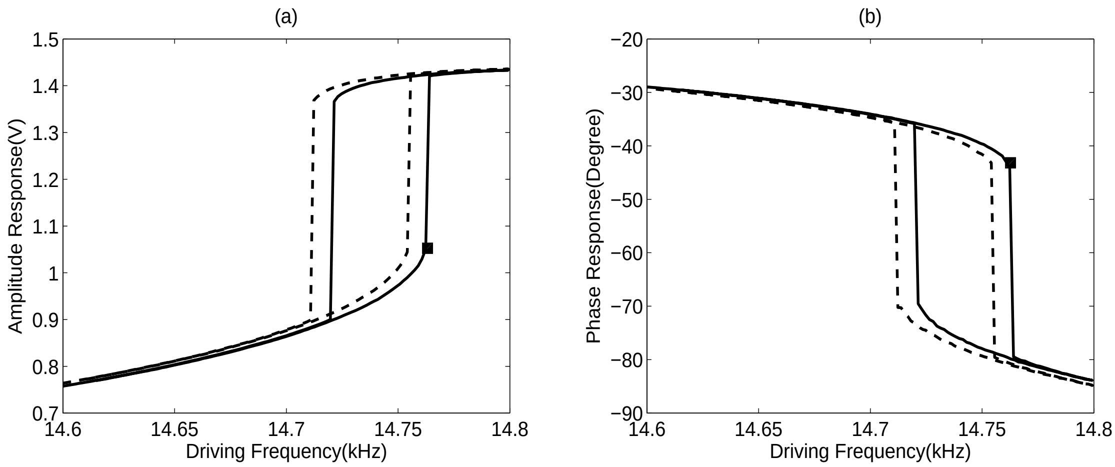

Figure 3.24: Comparison of amplitude (a) and phase (b) response of the softening Duffing circuit before (solid line) and after (dashed line) an 0.05% change in resonant frequency with $V_d = 1.22V$.

Since the initial condition for the jump frequency is on the lower stable state, the continuous sweep is not required to achieve the jump frequency. The softening resonator can be driven at the jump frequency obtained in Figure 3.24 directly with a signal generator. Figure 3.25 shows the expected jump in amplitude as well as phase response. The only difference from the hardening resonator is that the amplitude is increased following the resonant frequency change.

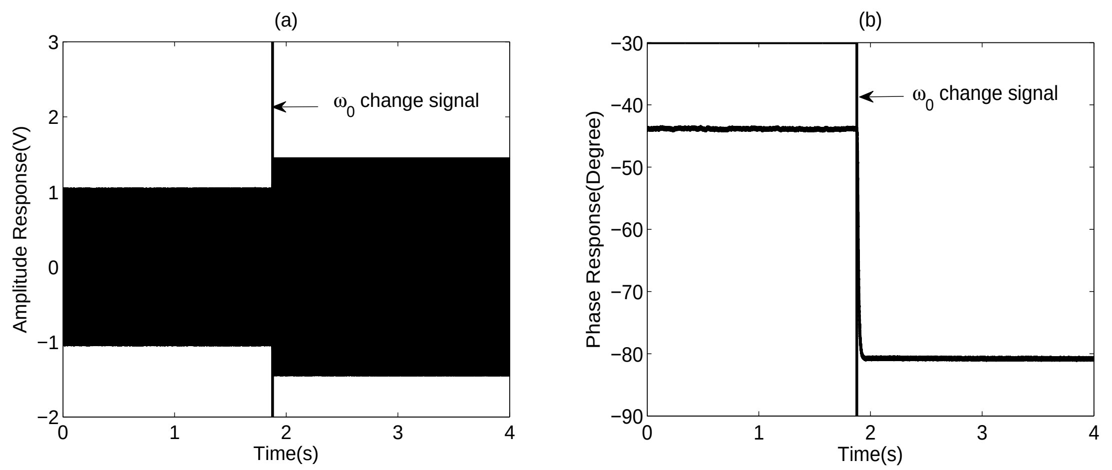

Figure 3.25: The measured transient amplitude (a) and phase (b)behaviour of the softening Duffing resonator at higher jump frequency and the resonant frequency changes by 0.05%. with $V_d = 1.22V$.

A strategy has been described to find the frequency at which the amplitude and phase of the non-linear resonator changes extremely rapidly. As expected a 0.05% change in resonant frequency of a Duffing resonator has been shown to create a dramatically larger change in amplitude and phase than the equivalent linear resonator when driven by an over-critical voltage.

3.4.5 Sub-critical driving voltage

Although an over-critical driving voltage shows benefit with large amplitude and phase change following a change in resonant frequency, the amount of the change can not be calculated from the phase change. The reason for this is because the discontinuity in amplitude and phase means that any changes in resonant frequency are likely to cause large phase changes but with similar magnitude. In this way, this can be considered as good alarm system to sense any change in resonant frequency but it is difficult to quantify the amount of the frequency change from the observed phase change. Therefore, if the change in resonant frequency is required then the phase response needs to be a continuous function of the resonant frequency. This can be achieved by reducing the driving voltage so that it is just below the critical value. Since the critical driving voltage is the threshold value to create a jump in amplitude and phase, those driving voltage just below this value will have a continuous phase response but also with a large value of $\frac{d\phi}{d\omega}$. These driving voltage will be referred to as sub-critical driving voltage in the following discussion.

For the Duffing resonator, if the driving force is smaller than the critical force then there is no hysteresis loop but the phase response is becoming increasingly vertical (Figure 3.5). To compare the phase change rate with linear resonator, Figure 3.26 illustrates the trend of the $\frac{d\phi}{d\omega}$ for the hardening and softening Duffing resonator. The linear curves in Figure 3.26 (a) and (b) are identical and the maximum phase change rate occurs at the resonance with a peak value of approximately $0.085°/Hz$. Small driving force for the non-linear resonator gives similar maximum $\frac{d\phi}{d\omega}$ as the linear one, as the driving force increases, the benefit of the non-linear resonator is more obvious.

To compare the sensitivity of the linear resonator and the Duffing resonator driven by the sub-critical driving voltage, an even smaller amount of resonant frequency change 0.005% has

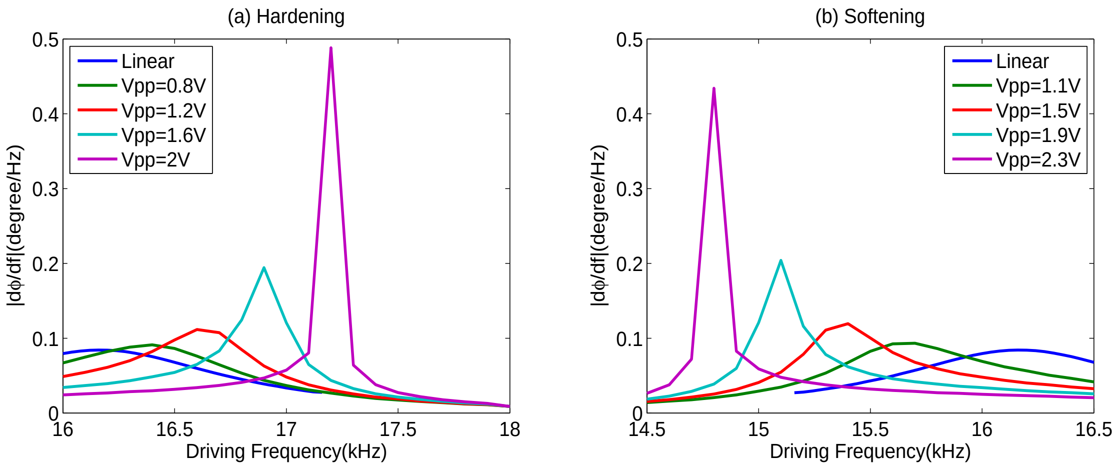

Figure 3.26: Phase change rate versus driving frequency for the hardening (a) and softening (b) resonator circuit.

been implemented by choosing C_3 to be $0.01\%C_2$. The transient phase response following this resonant frequency of the linear circuit is shown in Figure 3.27 and the phase noise makes the phase change quite difficult to detect which is less than a quarter of the noise level.

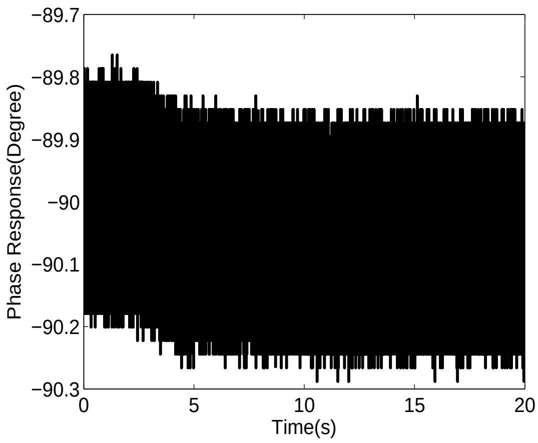

Figure 3.27: The measured transient phase response of the linear resonator at resonance following a change in resonant frequency of 0.005%.

The calculated critical driving voltage with the improved model of the Duffing circuit is $V_{d\_c} = 0.963V$ and Figure 3.15 shows no hysteresis loop but with high $\frac{d\phi}{d\omega}$. To identify a desirable sub-critical driving voltage, the driving voltages near $V_{d\_c} = 0.963V$ have been investigated with a two step search scheme. For the first step, two driving forces are chosen: one is definitely less than critical and the other one is obviously more than critical. Then the response of the driving force which is the mid-point of those two is recorded, and the next one depends on the smoothness of $\frac{d\phi}{d\omega}$ of the third driving force's response. The range of the potential critical driving voltage is narrowed down by looking for the mid-point between responses with and without a jump. Figure 3.28(a) shows this process and the driving frequencies have been scaled by the maximum $\frac{d\phi}{d\omega}$ frequencies for each driving voltage. It clearly shows a significant difference between the phase response of $0.95V$ and $0.975V$ at the maximum $\frac{d\phi}{d\omega}$ point. Therefore, it can be concluded that the critical driving voltage is within the range between these two voltages. A second search in this range is repeated with the same method as shown in Figure 3.28(b).

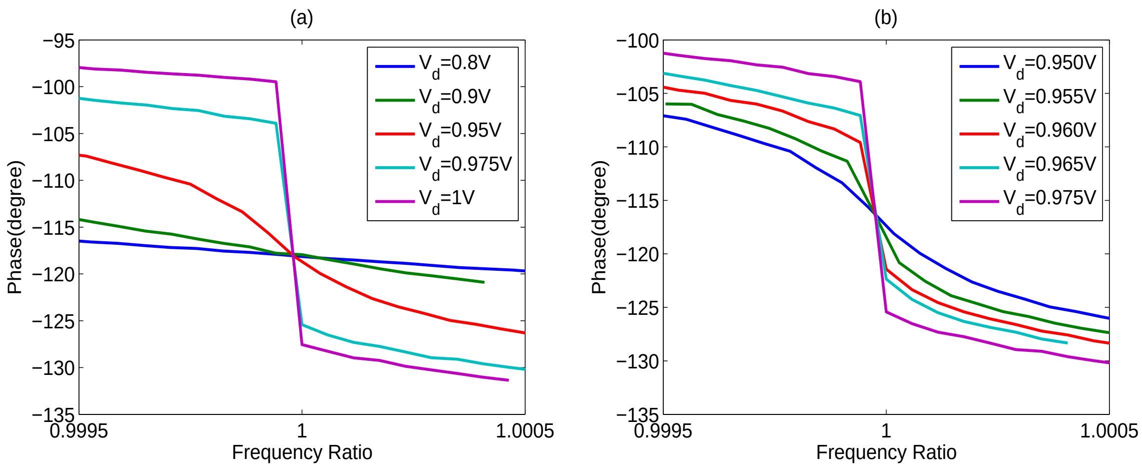

Figure 3.28: Phase response versus frequency ratio of the hardening Duffing resonator with different driving voltages.

Figure 3.28 shows that as the linear region of the phase response is smaller as when the phase change slope is higher which means that the dynamic range is reduced when the sensitivity is enhanced. In addition, it is very difficult to distinguish between a small jump and the continuous phase change but with high $\frac{d\phi}{d\omega}$ as shown in Figure 3.28 so the transient phase responses for $V_d = 0.95V$ and $V_d = 0.955V$ following the 0.005% change in resonant frequency are both recorded in Figure 3.29. The phase changes for two sub-critical driving voltages are approximately 1.7 degrees and 5 degrees respectively which means that $\frac{d\phi}{d\omega}$ has been increased significantly compared with the phase change of the linear resonator at resonance in Figure 3.27. Although the comparison of $\frac{d\phi}{d\omega}$ in Figure 3.26 shows that the peak value of the phase change rate of non-linear resonator can be increased by a factor of 5 compared with the linear response, the magnitude of the maximum $\frac{d\phi}{d\omega}$ is not accurate because of the 100Hz

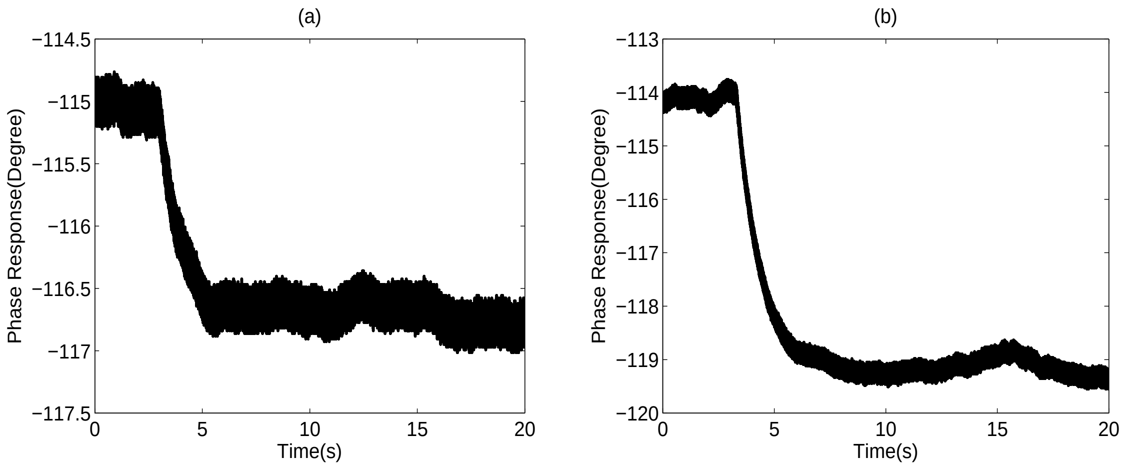

Figure 3.29: The measured transient phase response of the hardening Duffing resonator driven with $V_d = 0.95V$(a) or $V_d = 0.955V$(b) and the resonant frequency changes by 0.005%.

driving frequency intervals. In fact, the amount of phase change has been increased by more than 20 times when the hardening Duffing circuit is driven by a sub-critical voltage but the phase noise level is 0.5 degree which is similar to the linear resonator.

The same method of finding the sub-critical driving force and corresponding frequency with high $\frac{d\phi}{d\omega}$ using softening Duffing resonator as shown in Figure 3.30. Due to the positive non-linear damping term caused by the phase shift θ from the multipliers, the amplitude response and therefore the non-linear restoring force is smaller for the softening Duffing resonator if driven with the same voltage level with the hardening resonator. Consequently, the softening system has a greater critical driving voltage than the hardening one.

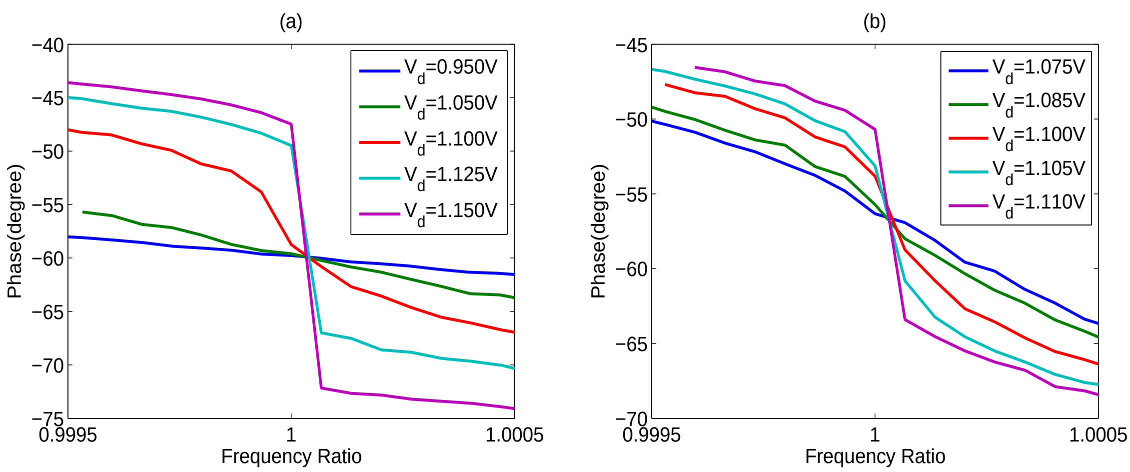

Figure 3.30: Phase response versus frequency ratio of the softening Duffing resonator with different driving voltages.

Figure 3.31 shows an example of the transient behaviour following the same resonant frequency change driven by a sub-critical voltage $V_d = 1.1V$. This 0.005% change in resonant frequency leads to approximately 2 degrees phase change which has been increased by a factor of 20 than the equivalent linear resonator approximately.

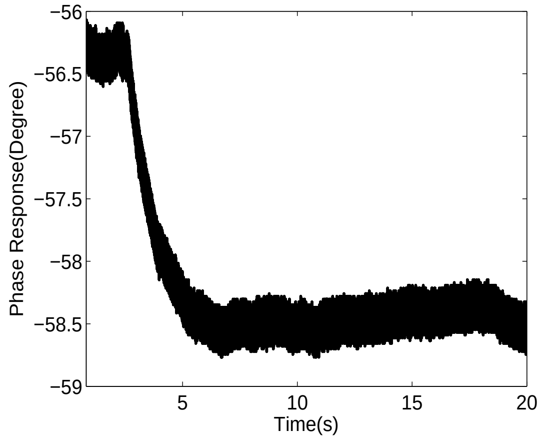

Figure 3.31: The measured transient phase response of the softening Duffing resonator driven with $V_d = 1.1V$ and the resonant frequency changes by 0.005%.

Comparing the raw data of the phase changes following the same resonant frequency change of different type of resonators in Figure 3.27, Figure 3.29 and Figure 3.31, it shows that both hardening and softening Duffing resonators show much larger step change than the linear resonator. The sensitivity of non-linear resonators driven by the sub-critical voltages depends crucially on the driving voltage and frequency. Although Figure 3.29 and Figure 3.31 shows different phase change following the same resonant frequency, there is no difference to implement a resonant frequency sensor using hardening or softening Duffing resonator driven by sub-critical driving voltage.

If a digital filter is available for the post processing further investigation of the noise might give a better comparison of these experimental results. To analyze the phase noise source, the power spectrum for voltage representing the phase response of the linear resonator is shown in Figure 3.32. Ideally, the spectrum of the phase response only contain DC component but Figure 3.32 shows that there are some high frequency noises. A second order Butterworth low pass filter with 5Hz cut-off frequency is implemented by MATLAB.

The filtered data of the linear resonator are shown in Figure 3.33(a) which gives a clear step

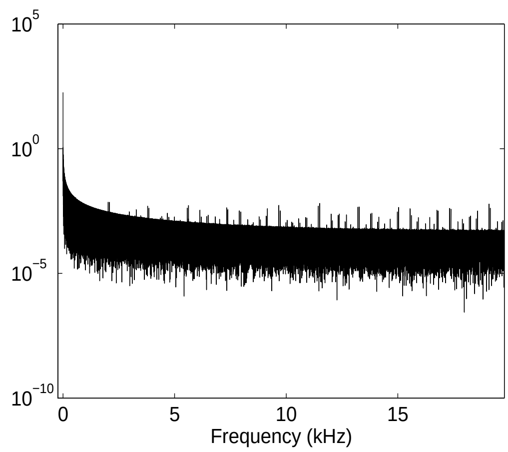

Figure 3.32: Power Spectrum for the output voltage representing the phase response of the linear resonator.

of around 0.06 degree phase change. After filtering, the phase response variation is reduced to approximately 0.01 degree. For the raw data in Figure 3.29(a), there is phase drift with about 0.3 degree after the same low pass filter process which is about 30 times greater than the linear drift. The filtered data for the non-linear resonators have similar signal to noise ratio to the linear resonators. There are two possible reasons for this increased phase variation. One reason could be that as the phase change rate is increased, the same frequency drift of the driving signal will result in more phase fluctuation. The 0.005% change in resonant frequency equals to $0.8Hz$ and the hardening resonator driven by sub-critical voltage shows a 1.5 degrees phase change following this amount of resonant frequency. Consequently, it can be predicted that if the driving frequency drifts about $0.16Hz$ the phase response will fluctuate by 0.3 degree which is plausible. The other reason is that the component values of the Duffing circuit are not perfectly stable either. No matter which mechanism caused the problem, however, it is always better to have a large signal to noise ratio as early as possible so that it can eliminate the inferences. Moreover, the system will be slowed down by this extra filtering.

3.4.6 Self-oscillation

During the characterisation of the hardening Duffing circuit, self-oscillation has been observed when the driving frequency is swept up and therefore the amplitude response is increased to a large value. This is probably caused by the phase shift of the multiplier. In Section 3.3.3,

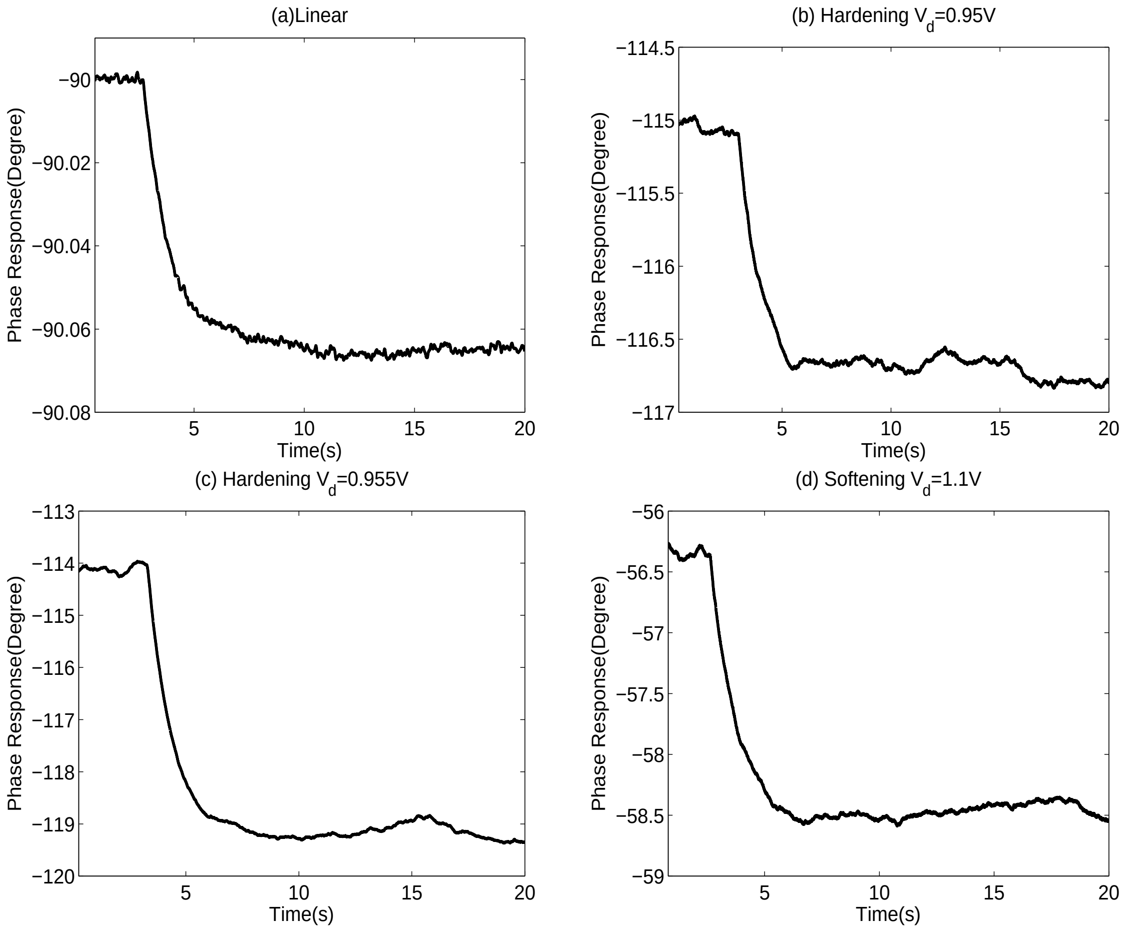

Figure 3.33: The filtered transient phase response of the linear(a) hardening (b,c) and softening (d) Duffing resonator following the resonant frequency changes by 0.005%.

the extra phase shift from the multipliers have been identified as the cause of the non-linear damping term in the Duffing model (Equation 3.16). For the hardening Duffing circuit, this non-linear damping term is negative and therefore the linear damping term will be partially cancelled if the ”displacement” is not too large. As magnitude of the output response increases a threshold value with a sufficient driving voltage, the non-linear damping term will cancel the linear damping term entirely so that the positive feedback loop causes the oscillation. Figure 3.34 shows a $1.5Hz$ change in the oscillation frequency has been observed following the same parameter change which is equivalent to a 0.005% change in resonant frequency of the Duffing resonator.

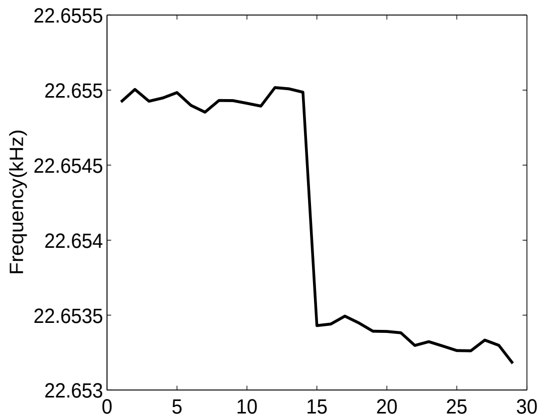

Figure 3.34: The measured oscillation frequency response of the hardening Duffing circuit when the resonant frequency changes by 0.005%.

Figure 3.34 also shows that oscillation frequency of the system does not remain constant before or after the parameter change which means that the system itself is not perfectly stable. The frequency noise is about $0.3Hz$ and the relative change to the resonance frequency is approximately $15ppm$. The temperature coefficient of the resistors used in the Duffing circuit is 100ppm/K which means that the frequency drift is probably caused by the temperature fluctuations. This also confirms the instability of the circuit itself is one of the causes for the observed phase variation when driven with the sub-critical voltages in Section 3.4.5. In this way, driving the Duffing resonator with the sub-critical voltage can be considered to be a good method to increase the sensitivity of the system in principle.

The magnitude of the Duffing self-oscillation is limited by the power rails so that the op-amps and other circuit component will not be damaged by the large voltage or current. It can be used as a technique to detect the parameter change of an electronic system. However, this method will not be used for the micro-mechanical system since the maximum displacement of the resonator needs to be restricted to less than the gap between the combs otherwise positive feedback will cause over-excitation and therefore destroy the resonator.

3.5 Summary

To confirm the simulated transient behaviour in Chapter 2 experimentally, a Duffing circuit has been designed with similar resonant frequency and Q value to the micromechanical resonator. The parameter values of the Duffing resonator circuit have been extracted and both softening and hardening models of the circuit have been confirmed with an extra nonlinear damping term caused by the phase shift of the multipliers. The experimental results fit with the improved model very well.

The transient behaviour following a resonant frequency change when the resonator is driven by a large voltage shows the long and varied response times. This proves that the simulated long transient responses in Section 2.2 are not caused by the numerical errors. This behaviour is not desired since the response time of a sensor is also essential as well as its sensitivity. This problem has been eliminated by driving the circuit with the over-critical voltage and the Duffing resonators show a much larger instant phase change following the same resonant frequency change at the higher jump point compared with the linear resonator. This is a good alarm system, but it can not quantify the resonant frequency change.

The resonant frequency change can be estimated by driving the resonator with sub-critical voltage because the phase response is continuous but with large phase change rate. The experimental results gave a larger phase change than the equivalent linear circuit for the same resonant frequency change. The phase noise of the raw data, includes the high frequency noise and the phase drifts resulting from the instability of the driving system or the resonator itself, are of similar magnitude for linear and non-linear resonator. If the high frequency noise is removed by a lowpass filter, the phase variation of the non-linear resonator is increased which means that the signal to noise ratio is not improved when using the non-linear resonator. However, it is always beneficial to have a large signal to noise ratio as early as possible and there is a disadvantage of the filter which will slow down the speed of system.

The self-oscillated Duffing circuit has shown frequency drifts which prove that the phase variation with sub-critical voltage might be caused by the instability of the circuit components. The Duffing oscillator can be implemented as a sensor to detect a parameter change potentially but this will not be used for the MEMS resonator since it might break.

Chapter 4

Actuation, measurement and characterisation of the micromechanical resonator

4.1 Introduction

A MEMS sensor is composed of a micromechanical resonator and electronics for actuation and readout. The micromechanical resonator used in this project was designed by Dr Carl Anthony from University of Birmingham and the devices were fabricated by QinetiQ using bulk micromachining technology. Discrete circuits instead of integrated ones are used for driving and readout electronics in this project as it is easier to modify the circuit at the first stage of implementing the sensor. It is possible to design an integrated circuit which can be packaged with the micromechanical resonator based on the discrete electronics.

4.2 Design of the micromechanical resonator

If the voltage across two plates, one of the plate is fixed while the other one is movable structure, is V then the electrostatic force between the plates is

$$F = \frac{V^2}{2}\frac{dC}{dx} \tag{4.1}$$

where $\frac{dC}{dx}$ is the capacitance change with respect to the displacement. To make sure that the driving force of the resonator is independent of the displacement, the interdigitated comb structure as shown in Figure 4.1 is used for the design of the resonator since such a comb structure can give a constant $\frac{dC}{dx}$ [56, 57]. If there are n pairs of static and movable combs and the gap between them is g, the capacitance of the whole system is

$$C = n\frac{\epsilon(l + x)d}{g} \tag{4.2}$$

where ϵ is the permittivity, l is the initial overlap and d is the thickness of the comb. The capacitance is proportional to the displacement which means that $\frac{dC}{dx}$ is constant. Consequently, the electrostatic force created by the voltage applied across one of these capacitances is independent of the displacement of the resonator. The movable comb normally is grounded and therefore the force applied on the resonator depends on the voltage applied on the static combs. Figure 4.1 shows that there are a pair of opposing driving combs forming a push and pull configuration. The resonator is excited by the difference between the electrostatic forces on these two static combs.

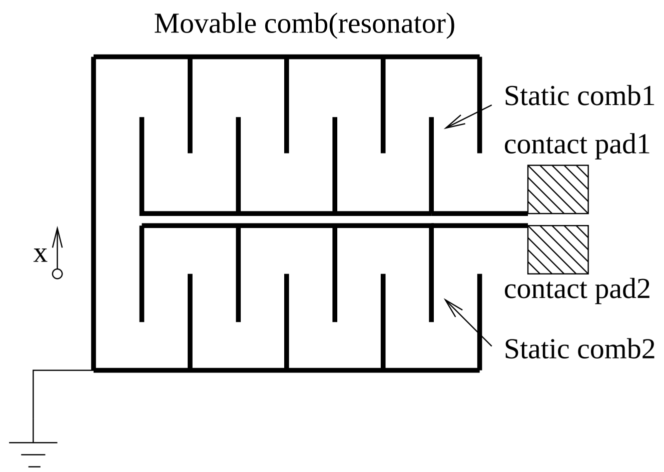

Figure 4.1: Simplified schematic diagram for the resonator and a pair of static comb.

The readout combs are of the same structure as the driving combs shown in Figure 4.1. The only difference is that the voltage applied on the static comb is a DC voltage V_s. Due to the movement of the resonator, the capacitance C of the whole system is varying while the voltage across the combs remains constant. Consequently, the amount of the electrical charge

Q on the comb is changing which is a current signal:

$$i(t) = \frac{dQ}{dt} = \frac{d(V_s C)}{dt} = C\frac{dV_s}{dt} + V_s\frac{dC}{dt} = V_s\frac{dC}{dx}\frac{dx}{dt} = V_s\frac{dC}{dx}\dot{x} \tag{4.3}$$

Since $\frac{dC}{dx}$ is independent of the displacement, the resulting current signal using this capacitive readout is proportional to the velocity of the resonator. There are a pair of sensing combs as well, and output signals from opposing static combs are the same magnitude but 180° out of phase. The readout electronics convert the output current to voltage signals which will be discussed in the next section.

A scanning electron microscope (SEM) image of the micromechanical resonator that has been used in the present study is shown in Figure 4.2. The resonators have been designed with four comb capacitors so that they can be used in two differential pairs, one pair to drive the resonator and one pair to detect the resulting motion. Each pair of combs are identical and the simplified schematic comb structure is shown in Figure 4.1. This resonator has four contact pads, each of which is connected to one side of one of four comb capacitances. The other side of each capacitance is formed by a comb that is attached to a movable frame supported by a spring in each corner of the movable frame. These supporting springs also form the electrical connection between the movable frame and an electrical connection to the substrate and this connection is used to ground the movable part of the resonator. [58].

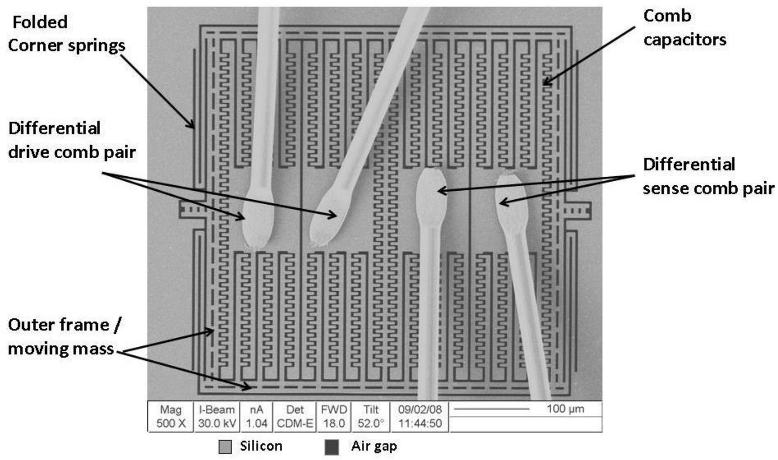

Figure 4.2: An SEM image of a resonator showing the four contact pads and comb capacitors.

4.3 Actuation and measurement electronics

There are two ways to apply the driving force, the simple one is to apply a cosine voltage $V_{ac}\cos\omega t$ on one comb and leave the other one free which is called single-ended driving method. The electrostatic force applied to the resonator is then

$$F_0 = \frac{1}{2}(V_{ac}\cos\omega t)^2\frac{dC}{dx} = \frac{1}{4}(1 + V_{ac}^2\cos 2\omega t)\frac{dC}{dx} \tag{4.4}$$

The frequency of the effective force is twice the driving frequency, and the magnitude of the force is proportional to the squared driving voltage.

The other driving method is called differential drive: The voltage applied on one of the comb is $V_{DC} + V_{ac}\cos\omega t$ while the voltage applied on the other comb is $V_{DC} - V_{ac}\cos\omega t$. The effective force resulting from the voltages on each comb is

$$\begin{aligned} F_+ &= \frac{1}{2}(V_{DC} + V_{ac}\cos\omega t)^2\frac{dC}{dx} \\ F_- &= \frac{1}{2}(V_{DC} - V_{ac}\cos\omega t)^2\frac{dC}{dx} \end{aligned} \tag{4.5}$$

The overall force on the resonator is the difference between the above two forces:

$$F_0 = F_+ - F_- = 2V_{DC}V_{ac}\cos\omega t\frac{dC}{dx} \tag{4.6}$$

Compared with single-ended driving, differential driving has no unwanted static force and the driving frequency is the same as the frequency of the voltage applied on the comb. The magnitude of the force can be adjusted linearly by varying V_{DC} or V_{ac}. Figure 4.3 shows the schematic diagram which generates the driving voltages. V_{ac} is the output from a signal generator and V_{DC} can be adjusted by changing the tapping point position of the variable resistor. Then the driving voltages $V_{DC} + V_{ac}\cos\omega t$ and $V_{DC} - V_{ac}\cos\omega t$ are generated by a few summing operational amplifiers (Op-amp).

A current that is proportional to the instantaneous velocity of the resonator can be detected by the each sensing comb. The comb structure means that the currents from the opposing readout are same magnitude but $180°$ phase difference. Each current can be converted to

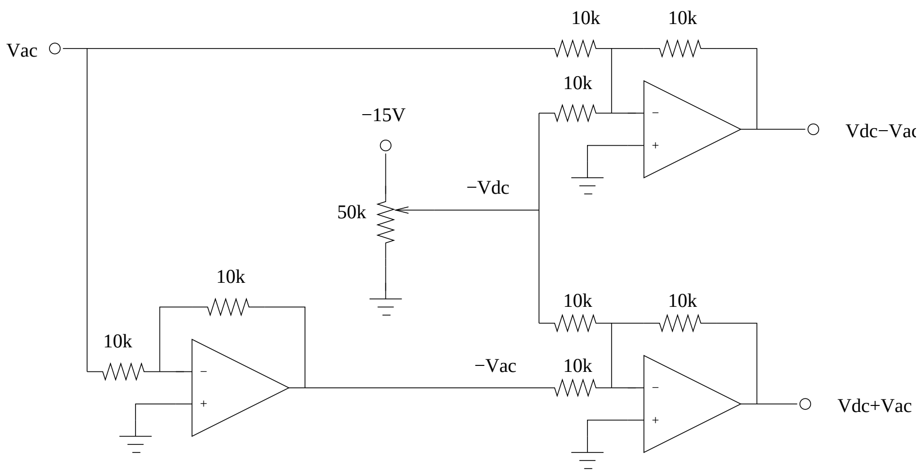

Figure 4.3: The electronic circuits for generating differential drive voltages.

a voltage that can be used to detect this motion using the electronic circuit in Figure 4.4. A transimpedance amplifier is used to convert the output current to voltage with a gain of

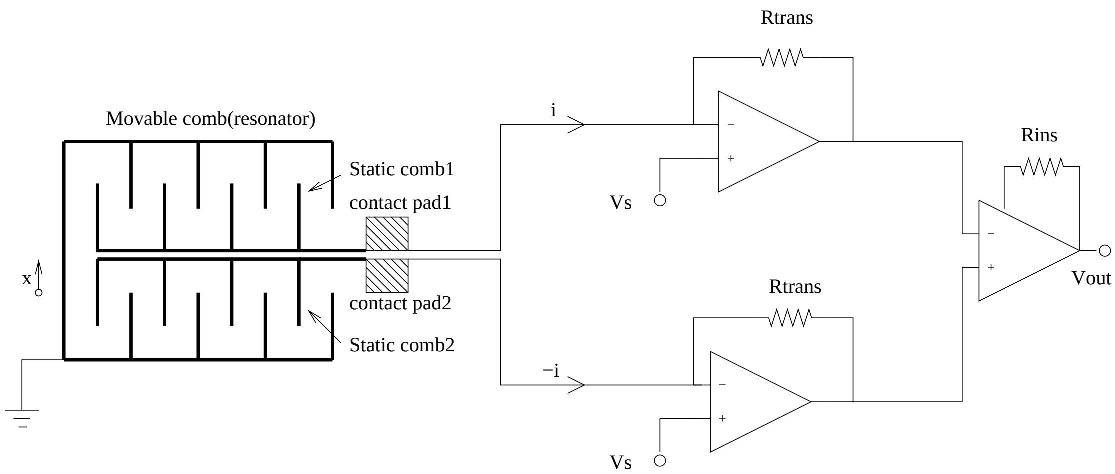

Figure 4.4: Differential readout electronic circuit to convert the output current to amplified voltage.

R_{trans} which is $1M\Omega$ in this project. An instrumentation amplifier is used after these two transimpedance amplifier to implement differential readout. The bias DC voltage is removed and the extra gain is added at this stage. The output voltage from the instrumentation amplifier is

$$V_{out} = G_{inst}[(V_s + iR_{trans}) - (V_s - iR_{trans})] = 2G_{inst}R_{trans}i \tag{4.7}$$

where G_{inst} is 10 in the following experiments and this is determined by the value of R_{ins} in Figure 4.4. Recall to Equation 4.3, the magnitude of resonator displacement can be calculated from V_{out} with Equation 4.8.

$$x = \frac{V_{out}}{2G_{inst}R_{trans}V_s j\omega \frac{dC}{dx}} \tag{4.8}$$

If one of the static combs is required to use for testing, single-ended readout is also feasible by connecting one of the inputs of the instrumentation amplifier to the V_s. The difference between these two readout methods is simply that the magnitude of the single-ended output voltage is half of the other one.

4.4 Characterisation of the micromechanical resonator

4.4.1 Feedthrough analysis

Due to the proximity of driving and readout channels, there is capacitive coupling between these channels which is called feedthrough in the thesis. The existence of the feedthrough means that the driving channels would interfere with readout channels and therefore the output from the readout channel is the sum of signal resulting from the movement of the resonator and the feedthrough signal due to the capacitive coupling with the driving channel.

If the single-ended driving method is used, the frequency of the resonator movement is doubled compared with the driving frequency. Consequently, the undesired feedthrough signal can be easily removed by a bandpass filter in place. For the differential drive, in theory, the feedthrough signal caused by the driving voltage V_{AC} on one comb can be cancelled by the feedthrough signal caused by the driving voltage $-V_{AC}$ on the other driving comb. This is true only when the two driving channels have the same coupling capacitances with the readout channel. However, practice experience shows that the coupling capacitances are not identical. The feedthrough signals of the resonator have been measured with single-ended drive for each comb and differential drive respectively. The readout combs are connected to the ground so that the measured voltage is the feedthrough voltage without any signal resulting from the movement of the signal. Figure 4.5 shows the feedthrough signal resulting from each driving comb with single-ended drive and the differential drive. The feedthrough signal of differential drive has been reduced by a factor of three or four. It also shows that the feedthrough signals for each driving comb with single-ended drive are different. The dots in Figure 4.5 show the difference of feedthrough signals from each comb with single-ended drive and it is the same as the feedthrough signal due to the differential drive. This explains why the differential drive can not fully eliminate the feedthrough signal.

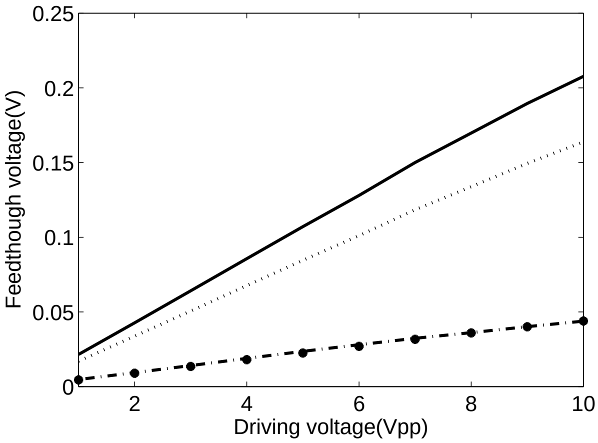

Figure 4.5: Comparison of feedthrough voltages of single-ended drive (solid line: comb A; dotted line:comb B) and differential drive (dash-dot line).

When the resonator is driven at the atmospheric pressure with differential drive, the minimum detectable output response magnitude $1mV$ requires V_{ac} to be $1.5V_{pp}$ if the V_{DC} is set to $4V$ in a typical driving mode. Figure 4.5 shows that the feedthrough signal due to $1.5V_{pp}$ differential drive is about $7mV$ which is much larger than the expected signal from the movement of the resonator. To avoid the interference of the feedthrough signal, for any experiment with direct drive it is better to choose single-ended drive because the desired movement output frequency is twice the feedthrough signal frequency which can be filtered easily.

4.4.2 Natural quality factor of the micromechanical resonator

The initial experiment was carried out in a vacuum to find the resonant frequency of the sample. Figure 4.6 gives the amplitude and phase response of the output voltage which represents the velocity of the resonator. The resonance peak is at $17.423kHz$ with a magnitude of $5mV$. The quality factor Q can be calculated with $-3dB$ frequencies which gives Q value around 1300. The expected phase response is observed with $0°$ at resonance and approaching $\pm 90°$ when the driving frequency is off resonance.

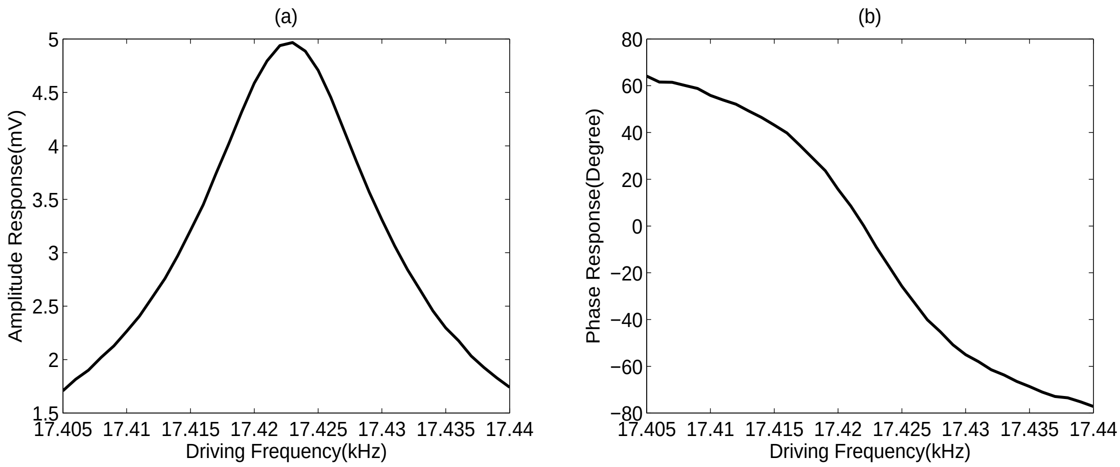

Figure 4.6: The amplitude (a) and phase response (b) of the resonator at a pressure of $7.7Pa$ with single-ended drive $V_{ac} = 1V_{pp}$.

If the resonator is exposed to the atmospheric pressure $10^5 Pa$, a much larger driving force is required to see the resonance peak since the damping term is increased significantly. Low Q means the amplitude response will be flat and wide as shown in Figure 4.7. It is difficult to tell the exact value of resonant frequency and Q drops to around 5.5 which is a bit lower than the designed value of 10 for air pressure.

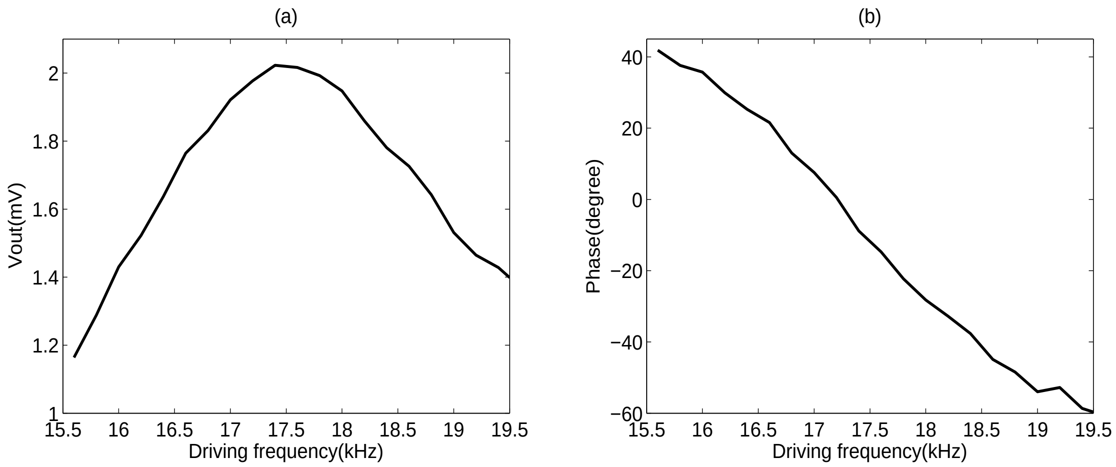

Figure 4.7: The amplitude (a) and phase response (b) of the resonator in air with single-ended drive $V_{ac} = 10V_{pp}$.

The quality factor of the resonator is closely related to the ambient pressure level. A series measurement have been performed to calculate the Q value under different pressures by taking the $-3dB$ frequencies. The relationship between the quality factor Q and ambient pressure is shown in Figure 4.8.

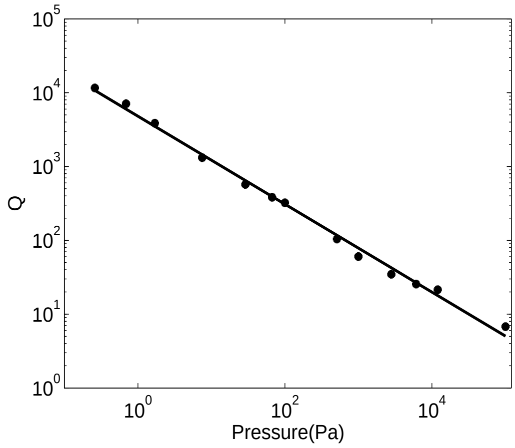

Figure 4.8: Relationship between the Q value and the ambient pressure.

Figure 4.8 shows that the Q is proportional to Pressure when both of them are plotted in the logarithm scale. A linear fit line is drawn in the figure and Equation 4.9 gives the relationship between the Q value and the pressure. This will provide a quick estimation to obtain the natural Q based on the ambient air pressure in the future experiments.

$$Q = 4816 \times Pressure^{-0.596} \tag{4.9}$$

4.4.3 DC voltage dependent resonant frequency (e-spring)

To confirm that the differential driving force obeys Equation 4.6 in Section 4.3, three different DC voltages V_{DC} are applied. The resonance is expected to occur at the same frequency but with different peak amplitudes because of different driving forces. The amplitude responses in Figure 4.9(a) shows the peak amplitude value increases as the V_{DC} grows as expected. However, there is a surprising resonant frequency change resulting from that. The zero degree phase shift point which indicates the resonant frequency in Figure 4.9(b) also confirms that DC voltage applied on the resonator has an effect on the resonant frequency.

Although the dominant contribution to the capacitance of the resonators will arise from the comb structures the higher resolution image in Figure 4.10 shows that the fingers of the combs have been made relatively short and the combs placed close together because this design was also for coupled resonators which requires the area for each single resonator is as small as possible. This means that there will be other contributions to the capacitance of the resonators,

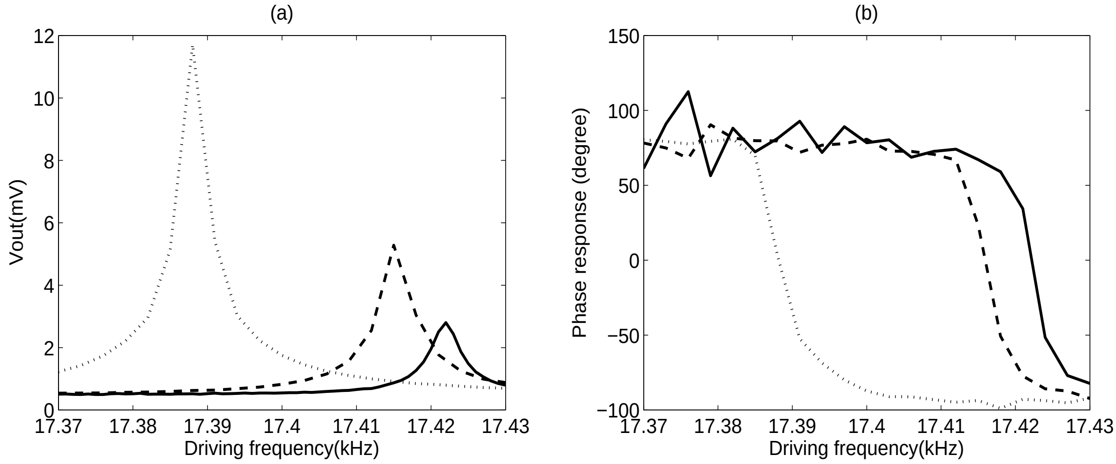

Figure 4.9: The amplitude (a) and phase response (b) of the resonator in vacuum ($1.1Pa$) with DC drive 1V(solid),2V(dashed) and 4V(dotted) ($V_{ac} = 10mV_{pp}$).

including a parallel plate capacitance between the backs of neighbouring combs.

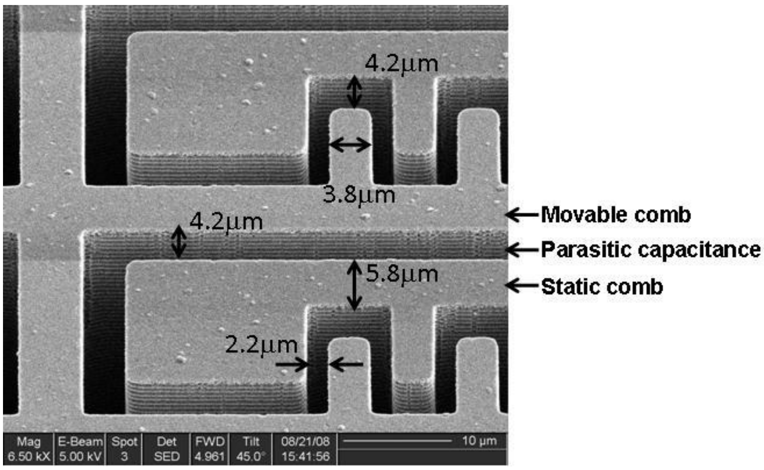

Figure 4.10: A high resolution image showing a few fingers of two comb capacitors and the parallel plate capacitor formed by the backs of comb arms.

To estimate the potential impact of these additional capacitances on the behaviour of the resonators the total capacitance of the comb set associated with each contact pad has been simulated with FEA modelling using COMSOL Multiphysics 3.4 by Dr Carl Anthony from University of Birmingham. The simulation was carried out in 2D using the electrostatics application mode (emes) in the MEMS module. The static comb boundary was set to ground and the moving comb boundary was set as a port with a port input voltage of $1V$. The capacitance of the structure was then found by scaling the capacitance matrix element 11 (given in the global data display and reported as Farads/meter thickness) by the thickness of the SOI layer used to make the resonator. The dimensions of the resonator used within these simulations were obtained from measurements of manufactured resonators and the capacitance was calculated over a wide range of displacements. The results in Figure 4.11 show that as the overlap between the combs is decreased (corresponding to a negative displacement) there is an increase in the predicted capacitance which is caused by the associated reduction in the gap of the parallel plate capacitance formed by the backs of the movable and static combs capacitances.

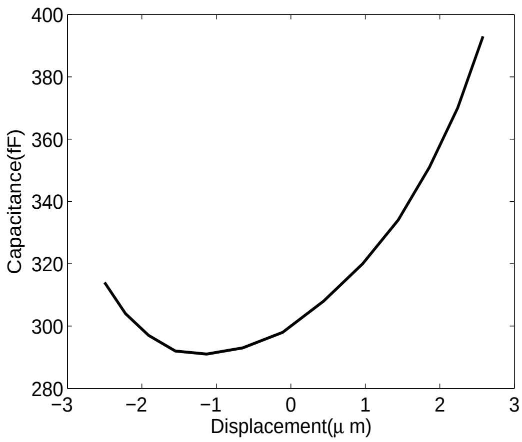

Figure 4.11: Resonator capacitance versus displacement simulated using COMSOL Multiphysics.

The electrostatic force that will result when a voltage is applied across one of the capacitances between the movable and the static combs is proportional to $\frac{dC}{dx}$. To determine the potential impact of the results in Figure 4.11 a polynomial function has been used to represent these results. Differentiating this polynomial with respect to displacement then gives

$$\frac{dC}{dx} = C_0 + C_1 x + C_2 x^2 + C_3 x^3 \tag{4.10}$$

where the values of the relevant coefficients are given in Table 4.1.

The significance of the various components of Equation 4.10 in determining the electrostatic forces on the resonator depends upon the displacement x. The output voltage in Figure 4.9(a) is between $1mV$ and $12mV$ which gives the range of displacement ranging approximately from 10nm to 100nm (Equation 4.8). The last two columns in Table 4.1 gives the values of each part of $\frac{dC}{dx}$ based on the condition that the amplitude of the resonator's mo-

Table 4.1: The values of the coefficients obtained from COMSOL Multiphysics and the maximum values contributing to the electrostatic forces when the maximum displacement of the resonator is $100nm$.

Parameter	Value	Units	Value contributing to $\frac{dC}{dx}$ $(x = 100nm)$	Units
C_0	14.7×10^{-9}	Fm^{-1}	14.7×10^{-9}	Fm^{-1}
C_1	10.1×10^{-3}	Fm^{-2}	10.1×10^{-10}	Fm^{-1}
C_2	-91.2	Fm^{-3}	-91.2×10^{-14}	Fm^{-1}
C_3	1.91×10^{9}	Fm^{-4}	1.91×10^{-12}	Fm^{-1}

tion is typically $100nm$. With this maximum displacement the contributions from the last two terms on the right hand side of Equation 4.10 will be negligible. In contrast the displacement dependent term in Equation 4.10 will contribute approximately 10% of the total electrostatic force. For displacements that give rise to two significant components to the electrostatic force on the resonator the equation of motion of the resonator is

$$\ddot{x} + \frac{c}{m}\dot{x} + \frac{k}{m}x = \frac{F_0}{m} + \frac{F(x)}{m} \tag{4.11}$$

where F_0 is the position independent force created by C_0 in Equation 4.10 whilst $F(x)$ is the displacement dependent force associated with C_1. Since this force is proportional to displacement then it can be written in the form $F(x) = k_e x$ so that the equation of motion becomes

$$\ddot{x} + \frac{c}{m}\dot{x} + \frac{k - k_e}{m}x = \frac{F_0}{m} \tag{4.12}$$

Equation 4.12 shows that since the electrostatic force generated by the resonators capacitance contains a component that is directly proportional to the displacement of the resonator, the effective spring constant of the resonator will be reduced. This apparent reduction in the spring constant will reduce the observed resonant frequency of the resonator by an amount that depends upon the DC voltages applied to the comb capacitances and therefore this DC voltage will be called the e-spring voltage in future discussion.

To confirm the predicted dependence of the resonant frequency on the DC voltages applied to the comb capacitances directly the response of a resonator was tested when it was driven with single-ended method. This particular driving method was chosen so that an AC voltage is applied to one of the comb capacitances while a DC voltage can be applied to the other drive comb without affecting either the driving force or the readout circuit. This means that any observed change in resonant frequency can only be caused by the DC voltage applied to the otherwise unused drive comb. If this DC voltage is V_e then the resulting force from the capacitor to which this voltage is applied is

$$F = \frac{V_e^2}{2}(C_0 + C_1 x) \tag{4.13}$$

which means that the change in the square of the resonant frequency is expected to be proportional to the square of the applied DC voltage, V_e. The resonators response to an AC driving voltage of $0.5V_{pp}$ at a pressure of 0.35Pa has been measured with different values of V_e. The results in Figure 4.12 show that the effect of applying the DC voltage was to reduce the resonant frequency of the resonator.

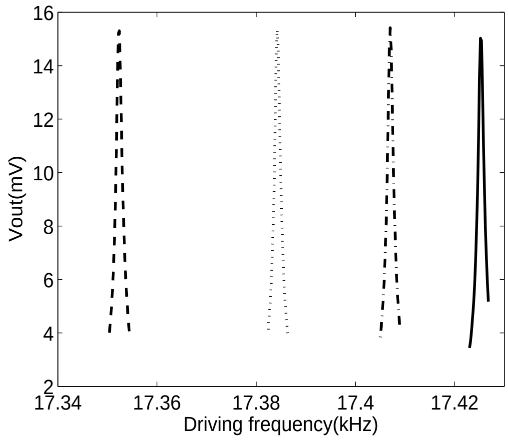

Figure 4.12: The response of the resonator when the V_e voltage is 0V (solid), 4V (dash-dot), 6V (dotted) and 8V (dashed).

Combining Equation 4.12 and Equation 4.13, the relationship between the measured resonant frequency ω_e and the DC voltage V_e is given by

$$\omega_e^2 = \frac{k - k_e}{m} = \omega_0^2 - \frac{C_1}{2m}V_e^2 \tag{4.14}$$

where ω_0 is the real resonant frequency of the resonator which can not be measured directly because voltages that must be applied to the combs to drive and sense motion will shift the measured resonant frequency. Figure 4.13 shows the linear relationship between ω_e^2 and V_e^2

which agrees with Equation 4.14.

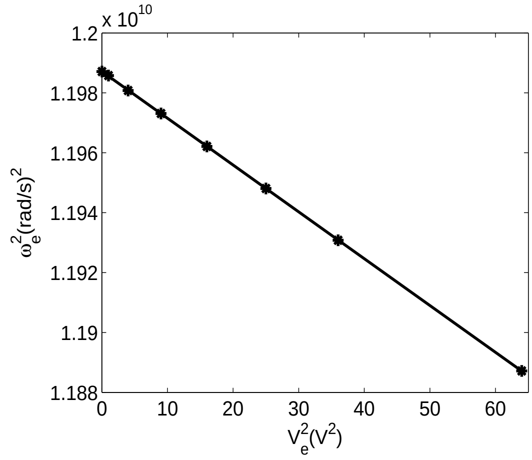

Figure 4.13: Relationship between the resonant frequency and the bias voltage applied on the resonator.

Figure 4.13 shows the effective resonant frequencies when one of the DC voltages applied on the combs varies. To estimate the parameters of the resonator, then V_e^2 in Equation 4.14 needs to expand to all the voltages applied on the combs and two driving methods will be discussed in turn. If the differential driving and readout method is used, the forces applied on the four combs are shown in Equation 4.15.

$$\begin{aligned}
F_{drive+} &= \frac{1}{2}(V_{DC} + V_{ac}\cos\omega t)^2(C_0 + C_1 x) \\
F_{drive-} &= \frac{1}{2}(V_{DC} - V_{ac}\cos\omega t)^2(C_0 - C_1 x) \\
F_{sense+} &= \frac{1}{2}V_S^2(C_0 + C_1 x) \\
F_{sense-} &= \frac{1}{2}V_S^2(C_0 - C_1 x)
\end{aligned} \tag{4.15}$$

Noticing that for the opposing combs the coefficient for displacement dependent in $\frac{dC}{dx}$ is of different sign because the relative displacement is opposite. The overall force F applied on the resonator is

$$\begin{aligned}
F &= (F_{drive+} - F_{drive-}) + (F_{sense+} - F_{sense-}) \\
&= 2V_{DC}V_{ac}\cos\omega t C_0 + (V_{DC}^2 + V_{ac}^2\cos^2\omega t + V_S^2)C_1 x \\
&= 2V_{DC}V_{ac}\cos\omega t C_0 + (V_{DC}^2 + \frac{V_{ac}^2}{2} + V_S^2)C_1 x + \frac{V_{ac}^2}{2}\cos 2\omega t C_1 x
\end{aligned} \tag{4.16}$$

The last term on the right hand of Equation 4.16 is ignored because it is a high order insignificant term. Then the effective resonant frequency is

$$\begin{aligned}\omega_e &= \sqrt{\omega_0^2 - \frac{C_1}{m}(V_{DC}^2 + \frac{V_{ac}^2}{2} + V_S^2)} \\ &= \sqrt{\omega_0^2 - k_e(2V_{DC}^2 + V_{ac}^2 + 2V_S^2)}\end{aligned} \tag{4.17}$$

where the effective e-spring constant $k_e = \frac{C_1}{2m}$.

The effective resonant frequency for the single-ended drive and differential readout is deduced with the same method:

$$\begin{aligned}\omega_e &= \sqrt{\omega_0^2 - \frac{C_1}{m}(\frac{V_{ac}^2}{4} + V_S^2)} \\ &= \sqrt{\omega_0^2 - k_e(\frac{V_{ac}^2}{2} + 2V_S^2)}\end{aligned} \tag{4.18}$$

To summarise both methods, the measured resonant frequency can be represented by the following equation:

$$\begin{aligned}\omega_e &= \sqrt{\omega_0^2 - \frac{C_1}{m}(\sum_{i=1}^{n}\frac{V_{DC^*(i)}^2}{2} + \sum_{j=1}^{m}\frac{V_{ac(j)}^2}{4})} \\ &= \sqrt{\omega_0^2 - k_e(\sum_{i=1}^{n}V_{DC^*(i)}^2 + \sum_{j=1}^{m}\frac{V_{ac(j)}^2}{2})}\end{aligned} \tag{4.19}$$

where the effective e-spring constant $k_e = \frac{C_1}{2m}$ and the V_{DC^*} in Equation 4.19 includes all the DC voltages applied on the comb: the driving voltage, the e-spring voltage and the sensing voltage.

The primary aim of the project is to detect a small mass change to the resonator by monitoring the amplitude or phase response. It is possible to use a focused ion beam(FIB) to deposit a small amount of platinum onto the surface of resonator to change its mass. However, it is very likely to be a one time process and it is difficult to repeat the experiments. The non-ideal displacement dependent comb capacitance can be used to change the effective spring constant which is equivalent to the effect of the mass as discussed in Section 1.3. A great deal of work has been done for mass sensing based on MEMS/NEMS but there is very little research on the transient behaviour following the mass change with experimental results in particular which is important to a sensor in addition to the sensitivity performance. One possible reason is that it is almost impossible to know the exact time when the mass is loaded which makes it quite difficult to monitor the response time after mass change occurs.

With this non-ideal displacement dependent comb capacitance, the resonant frequency change of the resonator can be effectively changed by the DC voltage V_e applied on the comb by any amount at any required time which can also be recorded by the data acquisition device accurately. Consequently, the implementation of the micromechanical resonator as a mass sensor will be achieved by changing the effective spring constant in the following experiments. Although it is a spring constant sensor if strictly speaking, the principle of this type of sensor is the same as the mass sensor because both of them characterise the resulting resonant frequency change after the parameter change occurs. To implement this method, it is therefore important to extract the parameters of the resonator to quantify the resonance change resulting from the e-spring voltage change.

4.4.4 Parameter extraction for the micromechanical resonator

The real resonant frequency ω_0 and the effective spring constant k_e can be obtained from the linear fit in Figure 4.13. The estimated mass for the resonator is $4\mu g$, and therefore the C_1 in $\frac{dC}{dx}$ can be calculated from Equation 4.14. Combining Equation 1.4, Equation 4.4 and Equation 4.8, the output voltage at resonance and the driving voltage can give the value of C_0 in $\frac{dC}{dx}$ as shown in Equation 4.20.

$$C_0 = \sqrt{\frac{2m\omega_e V_{out}}{R_{trans} G_{inst} V_S Q V_{ac}^2}} \tag{4.20}$$

where ω_e is the measured resonant frequency the maximum output voltage occurs. Equation 4.20 gives the method to calculate C_0 under conditions of single-ended drive and differential readout. The experimental data in Figure 4.6(a) have been used to extract C_0. To conclude, the parameters extracted from above method are shown in Table 4.2.

Table 4.2: The values of the coefficients from parameter extraction.

Parameter	Value	Units
C_0	18.038×10^{-9}	Fm^{-1}
C_1	12.9×10^{-3}	Fm^{-2}
k_e	1.613×10^{6}	Nm^{-1}
f_0	17497.81	Hz

4.5 Q-enhancement in air

The natural Q of the resonator in air is only around 5.5 and a high Q system is desirable to detect the same amount of the phase response(Equation 1.13). Turnbull et al. have implemented a method of Q-enhancement to partially cancel some of the damping term by feeding back a driving force which is proportional to the velocity signal [23].

4.5.1 Feedthrough compensation

The capacitive readout gives the output voltage which is proportional to the resonator velocity (Equation 4.3 and Equation 4.7). If single-ended drive is used then the feedback voltage representing the velocity signal requires to half the frequency which needs extra electronic circuit. It is better to use the differential driving method which produces the same output frequency as the driving signal. However, as mentioned in Section 4.4.1, the feedthrough signal is comparable with the desired movement signal when the differential drive is used. Therefore it is necessary to compensate the feedthrough signal before implementing the Q-enhancement. A method to remove the undesirable feedthrough signal by direct cancellation is described in this section [23, 47, 59, 60].

Figure 4.5 shows that the coupling capacitance between driving comb A and the readout channel is larger than the counterpart for comb B, and therefore the remaining feedthrough signal due to the differential drive is caused by the comb A. To compensate, the voltage on the comb B following an amplifier with variable gain can be applied to a small capacitor which is connected to the input of each transimpedance amplifier in Figure 4.4. For each sensing comb, the level of compensation can be varied by carefully adjusting the gain of the amplifier. To make sure that the feedthrough signal is reduced significantly, it can be observed by monitoring the fft of the output voltage on the oscilloscope. Figure 4.14 shows that after compensation the feedthrough signal has reduced by nearly two orders. In this case, the feedthrough signal in the observed output signal can be neglected.

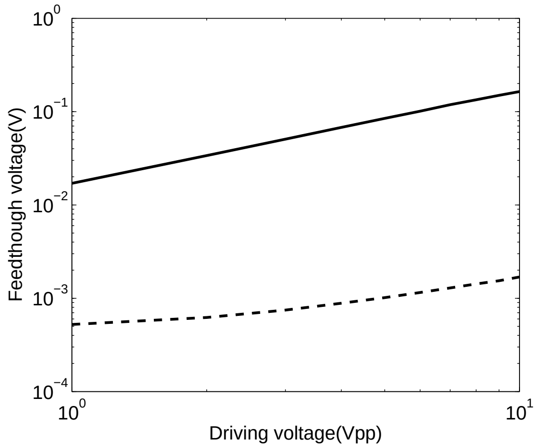

Figure 4.14: Comparison of feedthrough voltages before (solid) and after(dashed) compensation of differential drive.

4.5.2 Feedback electronics

To remove the noise, the output voltage which is proportional to the velocity of the resonator is bandpass filtered before it is fed back to the drive the resonator. An active bandpass filter composed from operational amplifiers, resistors and capacitors can be used by carefully mapping the centre frequency of the filter with the resonant frequency of the micromechanical resonator. There is a major drawback of this type of bandpass filter as the only way to change the characteristics of the filter is to change its components. It is not desirable because for the same design, the resonant frequency of the micromechanical resonators can vary after fabrication [54]. Moreover, even for a particular resonator, different actuation or sensing voltages could result in different resonant frequencies as discussed in the previous section. It is therefore better to implement a tuneable bandpass filter to cope with different situations and this can be realised by using a switched-capacitor bandpass filter. The centre frequency of such a bandpass filter is made directly proportional to the clock frequency which can be easily changed [61].

An 8th order Butterworth bandpass filter has been designed by cascading two 4-pole bandpass filters as shown in Figure 4.15. The LMF100 used in this configuration is a dual switched capacitor filter and the clock to frequency ratio is set to be 50:1.

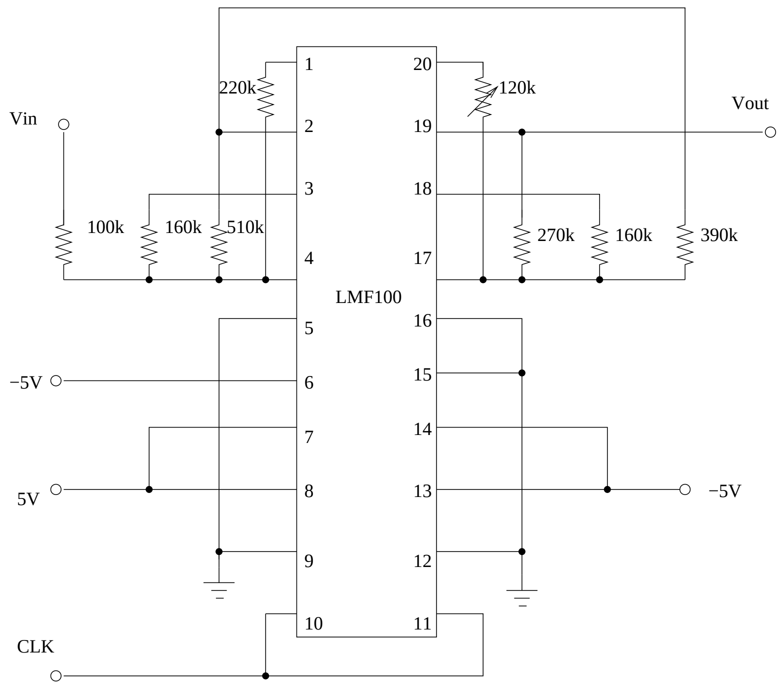

Figure 4.15: A 4th order switched-capacitor bandpass filter using LMF100.

The amplitude and phase response of the 8th order bandpass filter is shown in Figure 4.16 and the clock frequency is 950kHz. The centre frequency is 17kHz approximately and the quality factor is about 4. The bandpass filter is followed by several simple operational amplifiers which can produce a variable gain. Then a summing op-amp adds the feedback voltage to the primary drive from the signal generator. The sum of these two signals are considered as the V_{ac} in Figure 4.3.

An actuation and measurement system for a Duffing resonator circuit has been discussed in Section 3.3.1. A programmable waveform generator IC controlled by the FPGA produces the AC driving signal and driving frequency can be varied by the FPGA. An XOR gate followed by a low pass filter converts the phase difference between driving signal and displacement output signal to a DC voltage (Figure 3.2). A similar system can be used for the micromechanical resonator and the only difference is that the output of the Duffing resonator is proportional to the displacement while the output voltage of the micromechanical resonator is in phase with the velocity response of the resonator. The phase response of the velocity at resonance is zero degree as shown in Figure 4.6(b). The phase comparator in Figure 3.2 converts the phase difference between $0°$ and $180°$ to DC voltage from $0V$ to $10V$. Consequently, it is better to

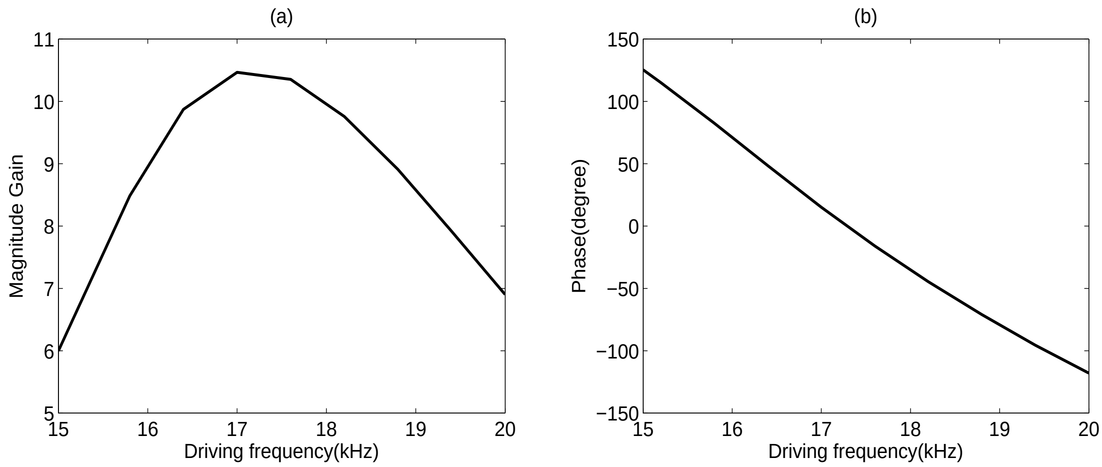

Figure 4.16: The amplitude (a) and phase response (b) of the 8th order bandpass filter with clock frequency $CLK = 950kHz$.

shift the driving signal or the output response by $\pm 90^{\circ}$ so that the phase of the output voltage will be centred at 90° and the DC voltage proportional to the phase response will be centred at mid-range $5V$.

A simple option for the phase shift circuit is an integrator or differentiator using op-amps. The problem with the integrator is that if the input voltage has DC offset then the output will saturate to the power rail. The differentiator can also be viewed as a highpass filter so higher order frequency noise will be passed which might lead to unstable behaviour of the circuit. Since the input signals of the phase comparator are digital signals a digital quadrature generator (DQG) using D-type flip flops can be used to generate a signal with 90° phase shift from the input voltage [62, 63]. The frequency of the output voltage from the quadrature generator is one fourth of the input frequency and therefore the quadrature generator is placed in a phase locked loop (PPL) as a frequency divider (n=4) as shown in Figure 4.17. Two D-type flip-flop are packaged in 4013B and both the linear voltage-controlled oscillator (VCO) and phase detector (PD) are in standard phase locked loop IC 4046. In order to comply with the resonator operating frequency range, the VCO range is set to generate frequencies between 40kHz to 80kHz and therefore the output frequency from DQG will be 10kHz to 20kHz. A type II phase detector is used which always locks when the phase difference is zero to make sure that the phase difference between the V_{out} and V_{in} is 90° [61]. This PPL including the DQG in Figure 4.17 is added between the second voltage comparator and the phase comparator in Figure 3.2 to shift the squared driving voltage by $90°$ and then the phase difference between the phase shifted driving voltage and the output voltage is converted to DC voltage by the phase comparator and the low pass filter in Figure 3.2.

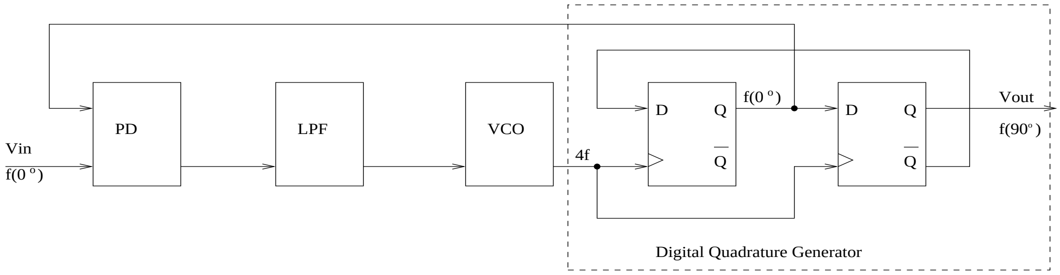

Figure 4.17: Phase lock loop and including a digital quadrature generator built from two D-type flip-flop stages.

4.5.3 Q-enhancement for the linear resonator

To investigate the response of the system to small changes in the resonant frequency the differential drive is implemented to make sure that the driving signal and output signal are the same frequency. For the sensing channel, single-ended readout with 8V sensing voltage V_S is used because the other comb is needed for applying the e-spring voltage which changes the effective spring constant of the resonator as discussed in Section 4.4.3. The e-spring voltage is set to be zero initially. In order to obtain a larger output voltage, the resonator is biased to $-5V$ so that the voltage across the sensing comb and the resonator V_s' is 13V and the effective DC voltage for driving is 9V. The initial effective e-spring voltage is then 5V.

When the e-spring voltage is changed from 5V to 5.4V, the expected resonant frequency change is 4.97Hz (Equation 4.19). Initially all experiments were performed in vacuum where the resonance peak of the resonator can be identified easily without Q-enhancement. When the resonator is operating in a vacuum the results obtained showed the expected change in the resonant frequency of approximately 5 Hz.

The same experiment was then repeated in air with the effective Q of the system enhanced by a factor of approximately 60 using velocity feedback. Figure 4.18(a) shows the amplitude of the response of the resonator at the driving voltage $V_{ac} = 100mV_{pp}$ before and after the e-spring voltage on the capacitance used to vary the resonant frequency of the resonator was increased from 5V to 5.4V.

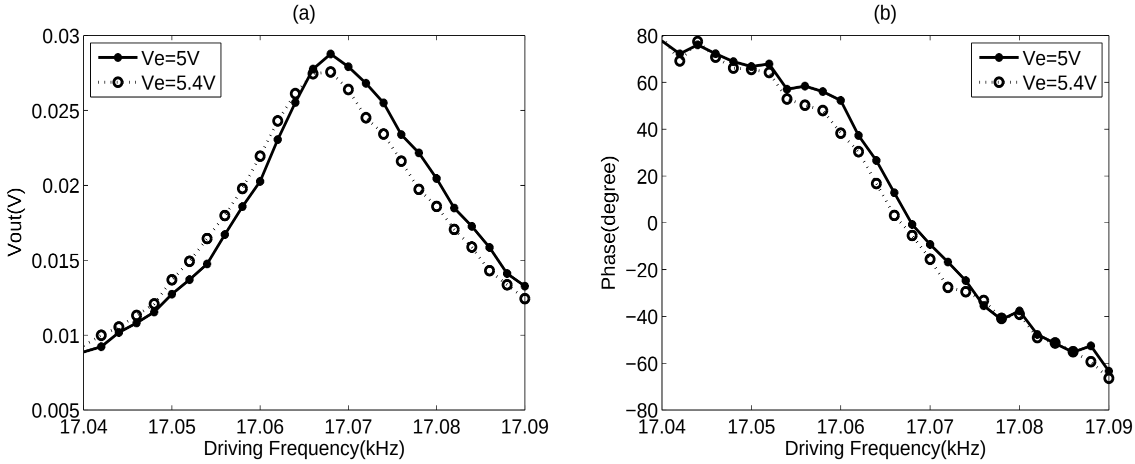

Figure 4.18: The linear amplitude (a) and phase (b) response when the voltage on the e-spring (Ve) is either 5V (solid line) or 5.4V (dashed line).

As expected the results show a decrease in the resonant frequency of the system. Although in this experiment the resonators' response has been measured at a range of frequencies in sensing applications the resonator would usually be driven at a single frequency. As described in Chapter 1 a convenient method of determining any change in resonant frequency is then to monitor the phase of the response of the resonator at this fixed frequency. Since the read-out circuit measures the velocity of the resonator the output voltage from the transimpedance amplifier is in phase with the driving voltage at resonance. By fitting the phase response near resonance when V_e is 5V the phase change rate versus frequency is $-5.5°/Hz$. The change in the phase of the resonator at the resonant frequency between the two sets of data shown in Figure 4.18(b) is 8 degrees. This suggests that the e-spring voltage change has caused a $1.45Hz$ change in resonant frequency. The resonant frequency change in Figure 4.18 is significantly less than one third of the expected value and since the expected resonant frequency change is observed when Q-enhancement is not required this reduction in the observed change in resonant frequency must be caused by the Q-enhancement circuit.

Supposing the feedback voltage is V_{FB}, the motion of the resonator with Q-enhancement is described by

$$\ddot{x} + \frac{\omega_0}{Q}\dot{x} + \omega_e^2 x = \frac{2V_{DC}V_{AC}C_0}{m} + \frac{2V_{DC}V_{FB}C_0}{m} \tag{4.21}$$

where ω_e is determined by Equation 4.19. If the feedback gain is η, then

$$V_{FB} = \eta \dot{x} V_S R_{trans} G_{inst} C_0 = G_{fb} \dot{x} \tag{4.22}$$

where $G_{fb} = \eta V_S R_{trans} G_{inst} C_0$ is a constant. The effective quality factor Q_{eff} is then determined by

$$Q_{eff} = \frac{\omega_0}{\frac{\omega_0}{Q} - \frac{2C_0 V_{DC} G_{fb}}{m}} = 349.49 \tag{4.23}$$

To compare with this effective Q value, the linear response when $V_e = 5V$ in Figure 4.18 is analysed. The peak amplitude response gives the effective resonant frequency $f_e = 17068Hz$ and the $-3dB$ frequencies give the effective quality factor $Q_{eff} = 858$ which is much larger than the expected value in Equation 4.23. Figure 4.19 shows the simulation results of the Q-enhancement model (Equation 4.21) with V_{FB} described by Equation 4.22. It is clear that the Q value of the experimental results is increased compared with the simulated model. Moreover, approximately $5Hz$ resonant frequency change is observed for the simulation which is much larger than the experimental value.

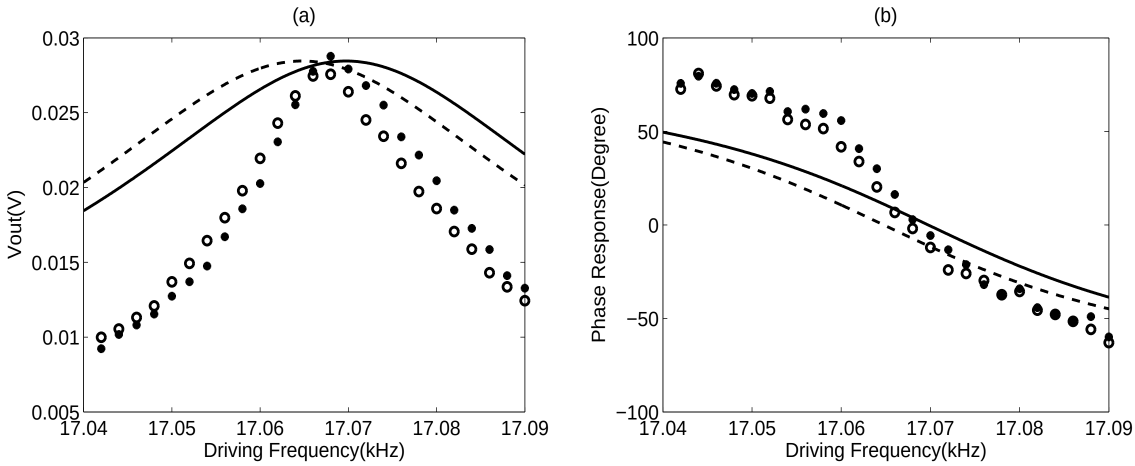

Figure 4.19: The simulated amplitude (a) and phase (b) response with ideal velocity feedback (lines) compared with the experimental response (markers) when the voltage on the e-spring (Ve) is either 5V (dots or solid line) or 5.4V (circles or dashed line).

In addition, the transfer function (Equation 1.4) of the simple harmonic motion (SHM) gives the peak output voltage at resonance with $Q_{eff} = 858$:

$$V_{peak} = \frac{2V_{DC}V_{ac}C_0Q_{eff}}{m\omega_e^2} \times C_0V_SR_{trans}G_{inst} = 0.076V \tag{4.24}$$

which is much greater than the measured peak magnitude $0.029V$ and this means that the model can not be described by SHM. This suggests that some important terms are missing from the model of Q-enhancement. To understand the unexpected effect of using Q-enhancement, we recall from Figure 4.16(b) that the phase response of the bandpass filter, which is used to remove the noise from the feedback loop used for Q-enhancement, varies slowly versus the frequency. The centre frequency of the filter is carefully set to the resonant frequency of the resonator so that the feedback voltage is in phase with the velocity signal. Because of the phase shift of the bandpass filter, the feedback voltage at frequencies other than the resonant frequency is the velocity signal plus a small displacement signal. By fitting the curve with a linear function, the gradient for the phase shift versus frequency in Figure 4.16(b) is $-0.0544°/Hz$ which is quite small in a 50Hz frequency range. As a result, this phase change has been assumed to be negligible previously. If the extra phase shift $\varphi(\omega)$ from the bandpass filter is included , then the feedback voltage is mixed with velocity and displacement signals as follows

$$\begin{aligned} V_{FB} &= \eta\dot{x}V_SR_{trans}G_{inst}C_0[\cos\varphi(\omega) + i\sin\varphi(\omega)] \\ &= G_{fb}\dot{x}[\cos\varphi(f) + i\varphi(\omega)] \\ &= G_{fb}\dot{x} - G_{fb}x\omega\varphi(\omega) \end{aligned} \tag{4.25}$$

Since $\varphi(\omega)$ is sufficient small $\cos\varphi(\omega)$ is considered to be unity and $\sin\varphi(\omega)$ equals to $\varphi(\omega)$ in Equation 4.25. Substituting Equation 4.25 into Equation 4.21 gives the equation describing the motion of the resonator (Equation 4.26). The damping term $\frac{\omega_0}{Q}$ in Equation 4.21 has been converted to $\frac{\omega_e}{Q'}$ for the simplicity of further discussion.

$$\ddot{x} + (\frac{\omega_e}{Q'} - \frac{2C_0V_{DC}G_{fb}}{m})\dot{x} + (\omega_e^2 + \frac{2C_0V_{DC}G_{fb}\omega\varphi(\omega)}{m})x = \frac{2V_{DC}V_{AC}C_0}{m} \tag{4.26}$$

where $\varphi(\omega)$ is obtained from Figure 4.16(b) and it is characterised by

$$\varphi(\omega) = \tau(\omega_{PS0} - \omega) = 1.5 \times 10^{-4}(\omega_{PS0} - \omega)(rads) \tag{4.27}$$

where ω_{PS0} is the frequency at which the phase-shift is zero, which is chosen to be as close as possible to the initial resonant frequency. For those frequencies greater than zero phase frequency ω_{PS0}, φ is negative and this means that it effectively reduces the effective resonant frequency by a small amount. Consequently, the amplitude response at the corresponding driving frequency is lower than the one with the original resonant frequency. The absolute value of the extra phase shift φ is proportional to the difference between the driving frequency and ω_{PS0} which means that the amplitude attenuation resulting from the effective resonant frequency shift is more serious if the driving frequency is farther away from ω_{PS0}. In addition, the absolute value of φ is symmetric with respect to the zero phase frequency which can be considered to equal to the resonant frequency. Consequently, the overall effect of the feedback force is cancelling the damping term partially and the effective Q value is increased further due to the phase shift. The transfer function of the velocity response of Equation 4.26 is

$$G(\dot{x}) = \frac{j\omega}{\omega_e^2 - \omega^2 + \lambda\frac{\omega\omega_e}{Q'}\varphi(\omega) + j(1-\lambda)\frac{\omega\omega_e}{Q'}} \tag{4.28}$$

where $\lambda = 2V_{DC}G_{fb}C_0Q'/(m\omega_e)$ which is the feedback fraction.

The amplitude transfer function, Equation 4.28, has been independently compared to both the measured data sets in Figure 4.19(a) using the curve fitting tool from MATLAB. In this fitting procedure the measured value of $\tau(1.5\times10^{-4})$ in Equation 4.27 was used and the known frequency at which the phase-shift through the feedback loop is zero was set to $17068Hz$. The fitting tool then determined the values of the resonant frequency, the unenhanced Q value and the feedback fraction (λ). As expected the Q and λ values obtained from the two data sets were almost identical with $Q' = 5.02$ and $\lambda = 0.984$. The resulting comparison between the model and both the amplitude and phase response of the resonator are shown in Figure 4.20. The stars represent the response with a $5V$ e-spring voltage while the circles show the results when the e-spring voltage is increased $5.4V$. Figure 4.20 shows a very good fit between the experimental results and the model with the phase shift taken into account. These results show that the small phase shift through the feedback loop has a significant effect on the system.

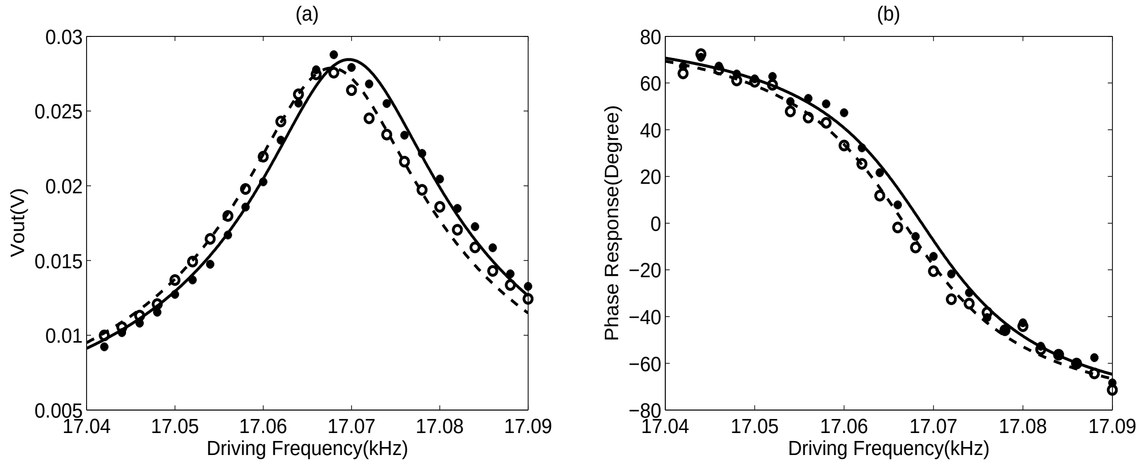

Figure 4.20: The simulated amplitude (a) and phase (b) response with phase shift model feedback (lines) compared with the experimental response (markers) when the voltage on the e-spring (Ve) is either $5V$ (solid line or stars) or $5.4V$ (dashed line or circles).

Combining the transfer function (Equation 4.28) and the phase change rate of the bandpass filter (Equation 4.27), the phase response the velocity can be described by

$$\phi = 90 - arctan\frac{(1-\lambda)\omega\omega_e/Q'}{\omega_e^2 - \omega^2 + \lambda\tau\omega\omega_e(\omega_{PS0} - \omega)/Q'} \tag{4.29}$$

If the zero phase-shift frequency ω_{PS0} equals to the effective resonant frequency ω_e, then the phase changing rate versus the frequency at resonance can be simplified to

$$\frac{d\phi}{d\omega} = -\frac{2Q'}{(1-\lambda)\omega_e}(1 + \frac{\tau\lambda\omega_e}{2Q'}) \tag{4.30}$$

The first term in this expression is the phase-shift that would be observed when there is no phase-shift in the feedback loop. The second term is then the effect of the small frequency dependent phase-shift in the feedback loop. For the extracted parameters values when the e-spring voltage is $5V$ the measure rate of change of phase will be

$$\frac{d\phi}{d\omega} = -2.58\frac{2Q'}{(1-\lambda)\omega_e} \tag{4.31}$$

which is a factor of 2.58 times larger than the rate of change of phase for a system without a frequency dependent phase-shift in the feedback loop. This means that the measured rate of change of phase with the feedback loop in operation, $5.5°/Hz$, gives a predicted rate of change of phase without the frequency dependent phase shift in the feedback loop of $2.13°/Hz$. Since the phase change due to a shift in the resonant frequency is measured at a fixed frequency, then it is the rate of change of phase when there is no frequency dependent phase-shift in the feedback loop that is relevant. The measured phase change at a constant frequency $8°$, is therefore consistent with a change in resonant frequency of $3.76Hz$. Correcting for the effects of the frequency dependent phase-shift through the feedback loop has therefore reduced the error significantly. The remaining error is probably caused by the error in the phase measurements in Figure 4.18.

Figure 4.21 shows amplitude and phase response when the e-spring voltage (V_e) changes from $5V$ to $5.4V$ at resonance. In these figures the time at which the resonant frequency of the system was changed by changing V_e is indicated. From Figure 4.21(a) it is clear that it is extremely difficult to detect this change from any change in the amplitude of the resonators' response. The envelope of the amplitude response has been averaged before and after the e-spring voltage change indicated by the blue line in Figure 4.21(a). A slight decrease in amplitude can be observed, in contrast the change in resonant frequency can be easily detected in the change of phase of the system as shown in Figure 4.21(b). To compare the phase change

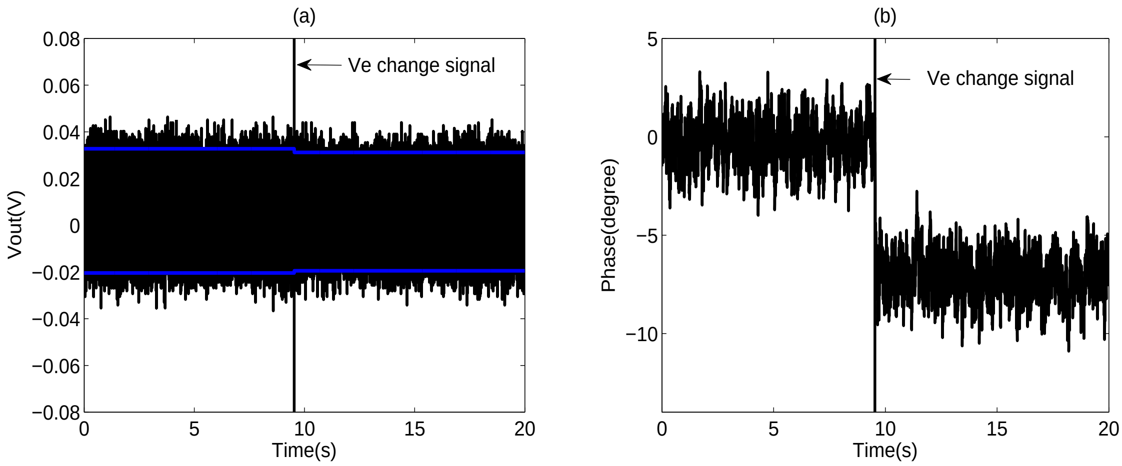

Figure 4.21: The transient amplitude (a) and phase (b) response of the resonator driven at resonance (($17.068kHz$, $100mVpp$) when the e-spring voltage (Ve) changes from $5V$ to $5.4V$ at the time indicated by the vertical line with Q-enhancement in air.

before and after Q-enhancement, the same e-spring voltage change is applied on the resonator without any feedback force in air. The resonance peak of the resonator with Q-enhancement is clear so that the resonant frequency shift can be quantified by comparing the amplitude peaks or the zero phase frequencies. It is difficult to obtain the resonant frequency change by comparing the resonator response in air pressure because the low Q system response is flat and broad. Figure 4.22 shows the transient response of the resonator in air when the e-spring voltage rises from $5V$ to $5.4V$. Due to the large damping at atmospheric pressure, the output magnitude change in Figure 4.22(a) is hardly identified even by comparing the averaged amplitude envelope (blue line in Figure 4.22(a)). The change in resonant frequency shows a step change in phase even though the noise level is higher than the step size.

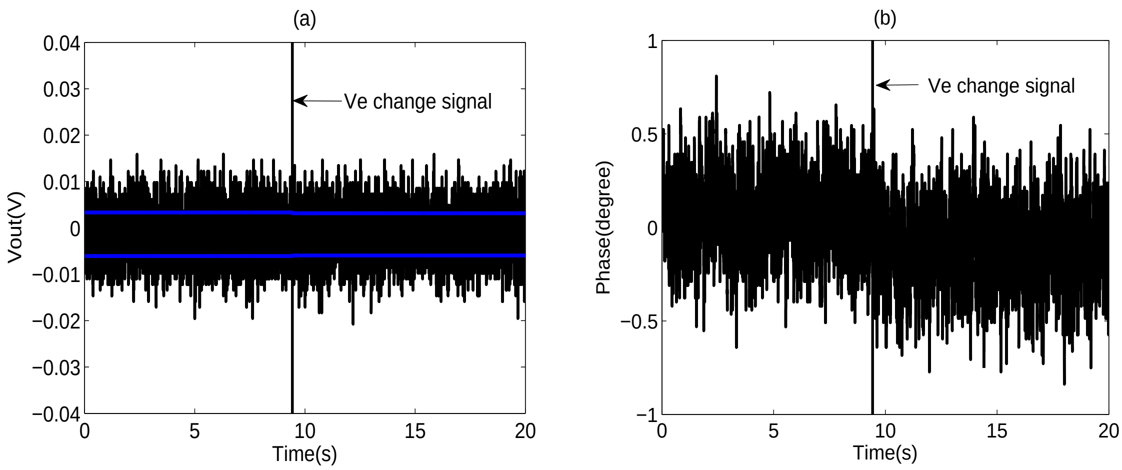

Figure 4.22: The transient amplitude (a) and phase (b) response of the linear resonator driven at resonance ($17.3kHz$, $4V_{pp}$) when the e-spring voltage changes at the time indicated by the vertical line without Q-enhancement in air.

As the phase change in Figure 4.21 (b) with natural Q is quite noisy it is quite difficult to identify the step change. To compare the phase change following the same e-spring voltage change before and after the Q-enhancement, a 1000-tap average filter is used to remove the noise for both signals as shown in Figure 4.23. For the natural Q, around $0.15°$ phase change is shown as expected, and it is still noisier compared with the Q-enhanced system. The Q-enhanced system gives a much larger phase change following the same e-spring change and also benefits from slightly better signal to noise ratio after filtering.

Figure 4.23 shows that the phase change for the Q-enhanced system is $10°$ which is there-

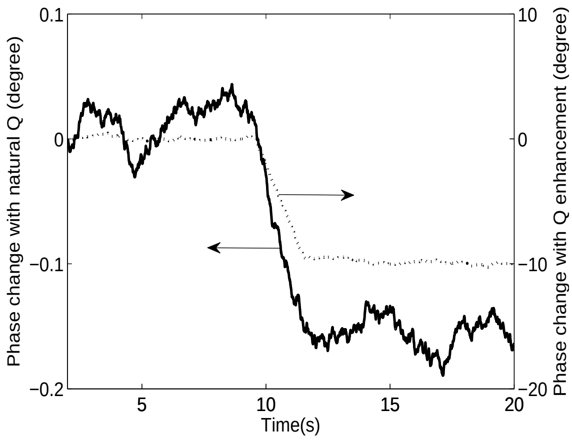

Figure 4.23: Phase change following the same resonance change with natural Q (solid) and Q-enhancement ($\frac{Q_{eff}}{Q} = 62.5$,dotted).

fore consistent with a $4.7Hz$ change in resonant frequency(Equation 4.31). The error has been reduced from a factor of more than three to less than five percent by including the model of the phase shift in the feedback loop. Although it is possible to compensate for the phase shift in the feedback loop the ideal situation is to design a system in which the phase-shifts are negligible. From Equation 4.30 the effect of the phase-shift will be negligible if

$$\frac{\tau \lambda \omega_e}{2Q'} << 1 \tag{4.32}$$

Since $\lambda \approx 1$ this is equivalent to

$$\tau << \frac{2Q'}{\omega_e} = \frac{2}{\Delta\omega} \tag{4.33}$$

where $\Delta\omega$ is the $-3dB$ bandwidth of the resonator. This means that it will be easier to ensure that phase shifts in the feedback loop are negligible for high Q systems, but harder for resonators with a high resonant frequency. Equation 4.33 can be used as a condition when the effect of phase shift is considered in the future design.

4.6 Summary

A micromechanical resonator and its actuation/readout electronics have been described. A capacitive driving technique has been chosen so that ideally the driving force is independent of the movement of the resonator. The differential capacitive readout channel gives the output voltage which is proportional to the velocity signal of the resonator.

However the design of the resonator structure means that the resonator also includes some small parallel plate capacitances. These small additional components to the resonators capacitance have an important consequence. They produce a small displacement dependent electrostatic force. This force can be used to change the resonant frequency of the resonator controllably and reproducibly in order to compare different methods of sensing changes in resonant frequency. This method is used to simulate the changes in mass of the micromechanical resonator. A DC voltage applied on one of the sensing combs has been used to control that force. The resonant frequency and coefficients of the comb have then been extracted.

Force feedback has been proposed as a useful method of partially cancelling the effects of viscous damping to increase the effective quality factor of a MEMS resonator. The resulting variability of the resonant frequency has been exploited to test a resonator when force feedback is employed. These tests have shown that an apparently negligible phase-shift in the feedback loop can have a dramatic effect on the user's ability to quantify any changes in resonant frequency. Results have been presented to show that it is possible to characterise the system to correct for this phase-shift. An inequality condition has also been suggested that allows the designers of future systems to determine if these phase-shifts will be have an effect upon their design. In addition, the phase change at resonance following an e-spring voltage change for the natural Q and Q-enhanced systems are compared. The Q-enhancement gives a larger phase change after the e-spring voltage change and also has a better signal to noise ratio.

Chapter 5

Q-enhancement to create non-linear behaviour

5.1 Introduction

Previously when the resonator was tested to extract the parameters or to confirm the expected DC voltage dependence of the resonant frequency a conservative driving force was used to characterise the response of the system at an estimated typical displacement at resonance of 100nm. At these small displacements the dominant displacement-dependent term in Equation 4.10 is the term that is directly proportional to displacement (Table 4.1). However, when the displacement of the resonator is larger the higher order terms in Equation 4.10 can become significant. In particular the comparison of forces in Table 5.1 suggests that, with larger displacements, the behaviour of the resonator could be influenced by forces that are proportional to the displacement cubed.

Table 5.1: The maximum values contributing to the electrostatic forces when the maximum displacement of the resonator is $1\mu m$.

Parameter	Value	Units	Value contributing to $\frac{dC}{dx}$ $(x = 1\mu m)$	Units
C_0	18.038×10^{-9}	Fm^{-1}	18.038×10^{-9}	Fm^{-1}
C_1	12.9×10^{-3}	Fm^{-2}	12.9×10^{-9}	Fm^{-1}
C_2	-91.2	Fm^{-3}	-91.2×10^{-12}	Fm^{-1}
C_3	1.91×10^{9}	Fm^{-4}	1.91×10^{-9}	Fm^{-1}

The parameters C_0 and C_1 in Table 5.1 were extracted in Section 4.4.4 while C_2 and C_3 are the simulated value from COMSOL Multiphysics. In this Chapter, the non-linearity arising from the third order displacement dependent term will be confirmed by applying a greater force. The parameter value C_3 will be extracted in vacuum and then the non-linear model with Q-enhancement will be characterised. In the end, two methods to detect the effective resonant frequency change when the resonator is operated in the non-linear region are compared in terms of the sensitivity and dynamic range.

5.2 Non-linear response with direct drive in vacuum

To extract the value of C_3, the resonator has been tested with a direct drive in vacuum where large displacements can be easily achieved. If all the significant displacement dependent terms in Table 5.1 are considered, then the motion of a resonator driven with single-ended drive and readout is

$$\ddot{x} + \frac{\omega_0}{Q}\dot{x} + \omega_e^2 x + \gamma x^3 = \frac{V_{ac}^2 \cos(2\omega t)}{4m}[C_0 + C_1 x + C_3 x^3] \tag{5.1}$$

where ω_e is the effective resonant frequency of the resonator and

$$\gamma = -C_3(\frac{V_{ac}^2}{4m} + \frac{V_S^2}{2m}) \tag{5.2}$$

in which the V_S is the sensing voltage to sense the movement of the resonator.

Although the equation of motion for the resonator (Equation 5.1) is quite complex the most significant driving force is the first term on the right hand side. The equation of motion is therefore very similar to Duffing Equation 1.17. Since the non-linear parameter (γ) in the equation of motion is negative this means that the resonator is expected to behave in a manner similar to a Duffing resonator with a softening non-linearity. As expected, the amplitude response showing an asymmetric resonance peak is shown in Figure 5.1 with the same ambient pressure as the linear response in Figure 4.6. A greater driving force is applied so as the displacement response is increased, so the expected Duffing like non-linearity is observed with high natural Q system.

To estimate the non-linearity coefficient γ in Equation 5.2, the steady state response for a

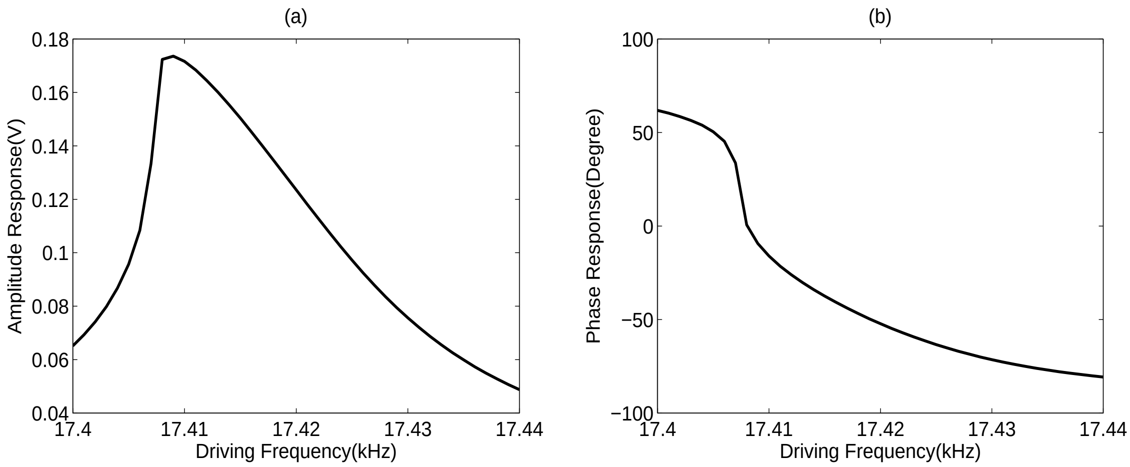

Figure 5.1: The amplitude (a) and phase response (b) of the resonator at a pressure of 7.7Pa with single-ended drive $V_{ac} = 6V_{pp}$.

set of frequencies have been simulated by solving Equation 5.1 with MATLAB $ode45$ solver. All the parameters except for C_3 in Equation 5.1 have been extracted in Section 4.4.4. As expected, the extracted parameters for the linear response in Figure 4.6 give a very good fit between the simulated and measured response as shown in Figure 5.2.

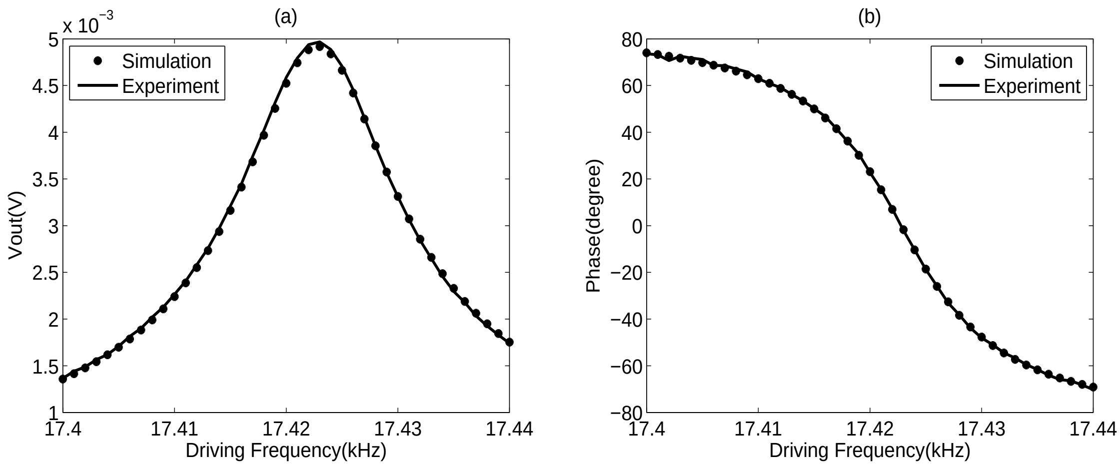

Figure 5.2: The amplitude (a) and phase (b) response of simulation and experimental result with single-ended drive $V_{ac} = 1V_{pp}$ in vacuum with ambient pressure of 7.7Pa.

The Q value obtained from the $-3dB$ frequencies is 1334.81 when the resonator is operated in the linear region. However, this Q value can not result in a good fit for the non-linear response in Figure 5.1 no matter what the value of C_3 is. Figure 5.3 shows the best fit between the simulated response and experimental results. The amplitude response in Figure 5.3 (a) shows that the damping term for the large magnitude is greater than those with small amplitude response. This suggests that there is an extra damping term missing in the model Equation 5.1.

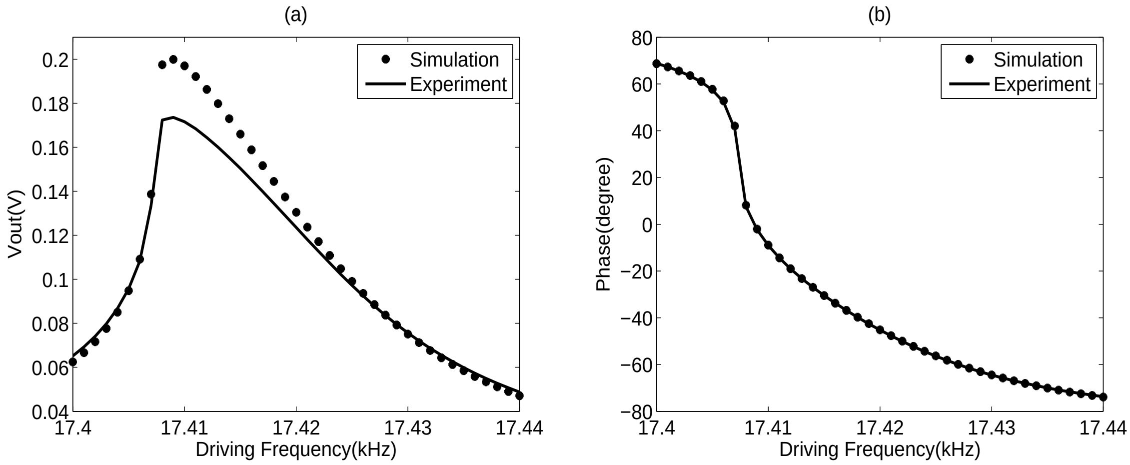

Figure 5.3: The amplitude (a) and phase (b) response of simulation and experimental result with single-ended drive $V_{ac} = 6V_{pp}$ in vacuum with ambient pressure of $7.7Pa$.

Previously, Lifshitz et al. argued that when the forces acting on a resonator have a term proportional to the cube of the displacement x^3 it is reasonable to add a non-linear damping term of the form $x^2\dot{x}$ which increases with the amplitude of motion [25]. Non-linearity in damping mechanisms is then considered, and it makes sense that when the displacement of the motion increases the damping term becomes significant and therefore the effective Q value is then reduced. With the non-linear damping term $\beta x^2\dot{x}$ added to the Equation 5.1, the equation describing the motion of the resonator becomes:

$$\ddot{x} + \frac{\omega_0}{Q}\dot{x} + \omega_e^2 x + \beta x^2\dot{x} + \gamma x^3 = \frac{V_{ac}^2\cos(2\omega t)}{4m}[C_0 + C_1 x + C_3 x^3] \tag{5.3}$$

The motion of equation therefore is symmetric for both damping term and spring constant. The simulated results of both driving voltages in Figure 5.4 shows a good fit after slightly adjust the C_3 and β. Table 5.2 concludes all the extracted parameters for the simulations in Figure 5.2 and Figure 5.4.

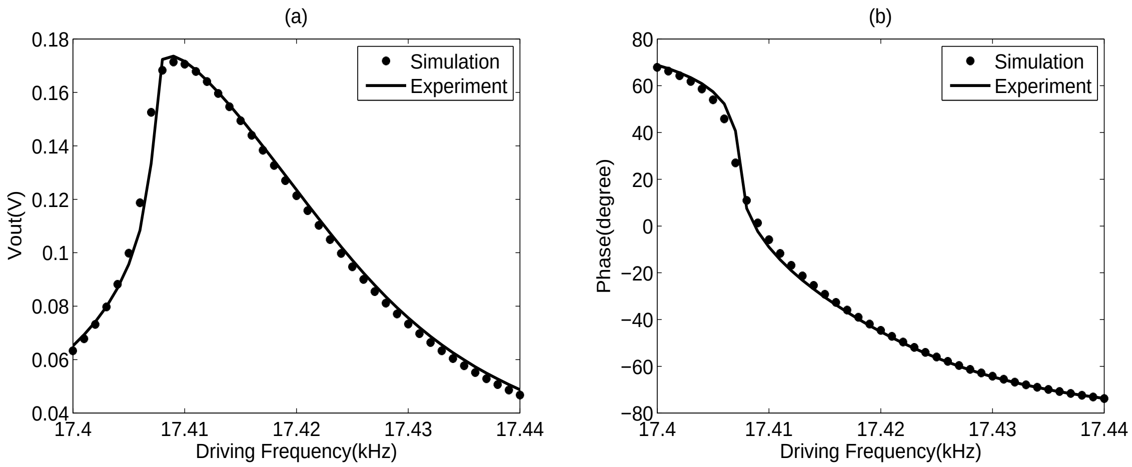

Figure 5.4: The amplitude (a) and phase (b) response of simulation with non-linear damping model and experimental results with single-ended drive $V_{ac} = 6V_{pp}$ in vacuum with ambient pressure of $7.7Pa$.

Table 5.2: The value of the coefficients from parameter extraction of the micromechanical resonator.

Parameter	Value	Parameter	Value
C_0	$18.038 \times 10^{-9}Fm^{-1}$	m	$4\mu g$
C_1	$12.9 \times 10^{-3}Fm^{-2}$	f_0	17497.81Hz
C_2	$-91.2Fm^{-3}$	Q	1334.81 (@7.7Pa)
C_3	$2 \times 10^{9}Fm^{-4}$	β	$5 \times 10^{13}Nskg^{-1}m^{-3}$

5.3 Non-linear response with Q-enhancement in air

The Duffing like non-linearity is observed in vacuum with a natural high Q when the resonator is driven harder which makes the displacement becomes larger. This non-linear behaviour is also expected to occur in the Q-enhanced system which has an effective high Q when it is excited by a larger force. As described in Section 4.5, it has been observed that damping severely limits the amplitude of response of the resonator. To obtain a detectable output signal this damping has been partially cancelled using a feedback force that is proportional to velocity. The resonator has therefore been tested in the presence of a feedback circuit that has been designed to create an electrostatic force that is proportional to the instantaneous velocity so that the effect of damping can be reduced. The displacement was limited below 100nm so that the response of the resonator is in the linear region where the higher order displacement terms of the non-ideal comb capacitance have been ignored (Table 4.1).

The results in Figure 5.5 show that as expected when the driving voltage is relatively small the response of the resonator can be described by the equation for simple harmonic motion. As the drive voltage, and therefore the amplitude of the resonators response increases, the frequency at which the maximum response occurs begins to decrease. In addition the amplitude response as a function of frequency becomes asymmetric. All these features are consistent with the behaviour of a non-linear resonator whose response is similar to the response of Duffing equation.

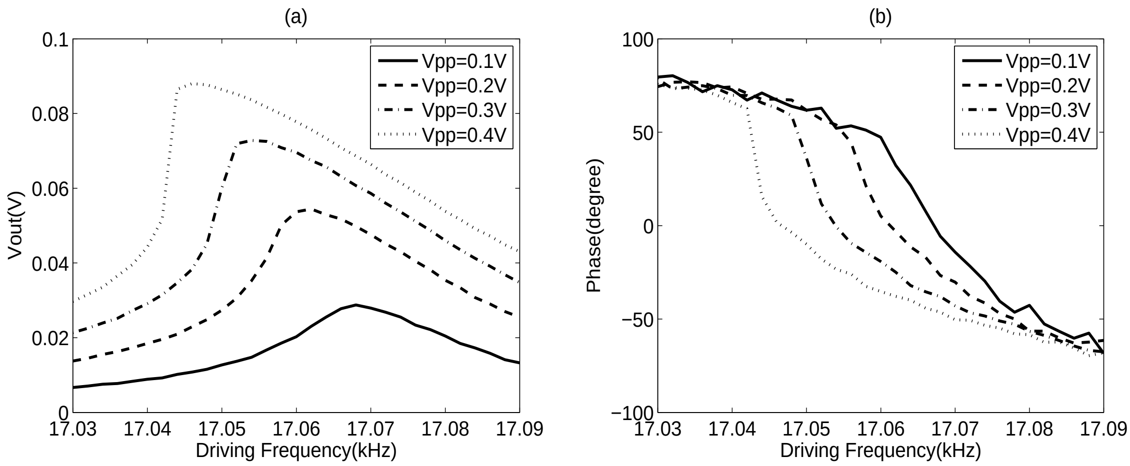

Figure 5.5: The amplitude (a) and phase (b) response of a resonator in air with feedback to reduce damping at different driving voltages.

To exploit the non-linearity of the Q-enhanced system, the model of the feedback system needs to be updated by including the higher orders terms of the comb capacitance. Since the amplitude and phase response of the Q-enhanced resonator in air is quite similar to a Duffing resonator, the critical driving voltage to just create a jump is expected to be calculated with the extracted parameters. In Section 5.2 we extracted the coefficients of the non-ideal comb and in this section how the displacement dependent comb capacitance contributes to the non-linearity of the system will be discussed.

For the Q-enhanced system, differential driving and single-ended readout is implemented and the spare sensing comb is used to apply the e-spring voltage V_e. The motion of the resonator is described by

$$\ddot{x} + \frac{\omega_0}{Q}\dot{x} + \omega_0^2 x + \beta x^2 \dot{x} = \frac{F_{sense}}{m} + \frac{F_{drive}}{m} \tag{5.4}$$

where β is the non-linear damping parameter which arises when the force applied has a non-linear term. The overall sensing force F_{sense} is

$$F_{sense} = \frac{1}{2}V_S^2(C_0 + C_1x + C_2x^2 + C_3x^3) - \frac{1}{2}V_e^2(C_0 - C_1x + C_2x^2 - C_3x^3) \tag{5.5}$$

in which the polynomials describing comb capacitances are different due to the opposite direction of displacement for each comb. The second harmonic term C_2x^2 is ignored because of the relative small value as shown in Table 5.1. The DC part $\frac{1}{2}C_0(V_S^2 - V_e^2)$ is just an offset which will not affect the amplitude of the displacement of resonator. Then the sensing force becomes

$$F_{sense} = \frac{1}{2}(V_S^2 + V_e^2)C_1x + \frac{1}{2}(V_S^2 + V_e^2)C_3x^3 \tag{5.6}$$

The first term in Equation 5.6 affects the effective resonant frequency of the system, and the second term is a part of displacement cubed non-linearity. The overall driving force F_{drive} is the difference between the following two forces applied on each driving comb separately:

$$F_{drive} = F_{drive+} - F_{drive-} \tag{5.7}$$

in which F_{drive+} and F_{drive-} can be described by

$$\begin{aligned} F_{drive+} &= \frac{1}{2}[V_{DC} + (V_{AC} + V_{FB})]^2(C_0 + C_1x + C_2x^2 + C_3x^3) \\ F_{drive-} &= \frac{1}{2}[V_{DC} - (V_{AC} + V_{FB})]^2(C_0 - C_1x + C_2x^2 - C_3x^3) \end{aligned} \tag{5.8}$$

where V_{FB} is the feedback voltage and the second harmonic terms in Equation 5.8 are ignored again since C_2x^2 is much smaller than the other terms as shown in Table 5.1. The feedback voltage V_{FB} is much larger than the primary driving voltage V_{AC} so all the terms related $V_{FB}V_{AC}$ and V_{AC}^2 are insignificant in comparison with V_{FB}^2 and therefore these terms are removed. Higher order terms whose degree is greater than three are discarded in this analysis. The overall driving force can be concluded as

$$F_{drive} = 2C_0V_{DC}V_{AC} + C_1V_{DC}^2x + C_3V_{DC}^2x^3 + 2C_0V_{DC}V_{FB} + C_1V_{FB}^2x \tag{5.9}$$

The first term in the overall force (Equation 5.9) is the primary drive, and the second and third term modify the effective resonant frequency and the displacement cubed non-linearity respectively. The fourth term has been discussed in Section 4.5.3 which cancels part of the damping term and phase shift of the bandpass filter increases the effective Q value of the system even further. The V_{FB} in the last term of Equation 5.9 is also substituted by the model with phase shift (Equation 4.25) and then the last term is expanded to

$$\begin{aligned} F_{drive1} &= C_1 x V_{FB}^2 \\ &= C_1 x G_{fb}^2(\dot{x} - \omega\varphi(\omega)x)^2 \\ &= C_1 G_{fb}^2 x\dot{x}^2 + C_1 G_{fb}^2\omega^2\varphi^2(\omega)x^3 - 2C_1 x G_{fb}^2\omega\varphi(\omega)x^2\dot{x} \end{aligned} \tag{5.10}$$

Supposing the displacement response of the resonator $x = A\cos\omega t$ then the first term in Equation 5.10 can be described by

$$\begin{aligned} F_{drive11} &= C_1 G_{fb}^2 x\dot{x}^2 \\ &= C_1 G_{fb}^2 A\cos\omega t(-\omega A\sin\omega t)^2 \\ &= C_1 G_{fb}^2\omega^2 A^3\cos\omega t\frac{1-\cos 2\omega t}{2} \\ &= \frac{1}{2}C_1 G_{fb}^2\omega^2 A^3[\cos\omega t - \frac{1}{2}(\cos\omega t + \cos 3\omega t)] \\ &= \frac{1}{4}C_1 G_{fb}^2\omega^2 A^3(\cos\omega t - \cos 3\omega t) \end{aligned} \tag{5.11}$$

For comparison, the cubed displacement term can be expanded to

$$x^3 = A^3\cos^3\omega t = \frac{1}{4}A^3(3\cos\omega t + \cos 3\omega t) \tag{5.12}$$

The third harmonic term in Equation 5.12 has been ignored to obtain the cubic equation 1.24 because its size is relative small. If the third harmonic in both Equation 5.11 and Equation 5.12 are ignored then $F_{drive11}$ can be considered to form part of the observed non-linearity as shown in Equation 5.13.

$$F_{drive11} \approx \frac{1}{3}C_1 G_{fb}^2\omega^2 x^3 \tag{5.13}$$

The second term in Equation 5.10 is a displacement cubed term with a magnitude that is dependent on different driving frequencies. In the frequency range of measured results, the largest value of this term occurs at $f = 17030Hz$ when φ^2 reaches it maximum 1.44×10^{-3} while the minimum value equals to zero at resonance where phase shift is zero. Compared with $F_{drive11}$ in Equation 5.13, the ratio between these two terms when $f = 17030Hz$ is

$$Ratio = \frac{C_1 G_{fb}^2 \omega^2 \varphi^2(\omega) x^3}{\frac{1}{3} C_1 G_{fb}^2 \omega^2 x^3} = 3\varphi^2(\omega) = 0.43\% \tag{5.14}$$

which shows that the contribution of the second term in Equation 5.10 to the overall non-linearity is insignificant compared with the first term and therefore the second term can be removed for simplicity of the model. The last term in Equation 5.10 is in the form of a non-linear damping term which will modify the inherent non-linear damping due to the large displacement as discussed in Section 5.2. To summarise, the model for the Q-enhanced resonance is described by

$$\ddot{x} + \frac{\omega_0}{Q_{eff}}\dot{x} + (\omega_e^2 + M)x + \gamma x^3 + (\beta + N)x^2\dot{x} = \frac{2V_{AC}V_{DC}C_0}{m} \tag{5.15}$$

where Q_{eff} is determined by Equation 4.23 and the effective resonant frequency ω_e can be calculated by

$$\omega_e = \sqrt{\omega_0^2 - \frac{C_1}{2m}(V_e^2 + V_S^2 + 2V_{DC}^2)} \tag{5.16}$$

The coefficients M and N and in Equation 5.15 are determined by the phase shift from the bandpass filter:

$$M = 2C_0 V_{DC} G_{fb} \omega \varphi(\omega)/m \tag{5.17}$$

$$N = C_1 G_{fb}^2 \omega \varphi(\omega)/m \tag{5.18}$$

where $\varphi(\omega)$ is determined by Equation 4.27 and the cubic non-linear parameter γ is

$$\gamma = \frac{1}{2}C_3(V_S^2 + V_e^2 + 2V_{DC}^2)/m + \frac{1}{3}C_1 G_{fb}^2 \omega^2/m \tag{5.19}$$

In a typical operating mode, the value for the term arising directly from the non-linear coefficient of the comb C_3 is around $9.1 \times 10^{19} N/kg$ which is also the origin of the non-linearity observed in vacuum. The value of the term caused by the combination of the displacement dependent term of the comb C_1 and feedback force which is meant to cancel part of the damping is between $8.23 \times 10^{20} N/kg$ and $8.28 \times 10^{20} N/kg$ in the measured driving frequency range which is around ten times larger than the non-linear term from the comb coefficient C_3. As expected, comparing the response with Q-enhancement in air (Figure 5.5) and that in vacuum (Figure 5.1), much smaller displacement is required to create a jump for the Q-enhance resonator because of the non-linear cubic parameter γ is greater than the counterpart in vacuum. This means that Q-enhanced feedback technique not only cancels part of the damping term but also can create an extra non-linearity.

The corresponding cubic equation to Equation 5.15 can be obtained by assuming $x = A\cos\omega t$, and the amplitude A is determined by

$$\begin{aligned}[(\frac{3}{4}\gamma)^2 &+ (\frac{\omega}{4}(\beta+N))^2](A^2)^3 + [\frac{3\gamma}{2}(\omega_e^2-\omega^2+M) + \frac{1}{2}\frac{\omega^2\omega_0}{Q_{eff}}(\beta+N)](A^2)^2 \\ &+ [(\omega_e^2-\omega^2+M)^2 + (\frac{\omega_0\omega}{Q_{eff}})^2]A^2 = (\frac{2V_{ac}V_{DC}C_0}{m})^2 \end{aligned} \tag{5.20}$$

and the phase response can be described by

$$\tan\phi = \frac{\frac{\omega_0\omega}{Q_{eff}} + \frac{\omega}{4}(\beta+N)A^2}{\omega_e^2-\omega^2+M+\frac{3}{4}\gamma A^2} \tag{5.21}$$

The simulation results for solving the above cubic are shown in Figure 5.6, and non-linear damping term β that increases with the amplitude of the resonator is carefully adjusted to $3 \times 10^{15} Nskg^{-1}m^{-3}$ so that the simulation fits well with the experimental results of all four different driving voltages.

5.4 Sensitivity enhancement using over-critical non-linearity

One possible response to the complexity of Equation 5.15 could be to limit the driving voltage applied to the resonator so that its displacement is small enough to be governed by the very

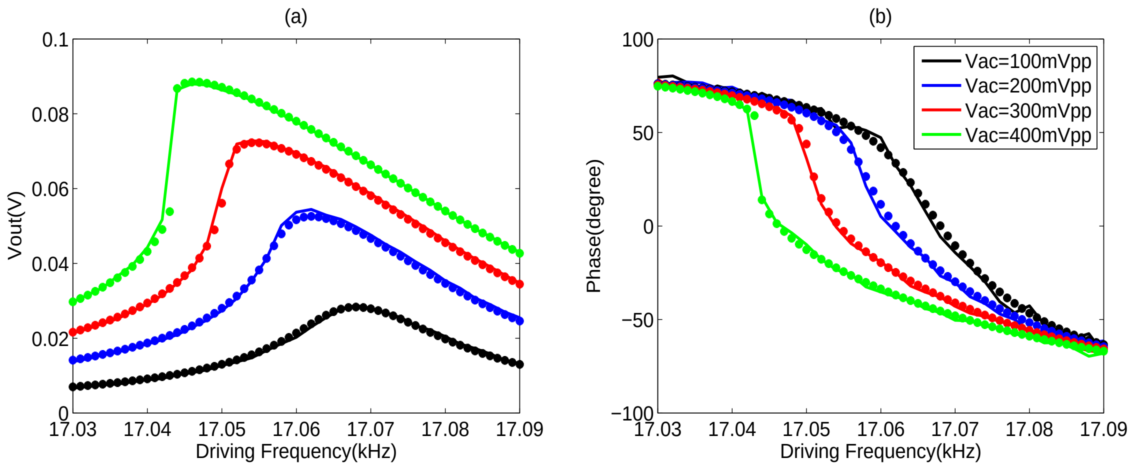

Figure 5.6: The amplitude (a) and phase (b) response of simulation (star) and experimental results (solid line) with different driving voltages with Q-enhancement in air.

well understood equation for simple harmonic motion as in Section 4.5. The sensitivity of the resonator's response to changes in the resonant frequency could then be increased using force feedback to increase the Q value of the resonator. To achieve an increase in the effective Q, a feedback force is used to partially cancel the effect of damping. However, if the feedback force completely cancels the force due to damping, this results in positive feedback and could cause damage to the resonator. The key problem with this approach is that the effective Q is critically dependent upon the feedback level and practical experience shows that it is difficult to increase the effective Q by more than a factor of 100.

An alternative approach to increasing the sensitivity of the resonators' response to changes in resonant frequency is suggested by the frequency dependence of the response of a Duffing resonator. When the driving force is larger than the critical driving force, there are two frequencies at which the amplitude and phase suddenly jump when the frequency of the driving force is changed continuously. Previous discussion in Section 1.4 also shows that if the resonant frequency of the corresponding linear resonator, ω_0 , changes then the two jump frequencies also change. The resulting dramatic changes in the amplitude or phase of the resonator when driven at one of these jump frequencies can potentially be exploited to detect a change in the resonant frequency of the linear resonator ω_0.

The critical driving voltage can be calculated from the cubic equation 5.20 with the same method discussed in Section 2.2. For the Q-enhanced system discussed above, the critical driving voltage is $V_{ac} = 375mVpp$ and the corresponding driving frequency is $f = 17045.6Hz$. The response of the resonator when the AC driving voltage is slightly greater than the critical driving voltage will be discussed. This over-critical non-linearity means that the driving voltage of the resonator is large enough to create a hysteresis so that there will be two jump frequencies but not too significant to cause the undesirable long transient response discussed in Section 2.2.

Choosing a driving voltage which is slightly greater than critical voltage, the amplitude and phase responses with $400mVpp$ have been investigated. If the resonator had retained a linear response then this higher driving voltage would correspond to an output voltage of 115mV. The observed maximum voltage, shown in Figure 5.7(a), is significantly lower than this expected value and the frequency dependence of the amplitude of the resonator's response is very different from that observed at lower amplitudes. Furthermore at this driving voltage there is hysteresis in the amplitude response of the resonator. All of these features of the observed response of the system are similar to the behaviour of a Duffing resonator. However, the most important aspect of the results in Figure 5.7(a) is that they show that the reduction in the resonant frequency, ω_0, has caused the expected shift in the frequency dependence of the response of the system.

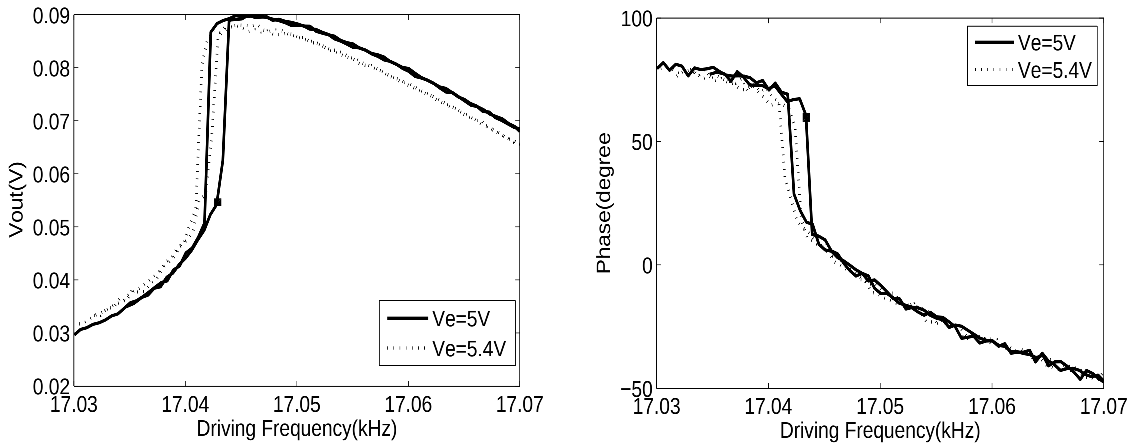

Figure 5.7: The non-linear amplitude(a) and phase(b) response when the voltage on the e-spring is either $5V$ (solid line) or $5.4V$ (dashed line).

As with the linear resonator, monitoring the phase response of the non-linear resonator at a constant frequency is a convenient method of sensing any changes in resonant frequency. The results in Figure 5.7 (b) show that like the amplitude response of the resonator the phase response also shows both hysteresis and a shift when the resonant frequency is changed. A close inspection of the phase changes when the resonant frequency is changed suggests that there is a drive frequency that could be used to sense a decrease in resonant frequency. A large change in phase response can be observed if the resonator is driven at a frequency corresponding to an initial phase of 60 degrees within the region of hysteresis, indicated by the black rectangles in Figure 5.7. Ideally, when driven at this frequency any decrease in resonant frequency can cause a phase change of approximately -40 degrees since the new phase response will be at the other stable state branch for the same frequency. These results suggest that by exploiting the non-linear response of the resonator it should be possible to increase the sensitivity of the system to changes in resonant frequency.

The sensitivity of this kind of system depends on the method to find the jump frequency and also the stability of the jump frequency. There are two methods to find the jump frequency. The first one is sweeping the frequency up slowly and the jump frequency can be recorded. Then the driving frequency can be set to the pre-recorded value directly. Since the initial condition that is required to sense a change in resonant frequency corresponds to the lower amplitude state of the resonator it has been found by simply driving the resonator from rest at the required frequency. The other method is to measure the DC voltage which is proportional to the phase response and then using the control system in Section 4.5.2 to find the driving frequency which can give the pre-measured phase value.

To check the stability of there two reference parameter, the jump frequency and the DC voltage representing the phase response are recorded for ten times of sweeping the frequency up repeatedly, driven with a 400mVpp AC drive voltage as shown in Figure 5.8. The relative standard deviation of the jump frequency is $1.95 \times 10^{-3}\%$ while the DC voltage is 1.1%. In this case it is more reliable to choose the jump frequency as the reference.

If the reference jump frequency is greater than the real value, the amplitude response will be at the higher stable state at which the decrease in resonant frequency will not show any sudden jump in amplitude or response. It is better to choose the minimum value of frequency from the repeating experiments in Figure 5.8. The condition to confirm the ability to detect a

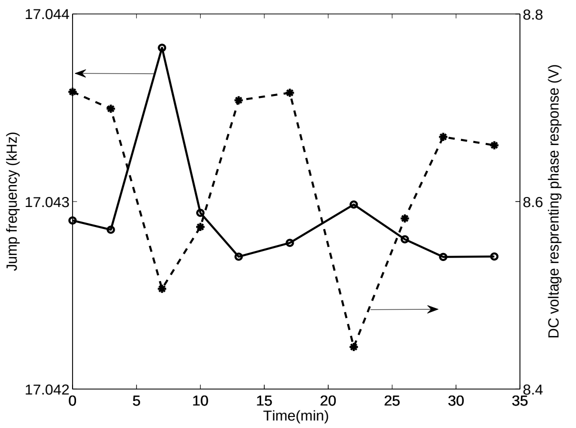

Figure 5.8: Jump frequency (solid line with circles) and DC voltage representing the phase response at the jump frequency (dashed line with stars) for sweeping the frequency repeatedly in a 30 minutes time window.

change in resonant frequency is to drive the resonator at a frequency of $17042.7Hz$. Once the resonator had achieved a steady state response both the amplitude and phase have been used to confirm that the resonator was in the low amplitude state within the hysteresis loop. Once this initial condition had been established the resonant frequency of the resonator was changed instantaneously by using SignalExpress program to control a power supply which added 0.4V to the existing 5V e-spring voltage. This is the minimum e-spring voltage that the resonator can detect and the resonant peak shift caused by this e-spring voltage change is 1.45Hz which is obtained by comparing the response of the same resonator in its linear mode when driven with AC signal $100mVpp$. The range of the jump frequency samples in Figure 5.8 is $1.12Hz$ and it is not surprising that the reliably detectable resonant frequency change is slightly greater than its fluctuation range.

The results in Figure 5.9 show the typical transient response of the resonator in the few seconds before and after the resonant frequency has changed. As expected, Figure 5.9(a) shows an increase in amplitude when the induced change in resonant frequency destroys the stable low amplitude response of the resonator to this drive voltage. This change of amplitude could easily be detected. However Figure 5.9(b) shows that the destruction of the initial state has caused an even more dramatic change in the phase response of the system.

In contrast, the transient response following the same resonant frequency change when the resonator is operated in its linear mode has been shown in Figure 4.21 in Section 4.5.3.

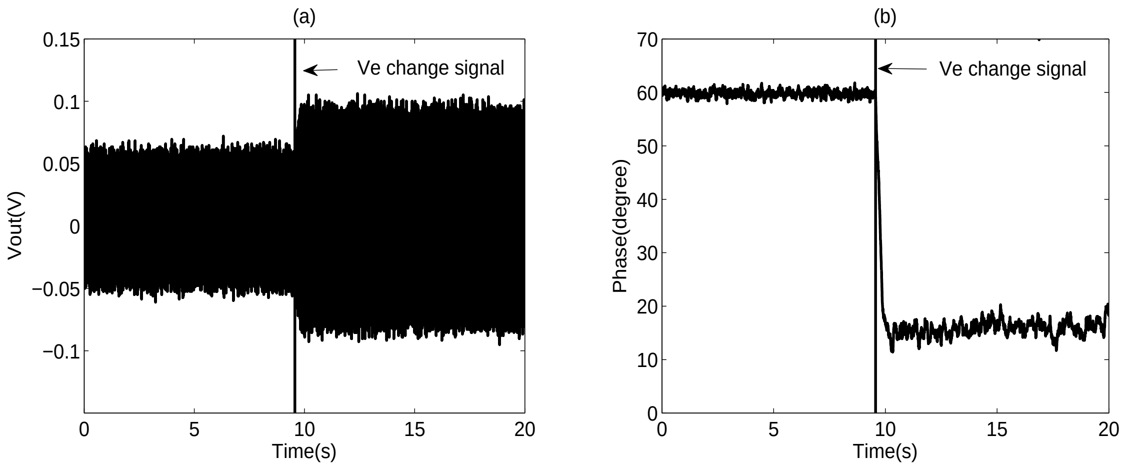

Figure 5.9: The transient amplitude (a) and phase (b) response of the resonator driven at 17.0427kHz with 400mVpp when the e-spring voltage (Ve) changes from 5V to 5.4V at the time indicated by the vertical line.

The amplitude change in Figure 4.21(a) can hardly be detected and the phase change in Figure 4.21(b) is only one fifth of the phase change when the same resonator is driven into its non-linear mode. Furthermore the results in Figure 4.21(b) and Figure 5.9(b) show that the phase noise of the resonator when operated in both linear and non-linear modes is approximately 5 degrees. This means that by operating in the non-linear mode the sensitivity to changes in resonant frequency has been significantly increased compared with the sensitivity in its linear model with the same feedback level. Moreover, if compared with resonator operated in air without any feedback, the non-linear resonator is approximately 300 times more sensitive.

5.5 Sensitivity enhancement using sub-critical non-linearity

The sensitivity of the resonator operating in the non-linear region with discontinuity in amplitude and phase is increased significantly compared with those in its linear mode. The ability to find the jump frequency determines the sensitivity of this method. Although this system can be implemented as a very sensitive alarm system, the amounts of the phase change caused by different changes in resonant frequency are almost the same which means that the resonant frequency change can not be easily quantified from the amounts of the phase change. This can be solved by reducing the driving voltage below the critical driving voltage so that the amplitude and phase response will be still continuous but with large rate of change of $\frac{d\phi}{d\omega}$ for a certain range of frequencies.

Figure 5.5 compares the amplitude and phase response of Q-enhancement with different AC driving voltages. As the driving voltage increases, the maximum $\frac{d\phi}{d\omega}$ in Figure 5.5 (b) grows. When a jump in phase occurs, in theory, the rate of change of phase versus frequency approaches infinity. As a result, if the driving voltage is just below the critical driving voltage, so called sub-critical non-linearity, the maximum $\frac{d\phi}{d\omega}$ will be larger than that at resonance in its linear mode. The phase change rate versus driving frequency with AC signal $300mV_{pp}$ is shown in Figure 5.10. It is clear that the peak phase change rate is at $17051Hz$ which is $17Hz$ smaller than the resonant frequency and it is not symmetrical with respect to the frequency where peak occurs.

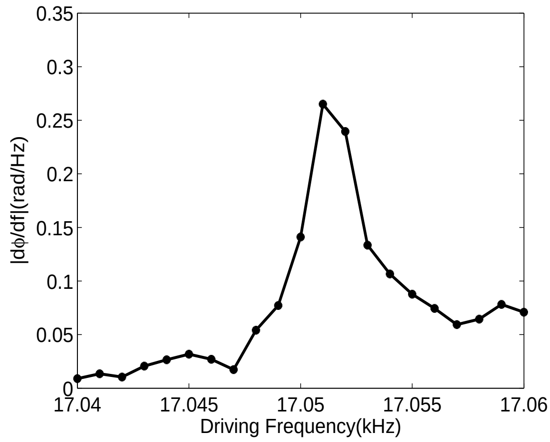

Figure 5.10: Phase change rate versus driving frequency when operating in sub-critical mode driven with AC signal $V_{ac} = 300mV_{pp}$.

The resonator is driven at this maximum $\frac{d\phi}{d\omega}$ point with $f = 17051Hz$ and then the transient response following the same e-spring voltage change from $5V$ to $5.4V$ as Figure 4.21 and Figure 5.9 is shown in Figure 5.11. The same resonant frequency change results in slight increase in amplitude and around 22 degrees phase shift which is about three times the phase shift in the linear mode (Figure 4.21).

It has been confirmed that phase change for the same resonant frequency change is increased as expected, and it is also important to consider the dynamic range as a sensing application. A series of resonance change between $-5Hz$ to $5Hz$ has been induced at the same

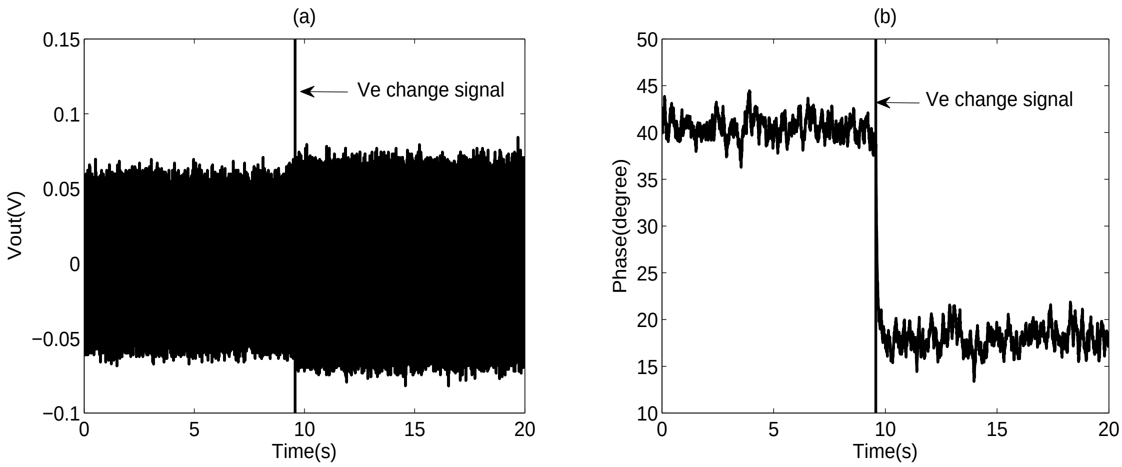

Figure 5.11: The transient amplitude (a) and phase (b) response of the resonator driven at with $V_{ac} = 300mV_{pp}$ at 17.051 kHz when the e-spring voltage (Ve) changes from 5V to 5.4V at the time indicated by the vertical line.

operating point as Figure 5.11. The phase change is expected to be proportional to the resonant frequency change and there should not be any phase change if resonant frequency is fixed. Consequently, it is expected to be a straight line crossing zero and symmetrical with respect to the zero. However, Figure 5.12 shows that the gradient for the positive Δf_0 is smaller than the negative ones. The cause of this asymmetry is the asymmetric phase response curve in Figure 5.5. With the benefit of the increased phase change rate the dynamic range is reduced.

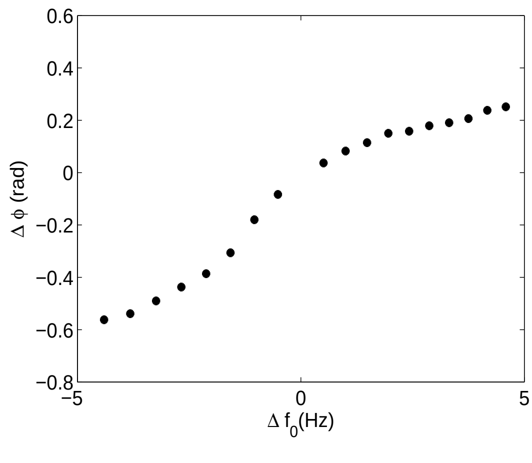

Figure 5.12: Relationship of phase change versus resonant frequency change measured by transient response driven with $V_{ac} = 300mV_{pp}$ at 17.051 kHz.

To compare the dynamic range, the same experiment is repeated for the linear mode ($V_{ac} = 100mVpp$) and the slightly bent response($V_{ac} = 200mVpp$) to implement the resonant frequency change for different values as shown in Figure 5.13. It also gives the linear fit for these three sets of the data, and the fit is obtained with the data points within $1Hz$ decrease in resonant frequency since the phase change rate of the increased resonant frequency when driven with $V_{ac} = 300mV$ is even smaller than that with $V_{ac} = 200mVpp$. This whole figure has shown that the symmetry against the zero point of the linear mode is the best and it becomes more asymmetric when the driving voltage increases which comply with the fact that the phase response becomes more asymmetric when it is driven harder. If only the negative resonant frequency part is considered, there are two points to conclude. The first is that as the driving voltage increases, the phase change increases obviously if the resonant frequency is reduced for the same amount. The other point is that the deviation of the measured data from the fitting line is more serious with the hard driven system as the absolute value of the resonant frequency change grows.

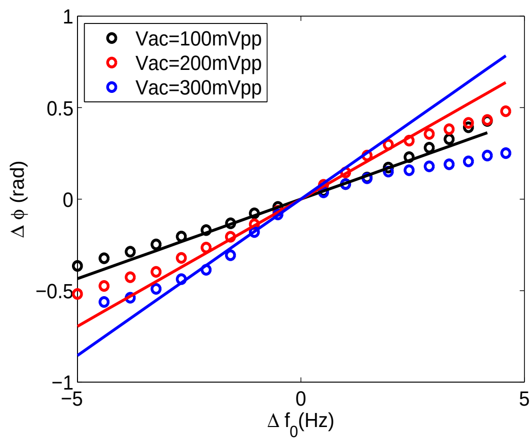

Figure 5.13: Comparison of measured (circle) and fitted (solid line)phase change versus resonant frequency change of different driving voltages.

To quantify the errors in assuming a linear relationship between phase change and resonant frequency change, the root mean square error(RMSE) is calculated with different driving voltages as shown in Figure 5.14. To work out the RMSE, only the negative resonant frequency change is considered. Figure 5.14 shows that for small resonant frequency change, say $-1Hz$, the deviation for all three driving voltage is similar. However, as the resonant frequency change increases, the RMSE which measures the precision of the linear fit is getting larger, especially for the greater driving voltage. This demonstrates that like all sensing systems using the phase response the sensitivity has to trade off against the range of detection.

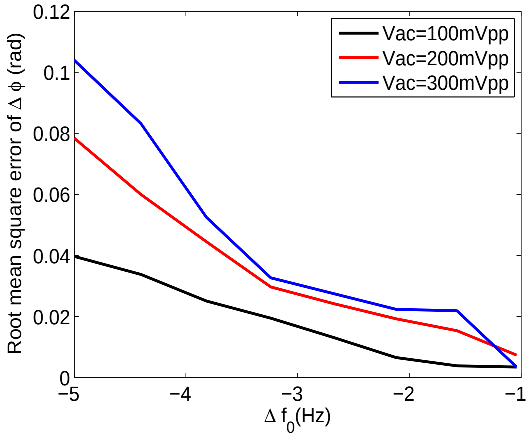

Figure 5.14: Comparison of root mean square error(RMSE) versus resonant frequency change of different driving voltages.

For the sensing application, the desired operating mode can be chosen based on the specific requirement of the application.

5.6 Summary

A micromechanical resonator with Q-enhancement has been driven harder and it shows Duffing-like non-linearity. The origins of a non-linear behaviour have been identified and characterised. The investigation starts with the resonator with large direct drive in vacuum and the source of the non-linearity is the displacement cubed term in the small parallel plate capacitances due to the design of the resonator. For the Q-enhanced system, in addition to this, the combination of the displacement dependent term in the non-ideal comb capacitance and the velocity feedback term plays a major role in the overall non-linearity which means that the Q-enhancement mechanism is a new method to create non-linearity.

Two methods have been discussed for sensitivity enhancement when the resonator is operated in its non-linear mode. The over-critical mode uses the well known jump edge of the Duffing resonator. The resonator is driven with a voltage which is slightly larger than the critical voltage at a frequency that corresponds to one edge of the hysteresis loop. A comparison of responses shows that the maximum phase change when the resonator is operating in its non-linear mode is much larger than the phase change for linear mode. Stability and repeatability of the initial condition has been investigated since it determines the sensitivity of the system.

Despite the desirable sensitivity of the over-critical mode, the resonant frequency change can not be calculated from the phase change. Another operating mode called sub-critical can make up for this deficiency but also increase the sensitivity compared with the Q-enhanced linear mode. The phase change following the effective resonant frequency change occurs when the driving voltage is below the critical driving voltage when the phase response is still continuous but maximum phase change rate is increased due to the non-linearity. The dynamic range has been then identified with different e-spring voltages causing different phase changes. The quantified deviation from the linear fitted curve show that there is a trade off between the sensitivity and the dynamic range.

To conclude, the non-linear mode increases the sensitivity of the resonator compared with the linear mode. If an extremely sensitive system is required and the amount of the resonant frequency is not required the over-critical mode will be desirable. The sub-critical mode can quantify the resonant frequency change with a better sensitivity than the linear mode.

Chapter 6

Sensitivity enhancement using non-linear feedback

6.1 Introduction

The non-linear behaviour of the resonator with Q-enhancement shows advantages in determining the resonant frequency change in Chapter 5. The non-linearity observed arises from the non-ideal comb capacitance which can not be changed once the resonator has been fabricated. Q-enhancement feedback is used to cancel part of the damping term to achieve a large displacement in atmospheric pressure and therefore the non-linear restoring force is increased. In Chapter 3, the Duffing resonator circuit was implemented using a linear resonator with a non-linear feedback. This suggests that non-linear feedback could be an alternative to create a user controllable non-linearity for the micromechanical resonator.

6.2 Driving electronics

The schematic diagram of the non-linear feedback system is shown in Figure 6.1. The capacitive readout of the resonator gives an output signal which is proportional to the velocity. To create a Duffing non-linearity, the measured velocity signal needs to be phase shifted by $90°$ to generate a signal that is in phase with the displacement. In Section 4.5.2, an 8th order switched capacitor bandpass filter was implemented to remove the noise and the centre frequency can

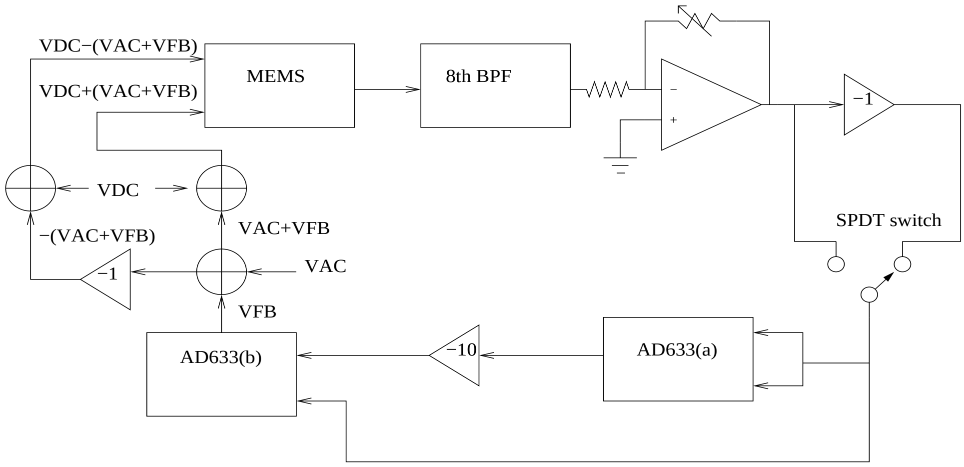

Figure 6.1: Schematic diagram of the non-linear feedback system.

be changed by varying the clock frequency of the filter. The velocity signal is obtained by setting the centre frequency to be the same as the resonant frequency. With the same bandpass filter in Figure 4.15, the displacement signal can be generated by adjusting the filter clock to shift the phase of the output signal by 90 degrees. Since it is an 8th order bandpass filter the maximum phase change through the filter is 720 degrees, this means that a 90 degree phase shift is only a small fraction of the available phase-shift. The clock frequency can therefore be changed to create a 90 degree phase shift through the filter at the driving frequency without a significant loss of gain. In addition, the bandpass filter is followed by an amplifier which can be used to compensate for the reduced gain and control the overall feedback gain. Supposing that the displacement of the resonator is $x = A\cos\omega t$ and the velocity $\dot{x} = -A\omega\sin\omega t$, the output voltage of the bandpass filter after a 90 degrees phase shift can be described by

$$V_1 = -G_{fb}A\omega\sin(\omega t \pm 90) = \mp G_{fb}A\omega\cos\omega t = \mp G_{fb}\omega x \tag{6.1}$$

Then the signal which is proportional to the displacement is amplified with a controllable gain. The sign of the feedback voltage can be controlled by the SPDT switch in Figure 6.1. This phase-shifted and amplified signal will be cubed by two AD633 multipliers that have been used previously in the Duffing resonator circuit (Figure 3.1). The output voltage from the multipliers is $V_{out} = -\frac{1}{10}V_{in}^3$ and similar to the implementation of Duffing resonator circuit, the non-linear feedback voltage that is proportional to the cubed displacement is added to the primary driving AC signal. The equation describing the motion of the resonator with non-linear feedback then becomes

$$\ddot{x} + \frac{\omega_0}{Q}\dot{x} + \omega_0^2 x = \frac{2C_0 V_{DC} V_{ac}\cos\omega t}{m} + \frac{2C_0 V_{DC} V_{FB}}{m} \tag{6.2}$$

where feedback voltage $V_{FB} = \pm\frac{1}{10}(G_{fb}\omega x)^3$ and Equation 6.2 can be modified to a Duffing equation:

$$\ddot{x} + \frac{\omega_0}{Q}\dot{x} + \omega_0^2 x \mp \gamma x^3 = \frac{2C_0 V_{DC} V_{ac}\cos\omega t}{m} \tag{6.3}$$

where the cubic non-linear parameter γ is determined by

$$\gamma = \frac{C_0 V_{DC}(G_{fb}\omega)^3}{5m} \tag{6.4}$$

Since the phase shift of the bandpass filter will only be 90 at one frequency, there will be extra phase shift at other frequencies and for an 8th order filter the rate of change of phase around the key frequency is approximately $0.05°/Hz$. Previous analysis, section 4.5.3, shows the small phase shift resulting from the bandpass filter affects the response of the Q-enhancement feedback system dramatically. For the non-linear feedback method, this phase shift has different effects as the Q value varies. Therefore, the model of the non-linear feedback will be discussed separately with a high Q when the resonator is operated in deep vacuum (Section 6.3) and when the Q value is small in medium vacuum or in air (Section 6.4).

6.3 Non-linear feedback in deep vacuum

6.3.1 Non-linear feedback model characterisation in deep vacuum

A new sample was used for the non-linear feedback experiment because the sample used for the Q-enhancement feedback experiments described in Chapter 4 and Chapter 5 lost one of its driving comb connections at the end of these experiments. The new sample was the same design as the previous sample and although it was fabricated at the same time the resonant frequency of the new sample is around 16.69kHz, which is slightly different from the resonant frequency of the previous one. The parameters of the new sample have been extracted with the same method as in Section 4.4, and these parameter values are summarized in Table 6.1.

Table 6.1: The values of the coefficients from parameter extraction.

Parameter	Value	Units
C_0	16.953×10^{-9}	Fm^{-1}
C_1	11.3×10^{-3}	Fm^{-2}
k_e	1.412×10^{6}	Nm^{-1}
f_0	16797.74	Hz

The higher order displacement dependent terms of the comb capacitance are not considered since the resonator will not be driven into the larger displacement region to create a non-linear force in this chapter. When the resonator is placed in a deep vacuum chamber with a pressure of $9.6Pa$, the Q value of the response is about 1250 (Equation 4.9). The bandwidth of such a high Q system is less than 15Hz and therefore the phase shift resulting from the bandpass filter is not expected to significant.

A softening or hardening non-linearity can be created using the sign of the feedback voltage. For each kind of non-linearity, there are two methods to realise it. If the filter clock frequency is set create a phase shift of 90 degrees and it is followed by an inverting amplifier then the feedback will result in a softening non-linearity. This can also be implemented by setting the filter clock to create a -90 degrees phase shift and followed by a non-inverting amplifier. Figure 6.2 shows the amplitude and phase response of the bandpass filter with the two clock frequencies which create either a leading or a lagging 90 degrees phase shift at the resonant frequency of the sample (16.69kHz). For both filter clock frequencies the non-linear feedback can be softening or hardening with an extra inverting or non-inverting amplifier following the filter. The magnitude response of both filter clocks in Figure 6.2 near resonance are similar. This means that the systems' response with either clock frequency will be very similar and so the softening and hardening behaviours with a filter clock frequency of 835kHz will be investigated in detail.

The velocity signal always leads the displacement signal by 90 degrees, so if the filter clock is 835kHz the output from the bandpass filter is in phase with the displacement of the resonator response. Figure 6.3 shows the amplitude and phase response of the resonator with different

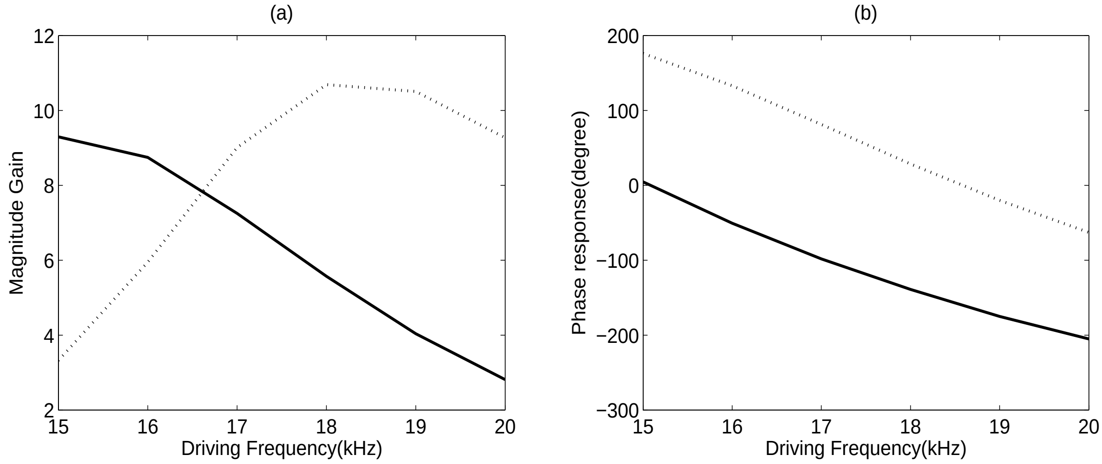

Figure 6.2: The amplitude (a) and phase (b) response of the bandpass filter with CLK=835kHz (solid line) and CLK=1010kHz (dotted line).

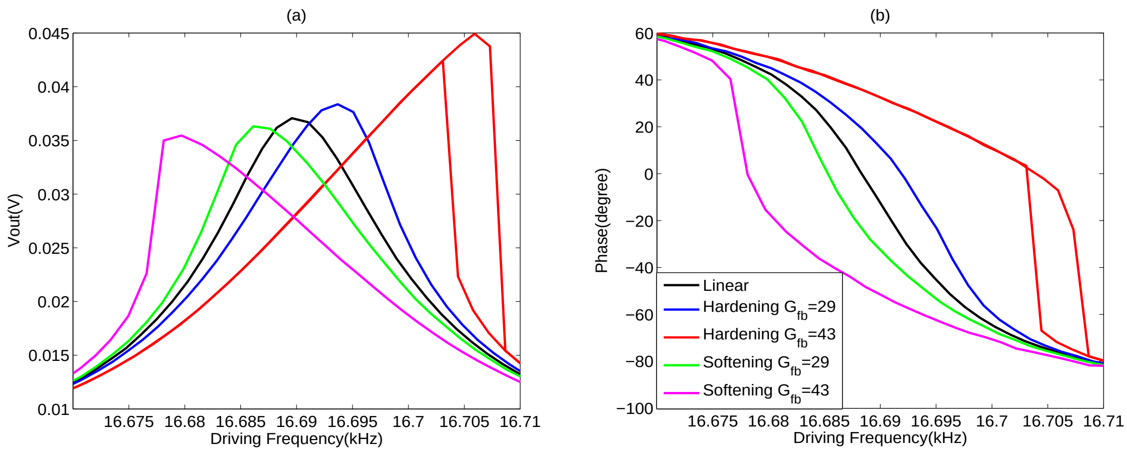

Figure 6.3: The amplitude (a) and phase (b) response of the resonator with different non-linear feedback gains in vacuum with a pressure of 9.6Pa.

levels of non-linear feedback gain, including no non-linear feedback. The amplitude response in Figure 6.3(a) shows that the peak amplitude responses of the five different feedback levels are different from each other. For an ideal Duffing resonator, the peak amplitude is expected to be the same if the primary driving force remains unchanged [52]. The maximum amplitude value is increased compared with the linear resonator as the hardening non-linearity becomes larger. On the contrary, an increase in the softening non-linearity causes a decrease in the peak amplitude. Recall from the analysis of the Duffing circuit in Section 3.3.3, the slight delay of the multiplier gives rise to a non-linear damping term. The non-linear feedback system has a similar behaviour as the Duffing resonator circuit. In addition, there is an extra phase shift φ due to the bandpass filter and the output of the bandpass filter can be described by:

$$V_1 = \pm G_{fb}\omega x[\cos\varphi + i\sin\varphi] = \pm G_{fb}(\omega x\cos\varphi + \dot{x}\sin\varphi) \tag{6.5}$$

where the phase shift φ can be obtained by fitting the phase response curve in Figure 6.2(b):

$$\varphi = 0.04575(f_{ref} - f)(degrees) \tag{6.6}$$

Recall from the model for the multipliers with extra phase shift θ, the feedback voltage is

$$\begin{aligned} V_{FB} &= \pm\frac{G_{fb}^3}{10}[\omega x\cos(\varphi+\theta) + \dot{x}\sin(\varphi+\theta)]^2(\omega x\cos\varphi + \dot{x}\sin\varphi) \\ &= \pm\frac{G_{fb}^3}{10}\{\omega^3\cos\varphi\cos^2(\theta+\varphi)x^3 + [sin2(\theta+\varphi)\cos\varphi + \cos^2(\theta+\varphi)\sin\varphi]\omega^2x^2\dot{x} \\ &\quad +[\sin 2(\theta+\varphi)\sin\varphi + \sin^2(\theta+\varphi)\cos\varphi]\omega x\dot{x}^2 + \sin^2(\theta+\varphi)\sin\varphi\dot{x}^3\} \end{aligned} \tag{6.7}$$

For the model in vacuum with Q value over 1000, the maximum phase shift φ caused by the bandpass filter is around $\pm 1^\circ$ with a measurement range of $40Hz$ in Figure 6.3 (Equation 6.6). The phase shift θ caused by the multiplier delay is approximately -4 degrees as extracted in Section 3.3.3 since the same system of multipliers has been used. Substituting the expected φ and θ value into Equation 6.7, the coefficient values are compared and the last two terms are significantly smaller than the first two. To simplify the model, the equation of the non-linear feedback in deep vacuum becomes:

$$\ddot{x} + \frac{\omega_0}{Q}\dot{x} + \omega_0^2 x \pm \gamma[x^3 + \frac{2\tan(\theta+\varphi)+\tan\varphi}{\omega}x^2\dot{x}] = \frac{2C_0V_{DC}V_{ac}\cos\omega t}{m} \tag{6.8}$$

where cubic non-linear parameter γ is determined by

$$\gamma = \frac{\cos^2(\theta+\varphi)\cos\varphi C_0 V_{DC}(G_{fb}\omega)^3}{5m} \tag{6.9}$$

This simplified model has a non-linear damping term which has opposite sign of the cubic non-linear parameter. As with the Duffing resonator circuit the phase shift through the non-linear feedback loop will introduce a non-linear damping term into the equation of motion for the system. When the feedback loop is used to create a softening non-linearity this extra damping term will be in addition to the existing linear damping and as a result the overall level of damping is expected to increase as the non-linear feedback gain increases. In contrast if the feedback loop is used to create a hardening non-linearity the extra damping term will have a different sign to the existing linear damping. Consequently the overall level of damping is expected to decrease as the non-linear feedback gain increases. In addition to changing the amplitude response the level of damping also affects the critical driving force, with lower levels of damping leading to a lower critical driving force. The fact that there will be less damping for the hardening system than the softening system is therefore consistent with the fact that the hardening response with $G_{fb} = 43$ (red curve) in Figure 6.3 shows a hysteresis loop while the softening response with the same feedback gain value (pink curve) is just about to show the jump. The results in Figure 6.3 are therefore consistent with a phase shift through the feedback loop creating a non-linear damping effect.

The amplitude response of the improved model described by Equation 6.8 can be calculated by solving the corresponding cubic equation:

$$\begin{aligned}&\{(\frac{3}{4}\gamma)^2 + [\frac{1}{4}(2\tan(\theta+\varphi)+\tan\varphi)\gamma]^2\}(A^2)^3 \pm \{\frac{3}{2}\gamma(\omega_0^2-\omega^2) + \frac{\omega\omega_0}{2Q}[2\tan(\theta+\varphi)\\&+\tan\varphi]\gamma\}(A^2)^2 + [(\omega_0^2-\omega^2)^2 + (\frac{\omega_0\omega}{Q})^2]A^2 = (\frac{2V_{ac}V_{DC}C_0}{m})^2\end{aligned} \tag{6.10}$$

and the phase response becomes:

$$\tan\phi = \frac{\frac{\omega_0\omega}{Q} + \frac{1}{4}[2\tan(\theta+\varphi) + \tan\varphi]\gamma A^2}{\omega_0^2 - \omega^2 + \frac{3}{4}\gamma A^2} \tag{6.11}$$

Solving the cubic equation gives the magnitude and phase of the displacement response from which the velocity response can be easily obtained. By comparing the experimental response to the simulated response obtained using the parameters in Table 6.1, the phase shift θ was found to be 4 degrees which is similar to the value expected form the results of the multiplier characterisation in Section 3.3.3. Figure 6.4 shows an excellent fit between the simulated and experimental response. This proves that a relatively small phase shift in the non-linear feedback loop has a significant effect on the response of the system and in particular upon the critical driving force.

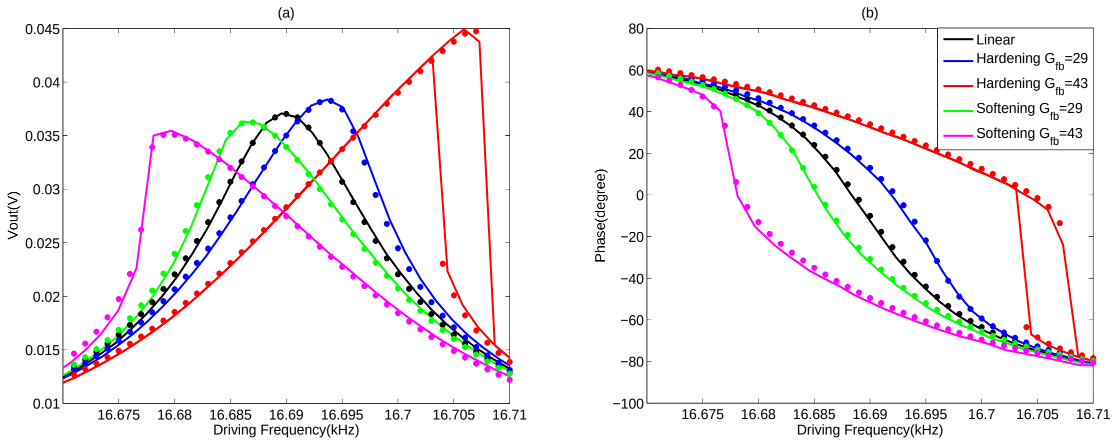

Figure 6.4: The amplitude (a) and phase (b) response of simulation (star) and experimental results (solid line) with different non-linear feedback gains in vacuum with a pressure of 9.6Pa.

6.3.2 Sensitivity of the non-linear feedback system in deep vacuum

The cubic non-linearity observed with direct drive in vacuum or with Q-enhancement feedback in air, is caused by the non-ideal comb capacitance which always shows a softening Duffing behaviour. For the non-linear feedback method either a softening or a hardening non-linearity can be realised easily. The following analysis will take the hardening feedback as an example to investigate the transient behaviour of the non-linear feedback system following a resonant frequency change.

When the non-linear feedback gain is small enough, the response of the system is expected to be the same as a linear resonator. Before investigating the sensitivity of the non-linear feedback system, the linear response with a small enough feedback gain has been studied. Figure 6.5 shows the linear response when the G_{fb} is 25 at pressure 14Pa. The amplitude and phase response is fitted with a linear transfer function with $Q = 858.6$ and $f_0 = 16691Hz$.

In Section 5.4, the minimum detectable resonant peak shift for the Q-enhanced system operated in over-critical region is 1.45Hz. To allow results obtained using non-linear feedback to be compared with these previous results a similar resonant frequency change will also be used for this investigation. Recall from Equation 4.19, 1.3Hz change in resonant frequency can be obtained when the e-spring voltage is changed from 0V to 1.1V with the extracted parameter in Table 6.1. Figure 6.5 shows that the expected 1.3Hz change in resonance peak is observed. This means that the phase shift in the non-linear feedback loop does not have an undesirable effect on the observed changes in the resonance frequency similar to those described in Section 4.5.3. The undesirable effect observed previously arose because a phase shift in the velocity feedback used for Q-enhancement introduced a frequency dependent term into the linear restoring force which determines where the resonant peak occurs. However, with the non-linear feedback used to create a Duffing resonator any phase shift in the feedback loop modifies the non-linear cubic term and the damping of the resonator but the resonant frequency is unaffected.

Figure 6.6 shows the transient amplitude and phase response following an e-spring voltage change from 0V to 1.1V when the resonator is driving at resonance. It is quite difficult to identify the amplitude change caused by the resonant frequency in Figure 6.6(a). However, there is a clear step change in phase following the e-spring change signal indicated by the vertical line in Figure 6.6(b). In theory, the phase change following a 1.3Hz change in resonant frequency is expected to be 7.7° which is calculated with Equation 1.11 using the extracted Q value and the resonant frequency. Comparison of the phase responses in Figure 6.5 gives a phase change of 7.8° with different e-spring voltages at resonance. The transient phase response in Figure 6.6(b) shows the expected 7.8° phase change.

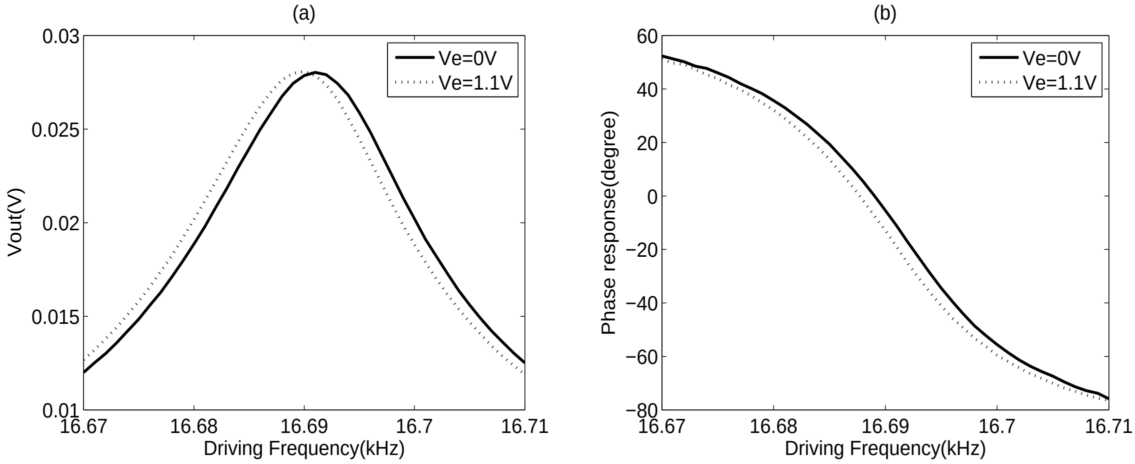

Figure 6.5: The linear amplitude (a) and phase (b)response of the resonator when the e-spring voltage is either 0V (solid line) or 1.1V (dashed line) when the driving voltage $V_{ac} = 150mV_{pp}$ and $G_{fb} = 25$ at pressure 14Pa.

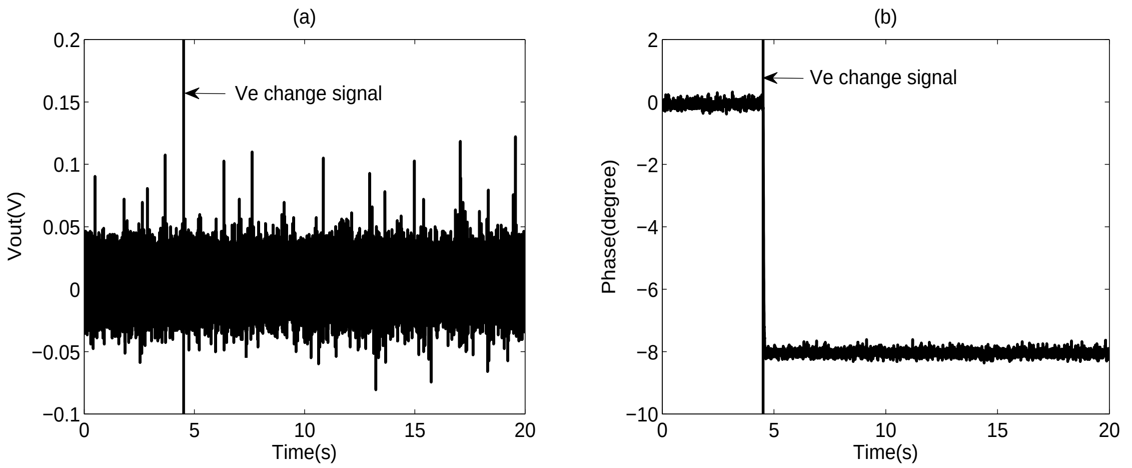

Figure 6.6: The transient amplitude (a) and phase (b)response of the linear resonator driven at resonance (16691 Hz) when resonant frequency is decreased by 1.3Hz at the time indicated by the vertical line.

Before investigating the sensitivity of the non-linear system, the critical feedback gain can be obtained from the cubic equation 6.10 which describes the amplitude response of the non-linear feedback model in deep vacuum. Using the same method as a typical Duffing resonator discussed in Section 2.2, the critical driving frequency and the critical feedback gain that can just create a hysteresis loop with $V_{ac} = 150mV_{pp}$ is calculated to be $16705.8Hz$ and $G_{fb} = 50.6$.

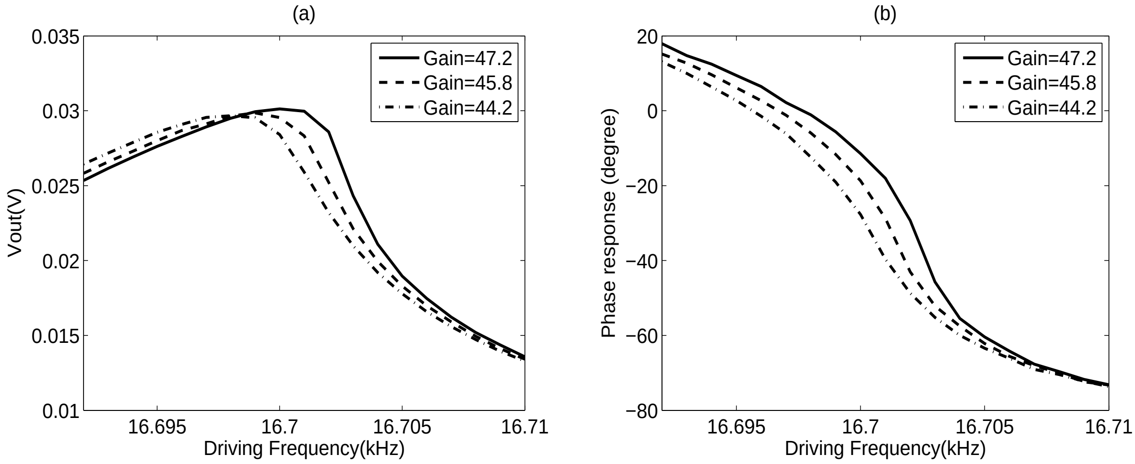

Figure 6.7: Comparison of amplitude (a) and phase (b)response of the resonator with different feedback gains driven with $V_{ac} = 150mV_{pp}$ at pressure $14Pa$.

Consequently, the sub-critical non-linear behaviour is observed when the feedback gain is slightly smaller than the critical value. Three sets of amplitude and phase response with different feedback gains are compared in Figure 6.7. As expected, the amplitude response becomes quite asymmetric but there is no jump in amplitude as the driving frequency changes. The phase response in Figure 6.7(b) shows the maximum $\frac{d\phi}{d\omega}$ increases as the feedback gain rises.

Figure 6.8 shows the rate of change of phase with frequency versus the driving frequency with three different feedback gains. The peak value of each curve corresponds to the driving frequency with the maximum phase change rate. As expected, as the feedback gain increases, the frequency where the maximum rate occurs increases as well and all these three frequencies are smaller than the calculated critical driving frequency 16705.8Hz.

For each of the three driving frequencies obtained in Figure 6.8, the e-spring voltage was changed from 0V to 1.1V and the transient response of the system was observed. The resulting

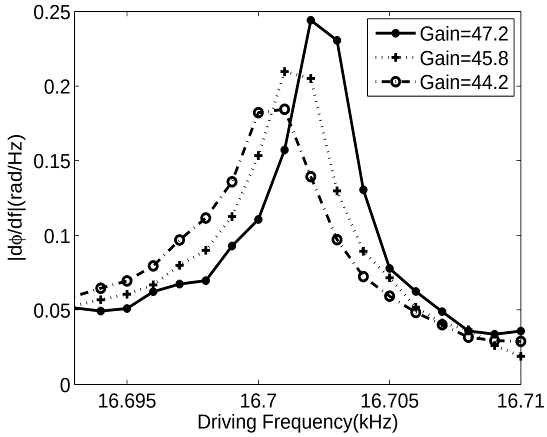

Figure 6.8: Phase change versus the driving frequency with different feedback gains driven with $V_{ac} = 150mV_{pp}$.

transient phase responses for these three different feedback gains are shown in Figure 6.9. These results show that the 1.3Hz change in resonant frequency causes changes in phase of $14.9°$,$17°$ and $20.7°$ respectively. From the peak magnitudes of $\frac{d\phi}{d\omega}$ in Figure 6.8 and these observed phase changes, the expected resonant frequency changes are calculated as 1.41Hz, 1.41Hz and 1.48Hz correspondingly. These values do not differ from the expected value $1.3Hz$ significantly and this is probably caused by the errors of the measured $\frac{d\phi}{d\omega}$ in Figure 6.8. The peak values of the $\frac{d\phi}{d\omega}$ can be smaller than the real ones if the frequency intervals are not small enough. However, compared with a $7.8°$ phase change of the linear resonator following the same e-spring voltage change in Figure 6.6, the phase changes for the resonator driven with the sub-critical driving voltages have been increased. In addition, the noise levels of all of these responses are approximately $0.5°$ which is similar to the noise level of the linear phase response in Figure 6.6. Therefore the signal to noise ratio of the phase response has been improved by driving the resonator with sub-critical feedback gain.

If the driving voltage is fixed then the hysteresis will not be observed until the feedback gain is increased above a critical value. For the model described by Equation 6.10 with $V_{ac} = 150mV_{pp}$, the critical feedback gain is 50.6. As expected, if the feedback gain is increased further so that it is beyond the calculated critical feedback gain of 50.6 then jumps in amplitude and phase are expected. Figure 6.10 shows a hysteresis loop with $G_{fb} = 58$. The comparison of the responses with different e-spring voltages applied shows that if the resonator is driven

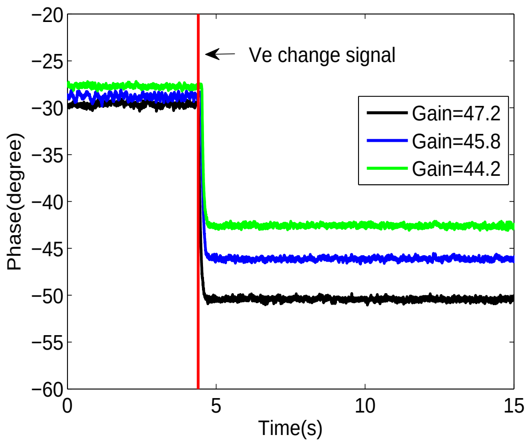

Figure 6.9: Comparison of transient response of the resonator with different feedback gains driven at each maximum $\frac{d\phi}{d\omega}$ frequency with $V_{ac} = 150mV_{pp}$.

at the higher jump frequency the e-spring voltage changing from 0V to 1.1V can be followed by the collapse of amplitude and phase.

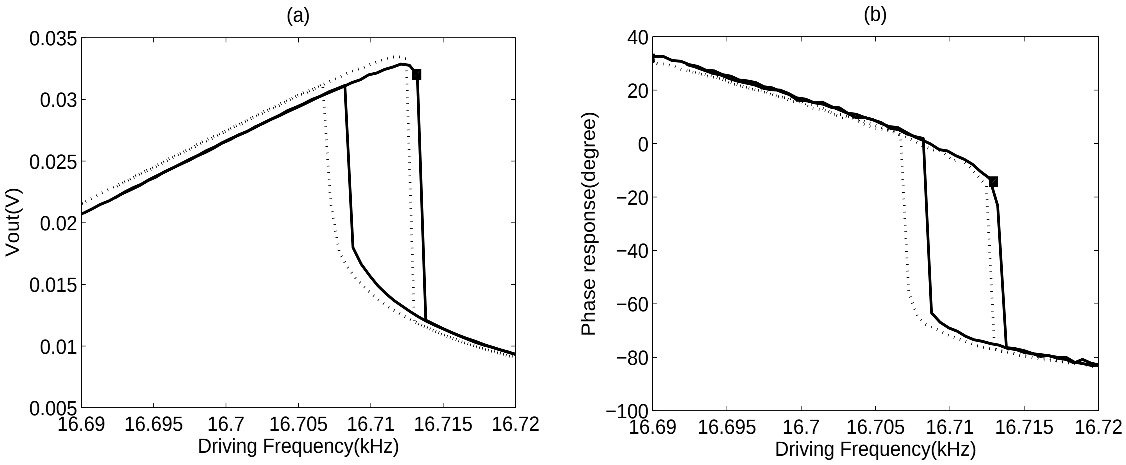

Figure 6.10: The amplitude (a) and phase (b) response of the resonator with a small hysteresis loop when the e-spring voltage is either 0V (solid line) or 1.1V (dashed line) when the driving voltage $V_{ac} = 150mV_{pp}$ and $G_{fb} = 58$ at pressure 14Pa.

Since the higher stable state of the hardening system can only be reached by increasing the driving frequency continuously from a frequency smaller than the lower jump frequency, the driving frequency of the resonator is generated by the DDS system in Figure 3.2 and the frequency control word is programmed by the FPGA so that the driving frequency will be increased gradually until it reaches the high jump frequency indicated by the rectangles in Figure 6.10. Then the same e-spring voltage change as linear and sub-critical system is implemented, and the transient response following the resonant frequency change is shown in Figure 6.11. Both amplitude and phase response shows an instant step change after the e-spring voltage change and the phase change of this over-critical response is approximately 70 degrees which is increased compared with the linear and the sub-critical responses as expected.

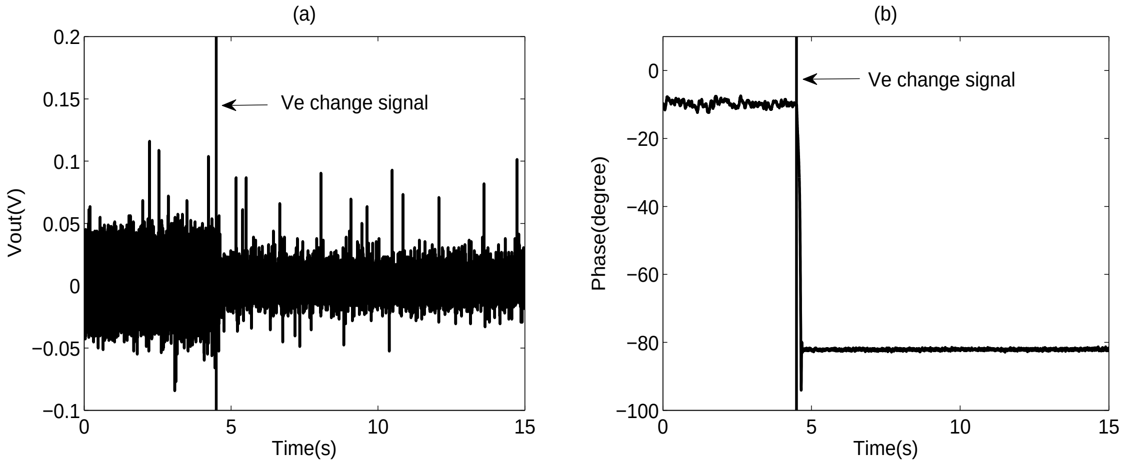

Figure 6.11: The transient amplitude (a) and phase (b)response of the resonator driven at the higher jump frequency (16713 Hz) when resonant frequency is decreased by 1.3Hz at the time indicated by the vertical line.

As discussed in Chapter 2, the simulation results show that when the driving force is far beyond the critical driving force, a resonant frequency change is followed by a delayed amplitude and phase response. This unexpected and undesirable behaviour is believed to be caused by the proximity of the stable and unstable state close to the driving frequency. In Section 3.4.3, the Duffing resonator circuit shows a similar undesirable temporal response. This ensures that this behaviour does not arise from the numerical methods in the simulation. With the micromechanical sample, the observed cubic non-linearity with direct drive in vacuum or Q-enhancement feedback in air is determined by the third harmonic term of the non-ideal comb capacitance and the displacement of the movement. The coefficient value of the third harmonic term is fixed once the resonator is fabricated. The maximum displacement is limited by the gap between the combs which also can not be changed. Under these two restrictions, the cubic restoring force is not sufficient to create a large hysteresis in Chapter 5. The non-linear feedback technique can create an extra cubic non-linear restoring force and therefore it is possible to use this method to confirm whether this problem occurs in the micromechanical systems.

The non-linear feedback gain G_{fb} is therefore increased further to 65, the amplitude and phase response with the e-spring voltage is either 0V or 1.1V are compared in Figure 6.12. It shows a large hysteresis loop both in amplitude and phase response. If there is a 1.3Hz resonant frequency change when the resonator is driven at the higher jump point, the phase response is expected to drop by more than 100 degrees.

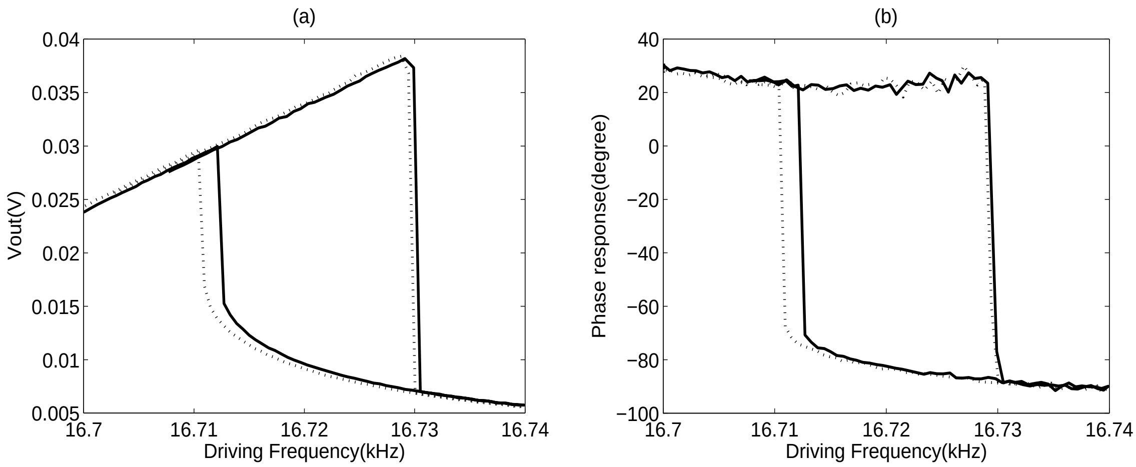

Figure 6.12: The amplitude (a) and phase (b)response of the resonator with large hysteresis loop when the e-spring voltage is either 0V (solid line) or 1.1V (dashed line) when the driving voltage $V_{ac} = 150mV_{pp}$ and $G_{fb} = 65$.

As shown in Figure 6.12(b), the phase response near the higher jump frequency is quite flat and a bit noisy. From the amplitude and phase response in Figure 6.12(b), the higher jump frequency is obtained to be $16730Hz$. When the driving frequency of the resonator is continuously increased to this pre-determined value, the response of the resonator can not be sustained at the high steady state and the amplitude collapses even before any e-spring voltage occurs. To avoid this problem the programmed stop frequency for the automatic sweeping is reduced to $16729Hz$ which is the maximum driving frequency the resonator can stay at the higher branch. The e-spring voltage change effective to a 1.3Hz change in resonant frequency does not lead to any expected jump of amplitude or phase. The minimum detectable resonance change is 2.7Hz and the response following this change varies. Figure 6.13 shows two of the transient responses after the e-spring voltage change. The response of the resonator in

Figure 6.13 suggests that the collapse in amplitude and phase occurs a significant time after the change in resonant frequency. In these circumstances, a change in e-spring voltage is followed by a period in which it has high amplitude, increasingly noisy phase response followed by a sudden collapse in amplitude and phase. In addition, the delay time for repeated experiments is different and unpredictable. This suggests that the undesirable long transient response exists in the micromechanical resonator systems as well. As discussed in Chapter 2, this problem can be avoided by reducing the feedback gain so that it can just create a hysteresis loop and the high amplitude stable state separates quickly from the unstable state. An immediate collapse in amplitude and phase has been observed in Figure 6.11 even for a smaller resonant change.

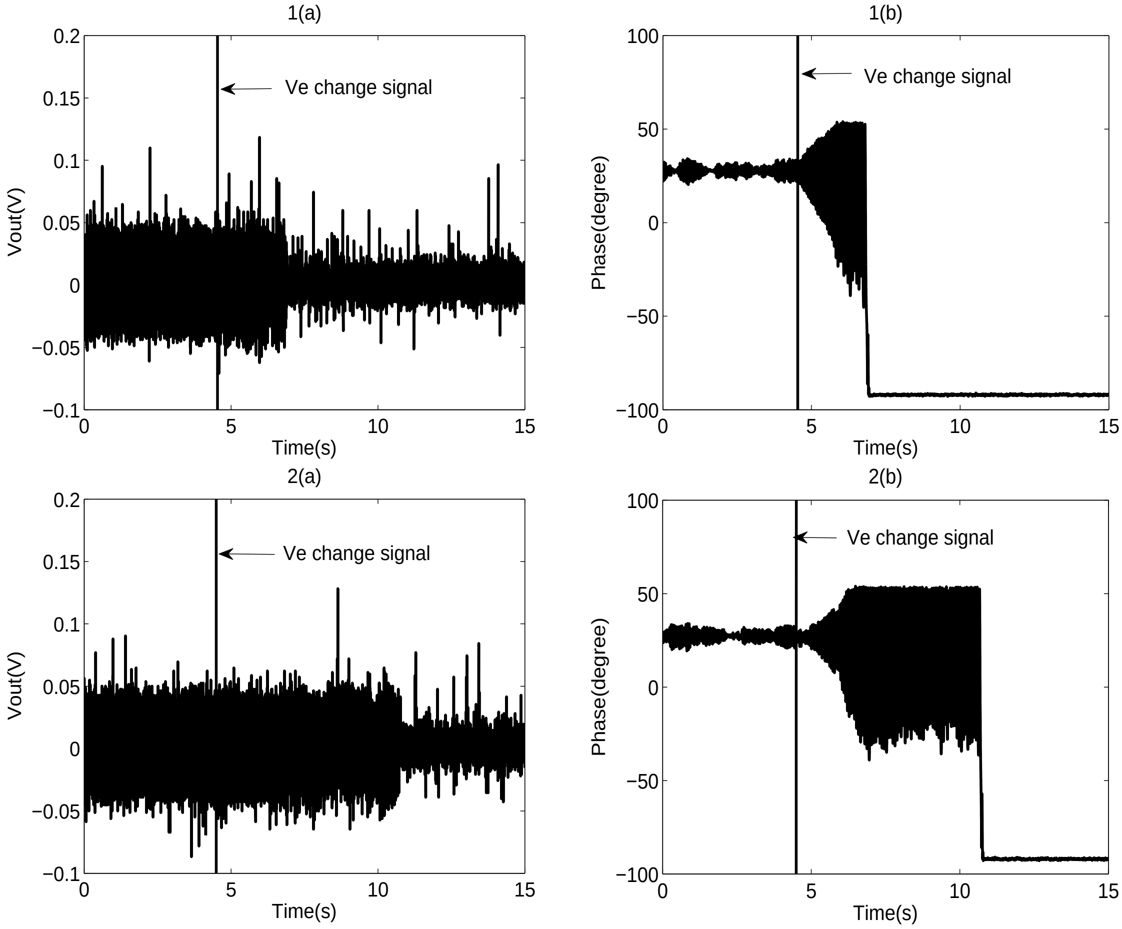

Figure 6.13: Two sets of measured transient amplitude (a) and phase (b) behaviours of the hardening Duffing resonator at higher jump frequency (16729Hz) and the resonant frequency is decreased by 2.7Hz at the time indicated by the vertical line.

6.4 Non-linear feedback in medium vacuum or in air

When the resonator is operated at a pressure of deep vacuum, the bandwidth of the resonance is quite narrow. Hence the frequency dependent phase shift φ from the bandpass filter can be considered to be an insignificant constant and therefore many terms related to φ in the feedback voltage (Equation 6.7) have been ignored. However, when the ambient pressure is increased to medium vacuum or atmospheric pressure, the Q value for the resonator becomes lower and the bandwidth will increase significantly. In particular if the resonator is operated in air, the Q value is approximately 5.5 as discussed in Section 4.4.2 and the bandwidth is approximately 3kHz which means that the value of phase shift φ could reach $\pm 68°$ at $-3dB$ bandwidth frequencies (Equation 6.6). Because of this, there are now several significant terms in the feedback voltage (Equation 6.7). Harmonic balance has therefore been used to simplify the analysis of the effects of phase shift in the feedback loop. This harmonic analysis is started by describing the output voltage of the bandpass filter by

$$V_1 = \pm G_{fb}\omega A\cos(\omega t + \varphi) \tag{6.12}$$

Substituting Equation 6.12 into the multiplier model Equation 3.13 gives the output of the multipliers:

$$\begin{aligned} V_{FB} &= \mp\frac{1}{10}(G_{fb}\omega A)^3[\cos^3(\omega t+\varphi)\cos^2\theta - \sin(\omega t+\varphi)\cos^2(\omega t+\varphi)\sin 2\theta] \\ &= \mp\cos\omega t[\frac{1}{10}(G_{fb}\omega A)^3(\frac{3}{4}\cos\varphi\cos^2\theta - \frac{1}{4}\sin\varphi\sin 2\theta)] \\ &\quad \mp\sin\omega t[\frac{1}{10}(G_{fb}\omega A)^3(-\frac{3}{4}\sin\varphi\cos^2\theta - \frac{1}{4}\cos\varphi\sin 2\theta)] \end{aligned} \tag{6.13}$$

where all the higher order harmonic terms are ignored. Suppose the amplitude response $x = A\cos\omega t$, substituting Equation 6.13 into Equation 6.2 gives

$$\begin{aligned} &[A(\omega_0^2-\omega^2) + \gamma A^3(\frac{3}{4}\cos\varphi\cos^2\theta - \frac{1}{4}\sin\varphi\sin 2\theta)]\cos\omega t + [-A(\frac{\omega_0\omega}{Q}) \\ &-\gamma A^3(\frac{3}{4}\sin\varphi\cos^2\theta + \frac{1}{4}\cos\varphi\sin 2\theta)]\sin\omega t = \frac{2V_{DC}V_{ac}C_0}{m}\cos(\omega t+\phi) \end{aligned} \tag{6.14}$$

where $\gamma = \pm C_0 V_{DC}(G_{fb}\omega)^3/(5m)$ and the corresponding cubic describing the magnitude of the displacement A can be obtained by using harmonic balance method:

$$\gamma^2(\frac{9}{16}\cos^4\theta + \frac{1}{16}\sin^2 2\theta)(A^2)^3 + [\gamma(\omega_0^2 - \omega^2)(\frac{3}{2}\cos\varphi\cos^2\theta - \frac{1}{2}\sin\varphi\sin 2\theta) + \gamma\frac{\omega\omega_0}{Q}(\frac{3}{2}\sin\varphi\cos^2\theta + \frac{1}{2}\cos\varphi\sin 2\theta)](A^2)^2 + [(\omega_0^2 - \omega^2)^2 + (\frac{\omega_0\omega}{Q})^2]A^2 = (\frac{2V_{ac}V_{DC}C_0}{m})^2 \tag{6.15}$$

and the corresponding phase shift is determined by

$$\tan\phi = \frac{\frac{\omega_0\omega}{Q} + \frac{1}{4}(3\sin\varphi\cos^2\theta + \cos\varphi\sin 2\theta)\gamma A^2}{\omega_0^2 - \omega^2 + \frac{1}{4}(3\cos\varphi\cos^2\theta + \cos\varphi\sin 2\theta)\gamma A^2} \tag{6.16}$$

When the resonator is operated in medium vacuum or in air, the damping term increases significantly. To increase the effective driving force and the output voltage, the resonator is biased to $-5V$ from ground. In this way, the effective DC driving voltage V_{DC} increases from $4V$ to $9V$ and the sensing voltage V_s is changed from $8V$ to $13V$. The resonant frequency with these applied DC voltage is then $16414Hz$ which is calculated using Equation 4.19 with the coefficient values in Table 6.1.

Previously the phase shift was set to be ideal at the resonant frequency and the resonator was always driven at a frequency very close to the resonant frequency in the deep vacuum. However, with a lower Q, hysteresis occurs at frequencies that are quite different from the resonant frequency. In this situation the phase shift should be ideal at the driving frequency which is chosen to be the critical driving frequency at which a hysteresis is about to occur. It is quite complicated to calculate the critical driving frequency from the cubic equation 6.15 if the reference frequency, at which the phase shift in the feedback loop is $90°$, is unknown. To simplify the process, the critical driving frequency can be calculated from Equation 2.5 which is obtained from the cubic equation of a standard Duffing resonator. In this way, critical frequency is calculated to be $19201Hz$ with $f_0 = 16414Hz$ and $Q = 5.5$. Although this is slightly different from the real critical frequency as the effective Q value of the non-linear feedback model is modified by the phase shift, this estimation can be set to be the reference frequency. Then the real critical driving frequency can be calculated from the cubic equation 6.15 of

$f_c = 19152Hz$. Before calculating the critical feedback gain, the G_{fb} in Equation 6.15 needs to be updated. In previous analysis, the feedback gain G_{fb} is described by

$$G_{fb} = G_{read} G_{filter} G_{amp} \tag{6.17}$$

where the readout gain $G_{read} = G_{inst} R_{trans} V_s C_0$ is constant which converts the velocity signal to the output voltage. The filter gain G_{filter} is determined by amplitude response of the bandpass filter in Figure 6.2(a)(solid line) which shows that the filter gain changes versus the driving frequency slowly. For the model with high Q, the filter gain change versus driving frequency has been ignored for a narrow bandwidth while for a system with a bandwidth of 3kHz in air, this effect can be significant to the response of the resonator. Therefore, the filter gain G_{filter} near $19kHz$ is represented by a linear function by fitting the amplitude response with a linear curve when the reference frequency is 19152Hz:

$$G_{filter} = 99.493 - 4.675 \times 10^{-3} f \tag{6.18}$$

The G_{amp} in Equation 6.17 is the gain of the amplifier following the bandpass filter and previous comparisons of the effect of different feedback gains have been performed by varying the value of G_{amp}. For the non-linear feedback model driven in air G_{fb} is a frequency dependent function, however for clarity in the following analysis the overall gain at the reference frequency will be referred to as the feedback gain G_{fb}. For the driving voltage $V_{ac} = 150mV_{pp}$ substituting Equation 6.17 and Equation 6.18 into the cubic equation gives a value of the critical feedback gain $G_{fb\_c} = 3656.01$. The simulated amplitude and phase response when the resonator is driven with the different feedback gains near this critical feedback gain value at the atmospheric pressure are compared in Figure 6.14. The response slightly below the critical feedback gain (dotted line in Figure 6.14) shows a high amplitude and phase change rate near the calculated critical driving frequency $19152Hz$ and as the feedback gain increases, a hysteresis loop is observed and then becomes larger.

The results in Figure 6.14 suggest that it will be possible to employ non-linear feedback even when the resonator is operating at atmospheric pressure. The experiment for the harden-

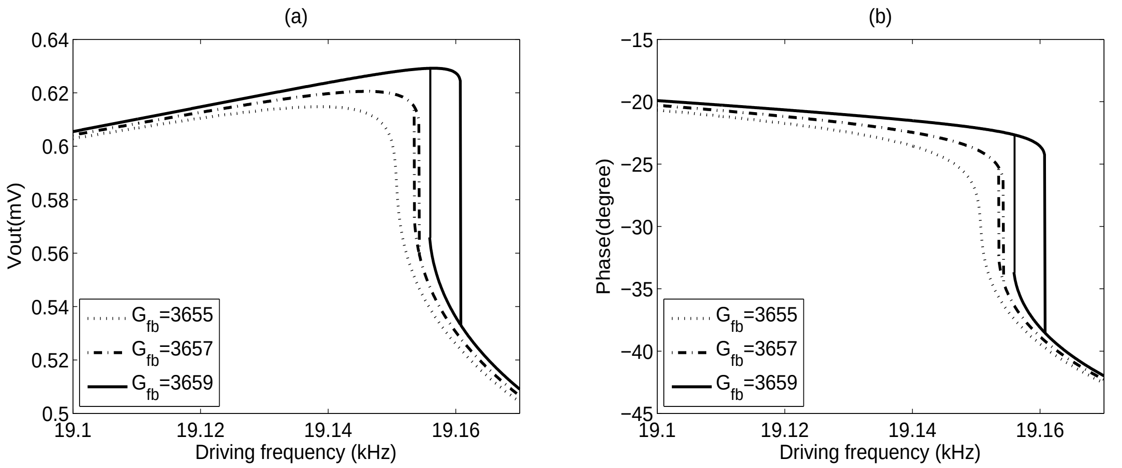

Figure 6.14: The simulated amplitude (a) and phase (b)response of the resonator with different feedback gains at a pressure of $10^5 Pa$ driven with $V_{ac} = 150mV_{pp}$.

ing feedback was conducted at a medium vacuum level before testing at atmospheric pressure. Figure 6.15 shows the amplitude and phase response of the resonator when it is operated at a pressure of $1500Pa$. Recall from Equation 4.9, the natural Q of this ambient pressure is approximately 60. With the reference frequency of around $17kHz$ and $G_{fb} = 320$, the hysteresis in both amplitude and phase are observed in Figure 6.15. This proves that this method is feasible in the medium vacuum. Unfortunately, during the experiments when the resonator was operated at atmospheric pressure, the sample was damaged before any hysteresis was observed. During the experiments in air, self-oscillations have been seen and the damage is probably due to the over-excitation when sweeping frequency into the range of the self-oscillation.

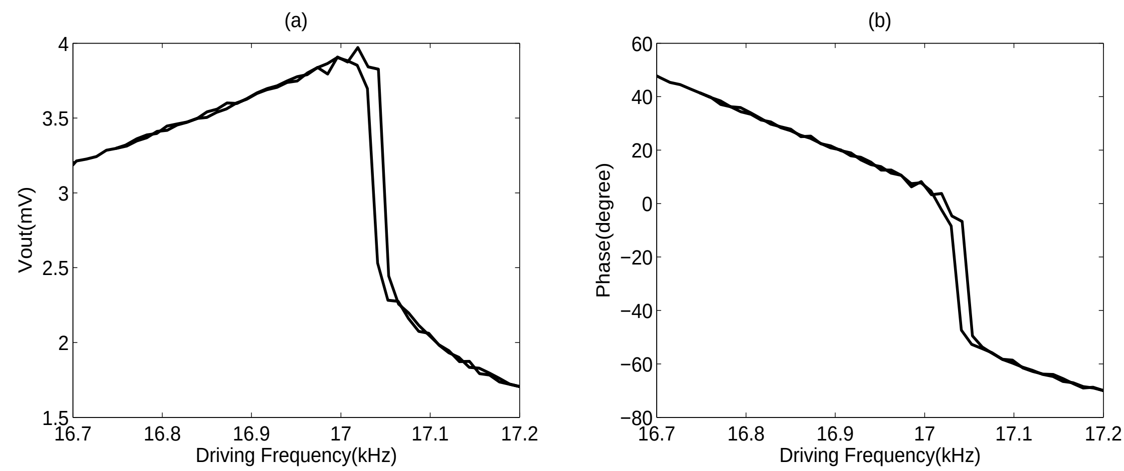

Figure 6.15: The experimental amplitude (a) and phase (b)response of the resonator at a pressure of $1500Pa$ driven with $V_{ac} = 150mV_{pp}$.

To investigate the reason for the self-oscillation, the response of hardening non-linear feedback was simulated with a wider range of frequencies at atmospheric pressure. As shown in Figure 6.16, the system response is very sensitive to both the driving frequency and the feedback gain. In particular Figure 6.16(a) shows the simulated amplitude response of the system when $G_{fb} = 3659$ over a wider range of driving frequencies. The frequency range I is the same response as the solid line in Figure 6.14(a) which is a Duffing-like response. However unlike a Duffing system there is now a second region, frequency range II, in which three solutions coexisting: two of them are steady state (solid line) and the other one is unstable state (dashed line). In addition, there is also now a frequency range, range III, in which there is no stable solution and region IV in which there is a single stable solution.

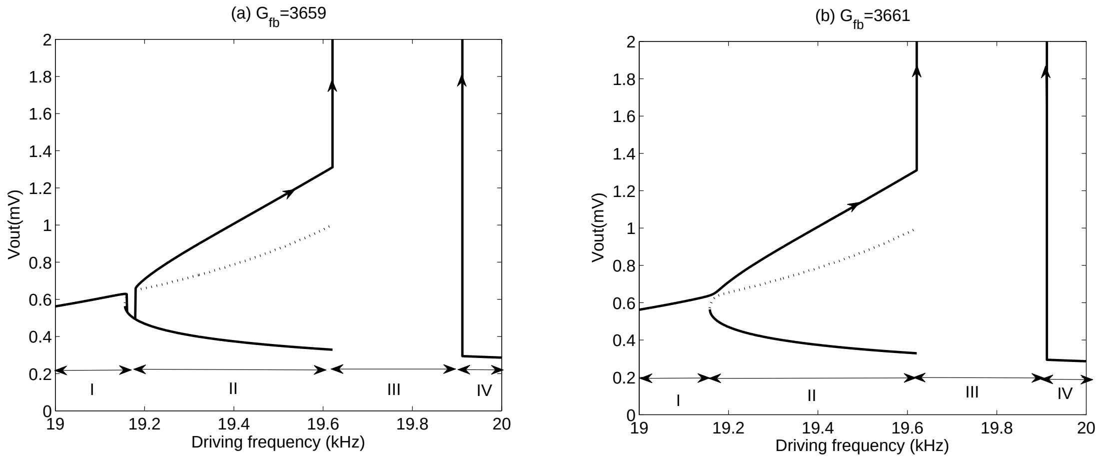

Figure 6.16: The simulated amplitude (a) and phase (b)response of the resonator with different feedback gains at a pressure of $10^5 Pa$ driven with $V_{ac} = 150mV_{pp}$.

This unexpected behaviour can be explained by the phase shift φ due to the bandpass filter. Equation 6.8, the model of the non-linear feedback system for high Q system, shows that when the driving frequency is larger than the reference frequency, the negative non-linear damping caused by the extra phase shift increases as the driving frequency grows. This means that the effective Q in range II gradually increases until the damping term has been fully removed by the feedback in range III. When the phase shift continues increasing, the negative damping term will change to positive eventually which is shown in range IV. Figure 6.16(b) shows that increasing the feedback gain to 3661 will have an unexpected effect on the response of the system. In this case the hysteresis loop in range I can not be observed because the expected

Duffing-like response merges with the three solutions from range II before the single low stable amplitude response arises.

The Duffing-like response will disappear when the feedback gain is increased by 0.14% from the critical value to $G_{fb} = 3661$ which is a very narrow range. This means that it will be very difficult to obtain the correct value of feedback gain when the resonator is operating at atmospheric pressure and even if the correct gain could be obtained it will not be sufficiently stable. The reason for this narrow range of desired feedback gains is because such a low Q system requires the non-linear damping term caused by the extra phase shift to cancel part of the linear damping term. However, due to the wide bandwidth, the frequency where the hysteresis loop occurs is very close to the frequency where the linear damping term is fully cancelled by the non-linear damping term. Hence if the feedback gain is too large, as the driving frequency is increased the amplitude response will increase along the high stable branch of the hysteresis loop and then become self-oscillated without jump down to the low stable branch as shown in Figure 6.16(b) because the damping term has been fully cancelled before the amplitude collapse. This suggests that the extra phase-shift helps to create enough non-linear restoring force by increase the magnitude of the displacement, but it also limits the non-linear feedback gain due to danger of causing positive feedback.

The above analysis is based on the system with hardening non-linear feedback. However, the response of a high Q system in Figure 6.3 shows that the damping term of the softening non-linear resonator is increased due to the extra phase shift and so it might be believed that the softening feedback resonator will not have the disadvantages of positive feedback. Recall from Equation 6.8, the phase shift θ caused by the multiplier is a negative constant of -4 degrees while the phase shift φ arising from the bandpass filter changes versus the driving frequency. When the driving frequency is limited within a range of $40Hz$, when Q is over 1000, the absolute value of φ is less than 1 degree which means that the sign of the non-linear damping term is always opposite to the displacement cubed term. However, as the range of the driving frequencies expand, the phase shift φ will become dominant. For the softening resonator, the non-linear damping term will change from positive to negative as the driving frequency decreases from the reference frequency. More importantly, the non-linear damping term from the phase shift is also needed for cancelling the linear damping. This means that the reference frequency for the softening non-linear feedback should be chosen slightly higher than calculated critical frequency to ensure the magnitude of amplitude response near the critical frequency is large enough to create a hysteresis loop. Consequently, both hardening and softening non-linear feedback systems with a low Q value have the disadvantage of narrow range of feedback gains to have the Duffing-like jumps.

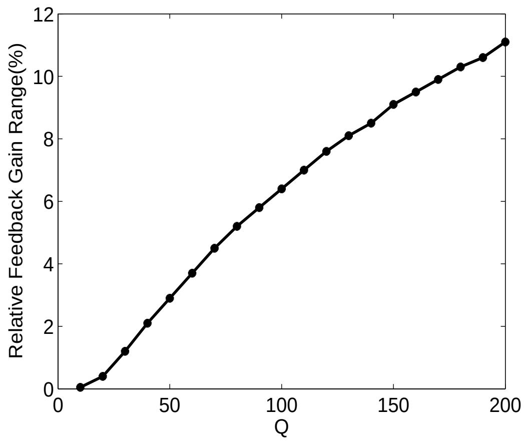

Figure 6.17: Relationship between Q values and the relative feedback gain range to create a Duffing hysteresis loop.

This problem arises when the natural Q is low in air and the linear damping term needs to be partially cancelled, as a result, it can be improved if a slightly better Q is available which means that less non-linear damping is required and the frequency where self-oscillation occurs is further away from the frequency where the hysteresis loop appears. Hence wider range of feedback gains will be able to create a Duffing-like non-linearity and therefore it is much easier to identify a desired feedback gain to implement a non-linear feedback. Experimental results in Figure 6.15 has shown that when the Q value is increased to 60, an appropriate feedback gain has been found to create two jumps in amplitude and phase response. To investigate the effect of Q value on the non-linear feedback gains, simulations with different Q values for the hardening resonators have been compared. The procedure of the simulation is the same as the one used for the responses with $Q = 5.5$ in Figure 6.14 and Figure 6.16. The range of the desired feedback gains is defined as the difference between the critical feedback gain and the maximum feedback gain that can create a Duffing-like hysteresis loop. Figure 6.17

shows the relationship between Q values and the relative feedback gain range which is the ratio between desired feedback range and the critical feedback gain. As expected, the percentage of range of the feedback gain with Q less than 10 is almost zero and as the rise of Q values the relative range for the feedback gain increases. This means that if the native Q of the resonator in air is increased to 50, for example, wider range of available feedback gains can be achieved of 3%. The slightly increased natural Q in air makes it easier to implement the non-linear feedback at atmospheric pressure. In this way, the non-linear feedback method can be therefore implemented in air to increase the sensitivity of the resonator.

6.5 Summary

The micromechanical resonator has driven with non-linear feedback to show a Duffing-like hysteresis. This is implemented by shifting the output voltage by 90 degrees using a bandpass filter. Then this voltage is cubed by two multipliers which was described in the Chapter 3 discussing the Duffing circuit. Both systems are composed with a linear resonator and a non-linear feedback which is same in principle. In the non-linear feedback loop, there are two main source of phase shift: one is the phase shift θ caused by the multipliers and the other one is the phase shift φ resulting from the bandpass filter. The phase shift θ is a positive constant of 4 degrees while the phase shift φ slowly changes versus the driving frequency. The effect of the extra phase shift is quite different with different Q values. Therefore, the system has been investigated in deep vacuum and medium vacuum or in air separately.

The resonator has native high Q when it is operated in deep vacuum and the bandwidth is quite narrow which means the phase shift φ from the bandpass filter is quite small and the phase shift θ from the multipliers is dominant. The consequence of the phase shift is a slightly modified non-linear parameter and an extra non-linear damping term. The equation of the motion with non-linear feedback in deep vacuum is obtained and it fits very well with the experimental results. The phase changes following a same change in resonant frequency with four different feedback levels are compared. The non-linear system with sub-critical and over-critical feedback gain shows benefits over the linear resonator. The undesired long transient response is also observed in the micromechanical system.

For the resonator in medium vacuum or in air, the natural Q has been reduced significantly. The bandwidth is subsequently increased and therefore the phase shift φ which varies versus the driving frequency becomes crucial. Simulation results show that the hysteresis loop occurs when the damping is partially cancelled by the extra phase shift. This phase shift has to be limited by choosing the feedback gain and the reference frequency carefully since it will lead to positive feedback if the damping term is fully removed by the extra phase shift. Experimental results in medium vacuum shows that the non-linear feedback is a feasible method in low Q system in principle. If a resonator design with a slightly higher native Q, the method of the non-linear feedback can be used in air to increase the sensitivity of the resonator.

Chapter 7

Conclusions

7.1 Executive summary

◇ The possibility of using non-linear behaviours of resonators to increase sensitivity to changes in resonant frequency have been investigated. This investigation has focused upon the possible exploitation of the well known jumps in amplitude and phase of Duffing resonators when they are driven with a force that is larger than a critical value.

- ◇ Sensitivity
  - When the resonator is driven with a force that is larger that the critical value the sensitivity to resonant frequency changes can be increased by a factor of nearly 300 times when compared to the equivalent linear resonator, but the discontinuous response curve means that it is impossible to quantify the change in resonant frequency. This mode of operation could be used to create extremely sensitive alarm sensors.
  - When the resonator is driven with a force that is slightly smaller than the critical value sensitivity is still increased but now it is possible to quantify any change in resonant frequency.
- ◇ Response time
  - Undesirable varied long delays following changes to the resonant frequency were observed in simulations when the resonator was driven much harder than

the critical force.

- Experimental results from a Duffing circuit confirmed that this phenomenon existed in real systems and it was not caused by the numerical errors in the simulation.
- A hypothesis to explain the delay was proposed that led to the suggestion that these delays could be avoided by driving the resonator with forces slightly larger than the critical value. This solution was shown to work for both the numerical simulations and the Duffing circuit.

◊ Two types of feedback technique were implemented to create Duffing-like non-linearities for a linear micro-mechanical resonator with a low native Q value at atmospheric pressure:

  ⋄ Velocity feedback was used to cancel damping so that the magnitude of the displacement increased. The combination of velocity feedback and the particular comb capacitors in a micromechanical resonator led to a softening Duffing non-linearity.

  ⋄ Non-linear feedback was created by generating an output voltage that was proportional to the displacement of the resonator. This voltage was then cubed and added to the primary drive to create the non-linear restoring force required to form a Duffing resonator. Both hardening and softening non-linearities were achieved.

◊ Characterisation of three different non-linear resonators (the Duffing circuit, micro-mechanical resonator with velocity feedback or non-linear feedback) were described. In all cases the models with the relevant extracted parameter values gave very good fits to the experimental data.

7.2 Summary

The small mass and large surface area of functionalised Microelectromechanical resonators makes them ideally suited for use as biological or chemical sensors. In these systems the presence of the target substance will cause a change in the resonant frequency of the resonator that can be detected by monitoring the amplitude or phase of the resonator. The sensitivity of the sensor is then proportional to the rate of change of amplitude or phase with resonant frequency. This makes the Duffing resonator with sudden changes in the amplitude and phase at two jump frequencies an attractive basis for a mass sensor. However the sensitivity of a sensor is only one of its critical characteristics, another important characteristic is its temporal response.

Numerical simulation results have shown that when the Duffing resonator is driven hard to enhance the change in amplitude a change in resonator parameters is followed by a delayed response. This amplitude change occurs when the resonator is driven at a frequency that corresponds to one edge of the hysteresis loop that is a well known feature of a resonator whose response is governed by the Duffing equation. It is possible that this unexpected and undesirable behaviour is caused by the proximity of the stable and unstable states over a range of frequencies close to the drive frequency. A solution to this problem that by driving the system with only just enough force for the required sudden changes to occur has been proposed. Results have shown that the undesirable delayed responses to parameter changes are avoided because in these conditions the stable and unstable states separate quickly near the drive frequency. To find the minimum driving force required to create a hysteresis, the harmonic balance method has been used obtain the cubic equation which describes the amplitude response of the Duffing resonator. The critical driving force was then calculated with this cubic equation by limiting the number of frequencies corresponding to multi-amplitude solution to be one. Due to manufacturing variations, parameter values for each resonator for the same design can be different. To determine the critical force for each resonator, a procedure to extract the parameters describing the response of the resonator has been suggested.

It is possible that the unexpected temporal responses following the simulated mass changes, arise from the numerical methods used in the simulation. To both ensure that this is not the case and to allow controlled reproducible experimentation this behaviour has been investigated using a circuit whose response is also governed by the Duffing equation. A control system for characterisation, actuation and measurement of the Duffing circuit has been described. A programmable waveform generator IC controlled by the FPGA is used to drive the Duffing circuit because the frequency of output can be increased/decreased continuously as programmed. The phase difference between the resonator's response and the primary drive was converted to a DC voltage by a phase comparator and a lowpass filter. A strategy has also been described to find the frequency at which the phase of the non-linear resonator changes extremely rapidly. The parameter values of the Duffing circuit have been extracted. Although the response of the ideal circuit should be represented by the Duffing equation it was found that the damping term varies for different driving forces. This unexpected behaviour has been explained by taking into account the phase shift of the multipliers which cause an extra displacement dependent damping term. An excellent fit between the new model and the data for both softening and hardening models of the circuit has been achieved. The corresponding critical driving voltage was calculated with the new model.

A comparison of the models of the mechanical Duffing resonator and the Duffing circuit shows that one capacitance is equivalent to the mass of a micromechanical resonator. When the effective "mass" of the circuit is increased when the circuit is driven hard to create a large hysteresis, there were varied delays in the response of the circuit to the same parameter change which is consistent with the systems behaviour observed in simulations. The solution proposed in the simulation analysis has also been confirmed by driving the Duffing circuit with a voltage slightly larger than the critical value which is called over-critical voltage. Using this choice of driving voltage the hysteresis loop normally associated with a Duffing resonator is small and the circuit's amplitude collapses as soon as the "mass" increases. The phase change of the Duffing resonator is significantly larger than that the equivalent linear resonator to the same changes in resonant frequency.

However, unlike the linear resonator, the Duffing resonator driven by the over-critical voltage can not quantify the resonant frequency change because its discontinuous phase response. To estimate the resonant frequency change, the resonator has been driven with the sub-critical voltage when the phase response is continuous but with large rate of change of phase. Experimental results show a larger phase change for the system driven with sub-critical voltage than the linear one but the phase noise for both systems is similar level. The phase responses after a lowpass filter have also been compared which shows that the phase variation of the non-linear resonator after filtering is also increased when the rate of change of phase rises. The increase in the phase variation is believed to be caused by the instability of the Duffing resonator itself because frequency drifts have been observed when the Duffing circuit becomes self-oscillation. As a result, the method to drive the Duffing resonator with sub-critical voltage is feasible to increase the sensitivity.

A micromechanical resonator with interdigitated combs structure, which has differential drive and readout, has been described. With this type of structure, the capacitive driving force is expected to be is independent of the movement of the resonator. However, due to the short combs and the proximity between the backs of the comb, the experiments show that the resonator also includes some small parallel plate capacitances. Two important consequences of these additional components to the resonator capacitance have been confirmed by the simulation and the experiments. The first is that they produce a small displacement dependent electrostatic force which has been used to change the effective resonant frequency of the resonator. This means that the comparison of different methods of sensing changes in resonant frequency is controllable and reproducible with a DC voltage and the changes in resonant frequency will also occur at a known time. The second important consequence is a non-linear force. This means that when the resonator is driven so that the amplitude of its response is several hundred nanometres the resonators response is governed by an equation similar to the Duffing equation and the resonator therefore has a non-linear mode of operation.

The natural Q value of the resonator in air is approximated 5.5 which is quite low and therefore force feedback has been employed as a useful method of partially cancelling the effects of viscous damping to increase the effective quality factor of the resonator. Since the resonator has been designed to be driven by a differential voltage and generate an output current proportional to its velocity, this type of force feedback was implemented in analogue circuits. The amplitude of the Q-enhanced resonator is limited within the linear region and the resulting phase chance at resonance has been increased by gives a factor of 60 after the velocity feedback force is applied. During the tests of varying the resonant frequency, an apparently negligible phase-shift in the feedback loop has a dramatic effect on the user's ability to quantify any changes in resonant frequency. The Q-enhanced system has been characterised to create a model which includes the effects of these phase shifts. In addition an inequality condition has been suggested that allows the designers of future systems to determine if these phase-shifts will be have an effect upon their design.

The simulation and the experimental results of the Duffing circuit suggests that the phase response of the Duffing resonator is more sensitive to changes in resonant frequency when the resonator is in its non-linear mode than it is operated in its linear mode. This has also been confirmed by a study of the response of the same resonator when its mode of response has been changed by simply driving the resonator harder. Before investigating the sensitivity of the non-linear resonator, the origins of the non-linearity have been identified and characterised. For the Q-enhanced system, one part of the non-linearity arises from the displacement cubed term in the small parallel plate capacitances due to the design of the resonator. More significantly, the combination of the displacement dependent term in the non-ideal comb capacitance and the velocity feedback term plays a major role in the overall non-linearity. This means that for a specific resonator design, the Q-enhancement mechanism is a new method to create non-linearity.

The experiment starts with calculating the critical driving voltage with the characterised model for the Q-enhancement. Then the phase responses with over-critical and sub-critical driving voltages following the effective resonant frequency change have been compared. The sensitivity of the method with over-critical driving voltage is determined by the accuracy of establishing the operation point and therefore the stability and repeatability of the initial conditions have been investigated. The minimum detectable resonant peak shift is 1.45Hz and the resulting phase change with over-critical driving voltage is 40 degrees. With the same feedback level, the maximum phase change when the resonator is operating in its linear mode is 10 degrees following the same resonant frequency change. Moreover, if compared with resonator operated in air without any feedback, the non-linear resonator is approximately 300 times more sensitive.

When the resonator is operated in its non-linear mode driven by sub-critical voltage, the amount of phase change following the same resonant frequency is also larger than the change when it is operated in the linear regime. The dynamic range of this method has also been identified by comparing the resulting phase changes from different effective resonant frequency variation. Results comparing the linear resonator and non-linear resonator with several sub-critical voltages show that there is a trade off between the sensitivity and the dynamic range. However, the method of driving the micromechanical resonator into its non-linear region has been confirmed to be a desired technique to increase the sensitivity of the resonator with same effective Q value as the linear mode.

An alternative method to create sufficient non-linearity for a micromechanical resonator is using a non-linear feedback force. With this method, the non-linear restoring force is controlled by the feedback gain instead of the magnitude of the displacement which was used in Q-enhancement. This non-linear feedback method is similar to the Duffing circuit in principle and the electronics to cube the "displacement" signal are identical for these two systems. However, for the micromechanical resonator extra electronics is required to shift the output voltage from the resonator by 90 degrees to create a signal proportional to the displacement. This is implemented using the same switched-capacitor bandpass filter described in the Q-enhanced system by changing the filter clock frequency. A new non-linear feedback model was created and two types of extra phase shift in the feedback loop have been investigated. The phase shift from the multipliers is a positive constant which has been extracted in the Duffing circuit analysis while the value of the phase shift due to the bandpass filter is frequency dependent. In deep vacuum with a high native Q, the effect of extra phase shift is to slightly modify the non-linear parameter and add a small non-linear damping term. As expected, the non-linear system with sub-critical and over-critical feedback gain shows benefits over the linear resonator. In addition, the feedback gain has been increased to create a large hysteresis loop and the undesired long transient response is also observed in the micromechanical system.

For the non-linear feedback with low Q value, the frequency dependent phase shift in the feedback loop affects the resonator's response significantly because of its wide bandwidth. Simulation results show the hysteresis loop occurs when the linear damping is partially cancelled by the non-linear term caused by the extra phase shift. It also suggests that the response is very sensitive to the feedback gain and the range of operating frequencies since positive feedback occurs if the damping term is fully removed by the extra phase shift. Consequently, the feedback gain is required to be greater than the critical feedback gain but smaller than the feedback gain value which will lead to self-oscillation. Simulation shows that the difference between these two criteria is reduced as the native Q value decreases. Experimental results in medium vacuum shows that the non-linear feedback is a feasible method in low Q system in principle. However, it has been very difficult to identify the desired feedback gain in air because of the narrow range of the available feedback gains. Although the non-linear feedback method is extremely difficult for this specific sample with native Q of 5.5 in air, this technique can be implemented to increase the sensitivity if a resonator is designed with a slightly higher native Q in air.

Sharp transitions in amplitude and phase response at the jump frequencies of the Duffing-like non-linearity have been exploited to increase the sensitivity of the resonator. Both Duffing resonator circuit and the micromechanical resonator show the benefits by driving the system into the non-linear mode compared with linear mode. There are two types of non-linear mode to increase the sensitivity. One is the over-critical force which is very sensitive to the changes in the resonant frequency. The drawback of this method is that it can only used as an alarms system because the amount of frequency change can not be quantified from any observed phase response. The other one is the sub-critical force can overcome this deficiency by sacrificing some amount of sensitivity. However, this sub-critical method shows the advantages in sensitivity compared with linear mode. For a linear micro-mechanical resonator, two different feedback strategies to create a Duffing-like non-linearity have been discussed. The velocity feedback is exploited to cancel part of the damping term which increases the magnitude of the displacement and therefore the non-linear restoring force. The non-linear feedback is to create a non-linear restoring force by varying non-linear feedback gain without increasing the displacement significantly. The phase shift in both feedback loops plays an important role in the response of the resonator and this has been identified and characterised. The non-linear feedback can be either softening or hardening non-linearity. It would be easier to choose the softening non-linear feedback if over-critical driving is employed because the jump frequency can be reached from rest without continuous sweeping the driving frequency. For the sub-critical driving force, it is the same to use softening or hardening non-linearity.

The transient response of the Duffing resonator following the changes in resonant frequency has been investigated. Both simulation and experimental results show that Duffing non-linear behaviour can be used to enhance the sensitivity with reliable response time. To implemented a MEMS sensor, the discrete electronic components used for the characterisation, actuation and measurement of the micromechanical resonators in this thesis can be converted to a microelectronic circuit.

7.3 Future work

Undesirable long transient responses following a change in the mass of a resonator when the resonator is driven hard have been predicted and observed. A practical solution to reduce the response time of the resonator to any change in mass was proposed and demonstrated in both simulations and experiments. However, the hypothesis that this problem is due to the proximity of unstable solution and stable solution needs to be confirmed.

The Duffing-like non-linearity observed using Q-enhancement in Chapter 5 is mainly caused by the combination of velocity feedback and the non-ideal driving combs, which have a displacement dependant component to their capacitance. This dependence of the amount of velocity feedback means that the amount of the non-linearity and the effective quality factor of the resonator can not be controlled independently. The independent control of these two key parameters could be achieved with a different resonator design. In the existing resonator design the displacement dependent component of the drive comb capacitance arises from the parallel plate capacitances between the movable combs and fixed combs. In a new resonator design, Figure 7.1, the drive combs could be separated into two parts, an ideal comb drive for Q-enhancement and a parallel plate capacitance to create a non-linear feedback force. Figure 7.1 shows that there are also one pair of differential drive capacitances and one pair of differential readout capacitances using interdigitated comb structure. Both of them are designed with less parasitic capacitances by using longer comb fingers and wider gap between the backs of combs which ensures that these comb capacitances can be considered to be constant without any displacement dependent terms. The differential drive comb can be used for

Q-enhancement feedback and the effective Q value can be controlled by this feedback gain while the differential sensing combs produce currents proportional to the velocity of the resonator as discussed in Chapter 5. The parallel plate capacitors should be designed to ensure that with the feedback voltages that are available the resulting non-linearity is large enough for the resonator to show hysteresis with an amplitude of response that is smaller than the gap between the drive combs but large enough to create a large output signal. Although this design would require one or two more contacts, it would then be possible to independently control the feedback that enhances the quality factor and the non-linear feedback required to create a non-linear resonator.

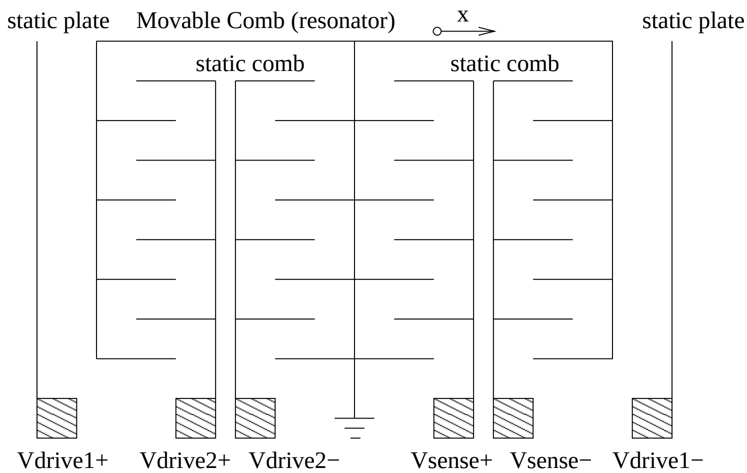

Figure 7.1: Conceptual diagram for the proposed comb structure.

The dynamic range of a resonant sensor when it is driven with a sub-critical driving voltage has been investigated in Chapter 5 using a linear approximation to the relationship between phase and resonant frequency. This linear approximation is a very straightforward and simple method to determine any change in resonant frequency from the observed change in phase. However, it is an approximation which limits the dynamic range of the sensor when a particular level of accuracy is required. The model for the resonators response that has been proposed and validated gives a relationship between the resonant frequency and phase change can be used instead of this linear approximation. For example a resonator could be characterised and the resulting parameters could be used in the model to generate a look-up table to convert an observed change of phase to an estimate of the change in resonant frequency. This would mean that the dynamic range of the sensor would no longer be limited by the range of validity of the linear approximation.

There are also several options to improve the sensing method using non-linear feedback in air. One option which has been proposed in Chapter 6 is to slightly increase the Q value of the resonator by modifying its design. Experimental results have shown that when the Q value is increased by a factor 10 a hysteresis loop is observed. A second option is suggested by the fact that a hysteresis loop has been observed in the response of the Duffing resonator circuit, with a similar Q value and the same feedback circuit as the micromechanical resonator. The main difference between the two resonators, which is also the main problem, is that the output response of micromechanical resonator needs to be shifted by 90 degrees using the bandpass filter. This bandpass filter causes a small but significant extra phase shift at all but one frequency and this extra phase shift creates a non-linear damping term which limits the maximum non-linear feedback gain that can be used without causing positive feedback. These problems can be avoided using a method, such as an optical detection technique [5, 18–20] which creates an output that is proportional to displacement. If this is not possible the feedback electronics can be modified in one of two ways. The first one is to avoid the extra phase shift in the band-pass filter by using the FPGA to generate the clock signal for the bandpass filter which ensures that the phase shift through the band-pass filter at the driving frequency is always 90 degrees. The other option is to switch the feedback control system to digital electronics. As shown in the block diagram, Figure 7.2, the output from the resonator is bandpass filtered to eliminate noise before it is converted to digital words by an ADC. Then the digitised signal is processed by the FPGA for different feedback requirements. The phase shift compensation, velocity to displacement conversion or even multiplication of cubed signal can be realised by the FPGA programming. After the signal processing, this digital output is converted to an analogue voltage by a DAC and this feedback voltage is then added to the primary drive. The digital feedback system can also improve the performance of the sensor by automatically finding the desired operating point. To do this the phase response of the resonator should be analysed by the FPGA to calculate the rate of change of phase as the drive frequency is varied. Particular care will be required to differentiate between a small jump and a very large $\frac{d\phi}{d\omega}$. This can be realised by monitoring the continuity of $\frac{d\phi}{d\omega}$ when determining the appropriate operating point. Once a technique to enhance the sensitivity of a non-linear resonant sensor has been demonstrated the circuits required by the technique could be integrated to create an inexpensive, easily used integrated sensor.

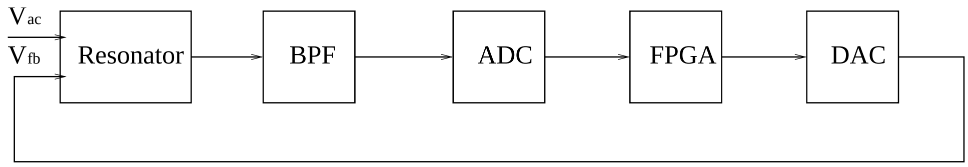

Figure 7.2: Block diagram of digitally controlled feedback system.

Bibliography

[1] Mohamed Gad el Hak. *MEMS: design and fabriation*. CRC Press, 2006.

[2] Masako Tanaka. An industrial and applied review of new mems devices features. *Microelectronic Engineering*, 84:1341–1344, 2007.

[3] E. A. Wachter and T. Thundat. Micromechanical sensors for chemical and physical measurements. *Review of Scientific Instruments*, 66:3662, 1995.

[4] Taeyun Kwon Kilho Eom, Harold S. Park Dae Sung Yoon. Nanomechanical resonators and their applications in biological/chemical detection: Nanomechanics principles. *Physics Reports*, 503:115–163, 2011.

[5] A. Malloy J. Tamayo, A.Humphris and M. Miles. Chemical sensors and biosensors in liquid environment based on mircocantilevers with amplified quality factor. *Ultramicroscopy*, 86:167–173, 2001.

[6] Wenhua Zhang Kimberly L. Turner. Design and analysis of a dynamic mem chemical sensor. *Proceedings of American Control Conference*, pages 1214–1218, 2001.

[7] C. Andreoli J. Brugger M. Despont P. Vettiger Ch. Gerber J. K. Gimzewski J. P. Ramseyer E. Meyer H. P. Lang, R. Berger and H.-J. Gntherodt. Sequential position readout from arrays of micromechanical cantilever sensors. *Applied Physics Letters*, 72:383, 1998.

[8] T. Thundat Zhiyu Hu and R. J. Warmack. Investigation of adsorption and absorption-induced stresses using microcantilever sensors. *Journal of Applied Physics*, 90:427, 2001.

[9] M. Zalalutdinov H. G. Craighead P. Neuzil C. Campagnolo B. Ilic, D. Czaplewski and C. Batt. Single cell detection with micromechanical oscillators. *Journal of Vacuum Science & Technology B*, 19(6):2825, 2001.

[10] S. J. Kennel K. B. Jacobson R. J. Warmack T. Thundat A. Subramanian, P. I. Oden and M. J. Doktycz. Glucose biosensing using an enzyme-coated microcantilever. *Applied Physics letters*, 81:385, 2002.

[11] G Abadal J Verd F Campabadal F Prez-Murano J Esteve N Barniol A Boisen S Ghatnekar-Nilsson, E Forsn and L Montelius. Resonators with integrated cmos circuitry for mass sensing applications, fabricated by electron beam lithography. *Nanotechnology*, 16:98, 2005.

[12] K. Aubin R. Reichenbach S. Krylov B. Ilic, Y. Yang and H. G. Craighead. Enumeration of dna molecules bound to a nanomechanical oscillator. *Nano Letters*, 5(5):925–929, 2005.

[13] S. Krylov W. Senaratne C. Ober B. Ilic, H. G. Craighead and P. Neuzil. Attogram detection using nanoelectromechanical oscillators. *Journal of Applied Physics*, 95:3694, 2003.

[14] H. P. Lang H. Rothuizen P. Vettiger E. Meyer H. J. Gntherodt Ch. Gerber1 and J. K. Gimzewski J. Fritz, M. K. Baller. Translating biomolecular recognition into nanomechanics. *Science*, 288(5464):316–318, 2000.

[15] Y. Yang B. Ilic and H. G. Craighead. Virus detection using nanoelectromechanical devices. *Applied Physics Letters*, 85:2604, 2004.

[16] M.L.Roukes K.L.Ekinci, X.M.H.Huang. Ultrasensitive nanoelectromechanical mass detection. *Applied Physics Letters*, 84:4469–4471, 2004.

[17] X.L. Feng K.L.Ekinci Y.T. Yang, C. Callegari. Zeptogram-scale nanomechanical mass sensing. *Nano Letters*, 6:583–586, 2006.

[18] O.Marti J.Mertz and J. Mlynek. Regulation of a microcantilever response by force feedback. *Applied Physics Letters*, 62(19):2344–2346, 1993.

[19] Humphris J. Tamayo, A and M. Miles. Piconewton regime dynamic force microscopy in liquid. *Applied Physics Letters*, 77(4):582–584, 2000.

[20] M.Alvarez J. Tamayo and L. Lechuga. Digial tuning of the quality factor of micromechanical resonant biological detectors. *Sensors and Actuators B: Chemical*, 89(1-2):33–39, 2003.

[21] C. Nguyen and R. Howe. An intergrated cmos micromechanical resonator high-q oscillator. *IEEE Journal of Solid-State Circuits*, 34(4):440–455, 1999.

[22] C. Nguyen and Howe R. Quality factor control for micromechanical resonators. *Electron Devices Meeting, 1992. Technical Digest, International*, pages 505–508, 1992.

[23] S. Collins R. Turnbull, M. Ward and C. Anthony. A simple technique to increase the quality factor of micro-mechanical resonators. *Micro- and Nanotechnology Sensors, Systems, and Applications*, 7318(1):73181G, 2009.

[24] Kimberly L. Turner Jeffrey F. Rhoads, Steven W. Shaw. Nonlinear dynamics and its applications in micro- and nanoresonators. *Jounal of dynamics systems, meausrement and control*, 132(3):034001, 2010.

[25] Ron Lifshitz and M. C. Cross. *Reviews of nonlinear dynamic and complexity*, volume 1. WILEY-VCH, 2009.

[26] Balakumar Balachandran Steven W. Shaw. A review of nonlinear dynamics of mechanical systems in year 2008. *Jounal of system design and dynamics*, 2(3):611–640, 2008.

[27] S. Aldridge. *The Duffing Oscillator for Nanoelectromechanical Systems, in Nonlinear Dynamics of Nanosystems*. Wiley-VCH Verlag GmbH & Co . KGaA, Weinheim, Germany, 2010.

[28] Kimberly L. Turner Steven W. Shaw Barry E. DeMartini, Jeffrey F. Rhoads and Jeff Moehlis. Linear and non-linear tuing of parametric excited mems oscillators. *Journal of microelectromechanical systems*, 16:310, 2007.

[29] Guang Meng Wen-Ming Zhang and Zhi-Ke Peng. Nonlinear dynamic analysis of atomic force microscopy under bounded noise parametric excitation. *IEEE/ASME Transactions on Mechatronics*, 16(6):1063, 2011.

[30] Oropeza-Ramos L.A. Miller N.J., Shaw S.W and Turner K.L. Analysis of a novel mems gyroscope actuated by parametric resonance. *In Proceedings of ENOC2008: The 6th EUROMECH Nonlinear Dyanamics Conference.*, 2008.

[31] Kimberly L. Turner Wenhua Zhang, Bajashree Baskaran. Effect of cubiic nonlinearity on auto-parametrically amplified resonant mems mass sensor. *Sensors and Actuators A: Physical*, 102:139–150, 2002.

[32] Rajashree Baskaran Wenhua Zhang and Kimberly L. Turner. Nonlinear behavior of a parametric resonance-based mass sensor. *Proceedings of IMECE ASME International Mechanical Engineering Congress & Exposition*, 2002.

[33] P.G.Hartwell N.C.Maconald S.H. Strogartz S.G. Atams K.L. Turner, S.A.Miller. Five parametric resonance in a microelectromechanical system. *Nature*, 396:149–152, 1998.

[34] Kimberly L. Turner Wenhua Zhang. Application of parametric resonance amplification in a single-crystal silicon micro-oscillator based mass sensor. *Sensors and Actuators A: Physical*, 122:23–30, 2005.

[35] Fadi Alsaleem Mohammad I. Younis. Exploration of new concepts for mass detection in electrostatically-actuated structures based on nonlinear phenomena. *Jounal of computational and nonlinear dynamics*, 4:021010, 2009.

[36] Kilho Eom Mai Duc Dai and Chang-Wan Kim. Nanomechanical mass detection using nonlinear oscillations. *Applied Physics Letters*, 95(20):20104, 2009.

[37] Bernard Yurke Buks.E. Mass detection with nonlinear nanomechanical resonator. *Physical review E*, 74, 2006.

[38] Malcolm J. Skove Apparao M. Rao Gayatri Keskar, Bevan Elliott and Steven M. Serkiz. Ultra-sensitive duffing behavior of a microcantilever. *IEEE Sensors Journal*, 8:1848–1855, 2008.

[39] B J Gallacher WH Waugh and J S Burdess. A high-sensitivity resonant sensor realized through the exploitation of nonlinear dynamic behaviour. *Measurement science and techonology*, 22:105202, 2011.

[40] Hendrik Ekowaluyo Jacob K. Miller George C. Marvin George T.C. Chiu Jeffrey F. Rhoads Vijay Kumar, J. William Boley. Linear and nonlinear mass sensing using piezoelectrically-actuated microcantilevers. *SEM Annual Conference and Exposition on Experimental and Applied Mechanics*, 2010.

[41] Y. Yang H. Ekowaluyo J. K. Miller G. T.C. Chiu V. Kumar, J. W. Boley and J. F. Rhoads. Bifurcation-based mass sensing using piezoelectrically-actuated microcantilevers. *Applied Physics Letters*, 98(15):153510, 2011.

[42] Mika Koskenvuori and Ilkka Tittonen. Towards micromechanical radio: Overtone excitations of a microresonator through the nonlinearities of the second and third order. *Journal of microelectromechanical systems*, 17(2):363, 2008.

[43] A. Kraus R. H. Blick G. Corso A. Erbe, H. Krmmer and K. Richter. Mechanical mixing in nonlinear nanomechanical resonators. *Applied Physics Letters*, 77:3102, 2000.

[44] Shtempluck.O Buks.E. Almog.R, Zaitsev. S. High intermodulation gain in a micromechanical duffing resonator. *Applied Physics Letters*, 88:213509, 2006.

[45] O. Shtempluck R. Almog, S. Zaitsev and E. Buks. Noise squeezing in a nanomechanical duffing resonator. *Physical review letters*, 98:078103, 2007.

[46] A.P. French. *Vibrations and Waves*. M.I.T. Press, 1971.

[47] Ross Turnbull. *Sensitivity enhancement in micro-electromechanical systems for sensor applications*. PhD thesis, University of Oxford, 2010.

[48] Singireshu S.Rao. *Mechanical vibrations*. Reading, Mass. ; Wokingham : Addison-Wesley, 3rd edition, 1995.

[49] Bernstein D.S. Padthe.A.K. A delay-duhem model for jump-resonance hysteresis. *Decision and Control, 2007 46th IEEE Conference on*, pages 1609–1614, 2007.

[50] Nikolai Nikolaevich Bogoliubov. *Asymptotic Methods in the Theory of Non-linear Oscillations*. Delhi : Hindustan Pub. Corp ; New York : Gordon and Breach, 1961.

[51] Peter Smith Dominic William Jordan. *Nonlinear Ordinary Differential Equations*. Oxford University Press, 1999.

[52] Dean T. Mook Ali Hasan Nayfeh. *Nonlinear oscillations*. John Wiley & Sons, Inc., 1979.

[53] A. S. Peters James Johnston Stoker, Kurt Otto Friedrichs. *Nonlinear Vibrations*. Interscience publishers.

[54] C Anthony H Ostadi R. Al-Dadah N H Saad, X Wei and M.C.L. Ward. Impact of manufacturing variation on the performance of coupled micro resonator array for mass detection sensor. *Procedia Chemistry*, 1:831–834, 2009.

[55] Wolfgang Schleich Frank Moss, Luigi A. Lugiato. *Noise and Chaos in Nonlinear Dynamical Systems*. Cambridge University Press, 1990.

[56] Roger T. Howe William C. Tang, Tu-Cuong H. Nguyen. Laterally driven polysilicon resonant microstructures. *Sensors and Actualors A*, 20:25–32, 1989.

[57] Michael W Judy William C Tang, Tu-Cuong H Nguyen and Roger T Howe. Electrostatic-comb drive of lateral polysilicon resonators. *Sensors and Actuators*, 20:328–331, 1990.

[58] Wei X Ward M Anthony C, Turnbull R and Collins S. Fabrication and quality factor control of a microelectromechanical system resonator with linear differential drive. *IET Science Measurement science and techonology*, pages 206–213, 2010.

[59] Y. Zhu J. Lee and A. Seshia. A bulk acoustic mode single-crystal silicon microresonator with a high-quality factor. *Journal of Micromechanics and Microengineering*, 18(6):064001, 2008.

[60] J. Lee and A. Seshia. Parasitic feedthrough cancellation techniques for enhanced electrical characterization of electrostatic microresonators. *Sensors and Actuators A: Physical*, 156(1):36–42, 2009.

[61] Paul Horowitz and Winfield Hill. *The art of electronics*. Cambridge University Press, 2nd edition, 1989.

[62] Fernandes J.R. Filanovsky I.M. Verhoeven C.J.M. Silva M.M. Oliveira, L.B. *Analysis and Design of Quadrature Oscillators*. Springer, 2008.

[63] R.M.Marston. *Modern CMOS circuits manual*. Oxford : Newnes, 1995.